Polytechnic of Turin

IOWEC: Design of the hull

Master's Degree Thesis in Mechanical Engineering

Supervisor

Giuliana Mattiazzo

Candidate

Pierluigi Moscogiuri

April 2018

A mio Padre

A mia Madre

Ai miei fratelli

A coloro che fanno del bene disinteressato

ACKNOWLEDGMENTS

Ho iniziato a sognare di scrivere questo paragrafo molto tempo fa, ancor prima di cominciare gli studi...ed ora che è finalmente arrivato il momento non riesco ancora a realizzarlo. Sono stati anni molto duri, a prescindere dalle difficoltà del percorso di studi e solo, non ce l'avrei mai fatta. Pertanto, ringrazio anzitutto i miei genitori che sono i principali artefici di tutti i miei successi tra cui questo che ritengo il più importante. Ringrazio Benedetto che da buon fratello maggiore mi ha sempre consigliato al meglio come superare gli ostacoli accademici e Paolo che con la sua ammirazione mi ha fatto capire che stavo procedendo nella direzione giusta e che non dovevo mollare. Ringrazio tutti i miei altri familiari che non mi hanno mai mancato del loro affetto nonostante la considerevole distanza che ci separa solo geograficamente, insieme ad Ivana e Claudio che ritengo ormai parte integrante della mia famiglia. Questa riga è per la mia ragazza Patricia, che è entrata nella mia vita a passi leggeri in un momento decisamente inaspettato e mi ha fatto riscoprire una forza a me sconosciuta. Un'importante fetta della mia riconoscenza va Sergej Antonello Sirigu che mi ha guidato nella redazione di questo lavoro e alla professoressa Giuliana Mattiazzo che lo ha reso possibile, oltre a tutti i ragazzi di Wave for Energy che mi hanno aiutato a districarmi in un mondo che per me era assolutamente nuovo. L'ultima espressione della mia gratitudine è per tutti i miei amici: quelli di sempre "di giù" e quelli nuovi ma che sento come se li conoscessi da tutta la vita incontrati durante questo incredibile percorso.

Contents

1 Introduction **1**

1.1 The sea: more than a simple cradle of life 1

1.1.1 Why develop renewable technologies 2

1.2 Wave energy conversion systems 3

1.2.1 Europe needs ocean energy 5

1.3 Iswec 6

2 Installation Site **9**

2.1 Linear wave theory 9

2.1.1 Equations of the surface motion 11

2.1.2 The dispersion relation 13

2.2 Irregular wave theory 15

2.2.1 Irregular waves 16

2.3 Study of the sites 18

2.3.1 Power density 19

2.3.2 Wave period 22

3 Design of the Hull **26**

3.1 Pre-Project conditions 26

3.2 First design attempt 28

3.2.1 Floating structure 29

3.3 The hulls 32

3.3.1 V1 32
3.3.2 V2 34
3.3.3 V3 36
3.4 Comparison of the hulls 37
3.5 Productivity 40

4 Pitch Resonance Tuning Tank **46**
4.1 Mathematical model of a U-tank 46
4.1.1 Euler's equation 49
4.1.2 Continuity equation 49
4.1.3 External forces 49
4.1.4 Final equation of the system 50
4.2 Coupling the hulls with the U-tube tank 51
4.2.1 V2 with PRTT 52
4.2.2 V1 and V3 with PRTT 65
4.2.3 Summary of the hulls productivity 65
4.2.4 V2: Rised Deck 71
4.3 Considerations about the productivity 74
4.3.1 Geometrical variations of the Prtt 79

5 Initial Stability **83**
5.1 Stability Diagram 87
5.1.1 Stability curve of the hull V2 89

6 Conclusions **90**

Appendix A **91**

Bibliography **124**

List of Figures

1.1 Comparison between the main renewable source of energy 1

1.2 Trend of CO_2 level and global temperature 3

1.3 Operating scheme of a gyroscopic group in ISWEC 6

1.4 Hull of Iswec 7

1.5 Iswec operating at a 800 m from the shore of the northwest side of Pantelleria island 8

2.1 Representation of a regular wave 10

2.2 Waves in a two-dimensional space 11

2.3 The hyperbolic tangent 13

2.4 Particle trajectories associated with linear waves 15

2.5 Superposition of regular waves 17

2.6 Example of wave record in short term statistic 18

2.7 Bathymetric maps of Easter island and Robinson Crusoe island 19

2.8 Statistical distribution of ocean wave heights 20

2.9 Power density map of Robinson Crusoe island 21

2.10 Percentage of time in which the wave height is higher than 1 meter . . 22

2.11 Wave period map 23

2.12 Magnifications of the site 3 24

3.1 Scatter plots of the site N3 27

3.2 First hull and its water plane 29

3.3 Scheme of the reference frame of the system 30
3.4 IOWEC Hull: version 1 33
3.5 Represetation of the most important fineness coefficients 34
3.6 IOWEC hull: version 2 35
3.7 IOWEC hull: version 3 36
3.8 RAO of the hulls V1, V2, V3 37
3.9 Trend of the added masses 38
3.10 Energy production scatter - V1 44
3.11 Energy production scatter - V2 44
3.12 Energy production scatter - V3 44

4.1 Example of PRTT installation - V2 47
4.2 PRTT coordinate system 48
4.3 PRTT dimensions 48
4.4 Representation of the dimensions in Tab. 4.1 53
4.5 Response of the V2 with PRTT 54
4.6 Overlap between δ and ε - V2 - PRTT On 56
4.7 Overlap between δ and τ - V2 - PRTT On 56
4.8 Gross and net productivity - V2 - PRTT On 57
4.9 Torque transmitted to the PTO - V2 - PRTT On 57
4.10 Production scatter - V2 - PRTT enabled 59
4.11 Overlap between δ and ε - V2 - PRTT Off 60
4.12 Overlap between δ and τ - V2 - PRTT Off 60
4.13 Gross and net productivity - V2 - PRTT Off 61
4.14 Torque transmitted to the PTO - V2 - PRTT Off 61
4.15 Production scatter - V2 - PRTT disabled 63
4.16 Utilization of the U-tank in dependence of the waves - V2 64
4.17 Production scatter of V2 with the optimal use of the U-tank 65
4.18 Performance graphs - V2 - group 1 66

4.19 Performance graphs - V2 - group 2 66

4.20 Performance graphs - V2 - group 3 67

4.21 Performance graphs - V2 - group 4 67

4.22 Response amplitude operator of the V2 with the rised deck 71

4.23 Comparison between the wave and the hull - Case study 1 76

4.24 Comparison between the wave and the hull - Case study 2 76

4.25 Comparison between the wave and the hull - Case study 3 77

4.26 Comparison between the wave and the hull - Case study 4 77

4.27 PRTT dimensions 79

4.28 Map of the productivity 79

4.29 RAO with $h_r = 5,5m$ 80

4.30 Ratio τ/δ with $h_r = 5,5m$ 81

4.31 RAO with $h_d = 3m$ 81

4.32 Ratio τ/δ with $h_d = 3m$ 82

5.1 Initial position 83

5.2 Equilibrium conditions in dependence of B 84

5.3 Geometrical representation of the relation among B, G, M 85

5.4 Metacentric involute for $\alpha > 10$ 86

5.5 Relations among the characteristics of the hull and the stability curve . 88

5.6 Stability curve - hull V2 89

1 Response of the V1 with the PRTT 92

2 Overlap between δ and ε - V1 - PRTT On 93

3 Overlap between δ and τ - V1 - PRTT On 93

4 Gross and net productivity - V1 - PRTT On 94

5 Torque transmitted to the PTO - V1 - PRTT On 94

6 Production scatter of V1 with PRTT activated 95

7 Overlap between δ and ε - V1 - PRTT Off 96

8 Overlap between δ and τ - V1 - PRTT Off 96
9 Gross and net productivity - V1 - PRTT Off 97
10 Torque transmitted to the PTO - V1 - PRTT Off 97
11 Production scatter of V1 with PRTT disabled 101
12 Utilization of the U-tank in dependence of the waves - V1 101
13 Production scatter of V1 with the optimal use of the U-tank 102
14 Performance graphs - V1 - group 1 102
15 Performance graphs - V1 - group 2 103
16 Performance graphs - V1 - group 3 103
17 Performance graphs - V1 - group 4 104
18 Hull V3 with PRTT 104
19 Response of the V3 with PRTT 105
20 Overlap between δ and ε - V3 - PRTT On 106
21 Overlap between δ and τ - V3 - PRTT On 106
22 Gross and net productivity - V3 - PRTT On 107
23 Torque transmitted to the PTO - V3 - PRTT On 107
24 Production scatter - V3 - PRTT enabled 108
25 Overlap between δ and ε - V3 - PRTT Off 109
26 Overlap between δ and τ - V3 - PRTT Off 109
27 Gross and net productivity - V3 - PRTT Off 110
28 Torque transmitted to the PTO - V3 - PRTT Off 110
29 Production scatter - V3 - PRTT disabled 111
30 Utilization of the U-tank in dependence of the waves - V3 111
31 Production scatter of V3 with the optimal use of the U-tank 112
32 Performance graphs - V3 - group 1 112
33 Performance graphs - V3 - group 2 113
34 Performance graphs - V3 - group 3 113
35 Performance graphs - V2 - group 4 114

36 Overlap between δ and ε - V2 RD - PRTT On 115
37 Overlap between δ and τ - V2 RD - PRTT On 115
38 Gross and net productivity - V2 RD - PRTT On 116
39 Torque transmitted to the PTO - V2 RD - PRTT On 116
40 Production scatter - V2 RD - PRTT enabled 117
41 Overlap between δ and ε - V2 RD - PRTT Off 118
42 Overlap between δ and τ - V2 RD - PRTT Off 118
43 Gross and net productivity - V2 RD - PRTT Off 119
44 Torque transmitted to the PTO - V2 RD - PRTT Off 119
45 Production scatter - V2 RD - PRTT disabled 120
46 Utilization of the U-tank in dependence of the waves - V2 RD 121
47 Production scatter of V2 RD with the optimal use of the U-tank 121
48 Performance graphs - V2 RD - group 1 122
49 Performance graphs - V2 RD - group 2 122
50 Performance graphs - V2 RD - group 3 123
51 Performance graphs - V2 RD - group 4 123

List of Tables

2.1 Spectrum of site N3 25

3.1 Wave characteristics of the site N3 28
3.2 Percentages of reduction with respect to V1 37
3.3 Hydrostatic datas 39
3.4 Productivity and main parameters for the design wave 42
3.5 Productivity and main parameters weighed on the scatter 43

4.1 Dimensions of U-tube tank 52
4.2 Mass of the components with respect to the total mass 52
4.3 Hydrostatic datas V2 with PRTT 53
4.4 Production and main parameters - V2 - PRTT On 58
4.5 Production and main parameters - V2 - PRTT Off 62
4.6 Performance parameters of all V2 versions for the design wave 68
4.7 Performance parameters of all V2 versions weighed on the scatter . . . 69
4.8 Productivity of all the hulls 69
4.9 Hysrostatic datas of V2 - rised deck 72
4.10 Performance parameters of the hull V2 - RD for the design wave 73
4.11 Productivity and main parameters weighed on the scatter - V2 RD . . 74
4.12 Welch's method parameters used in the PSD estimation 75
4.13 Natural frequencies of the hull 75
4.14 Main parameters of the waves used for the frequency analisys 75

4.15 Avarage pitch amplitude of the four case studies 76

1 Hydrostatic datas of V1 with the PRTT 92

2 Performance parameters of all V1 versions for the design wave 98

3 Performance parameters of all V1 versions weighed on the scatter . . . 99

4 Hydrostatic datas - V3 - PRTT 99

5 Performance parameters of all V3 versions for the design wave 100

6 Performance parameters of all V3 versions weighed on the scatter . . . 105

CHAPTER 1

Introduction

1.1 The sea: more than a simple cradle of life

Since prehistoric times we have looked at the sea as a source of life, the place in which the first living organisms developed. But today it represents much more than this, because we can look at the sea as an incredible source of energy. Nowadays we have a lot of renewable energy sources and potentially the best one is the wave energy conversion from the sea waves, as is shown in the figure 1.1.

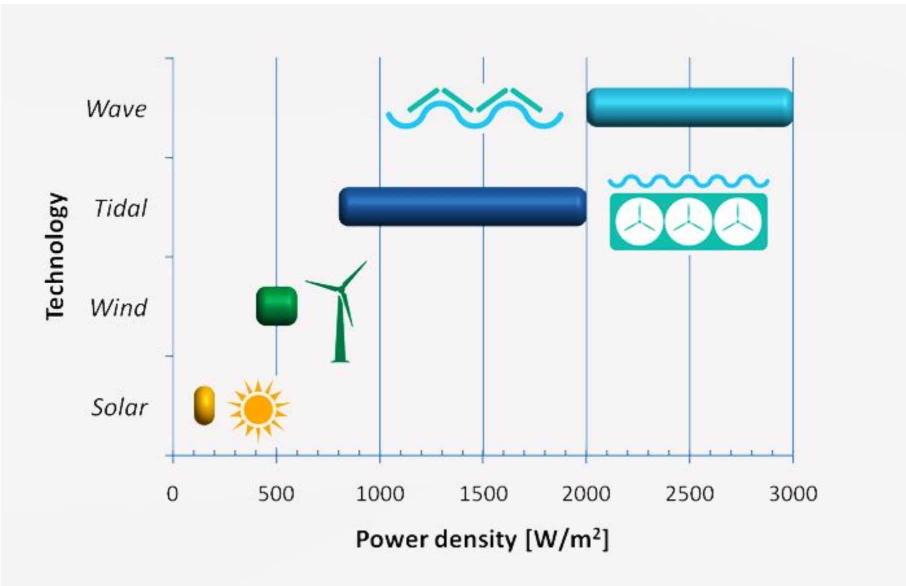

Figure 1.1: Comparison between the main renewable source of energy

1.1.1 Why develop renewable technologies

Air pollution during the last five years is increased with the highest ever grow rate reaching in some cities in the Middle East, South-East Asia and the Western Pacific levels at five to ten times above WHO(World Health Organization) recommended limits [1]. According to an estimation of the WHO air pollution causes seven million

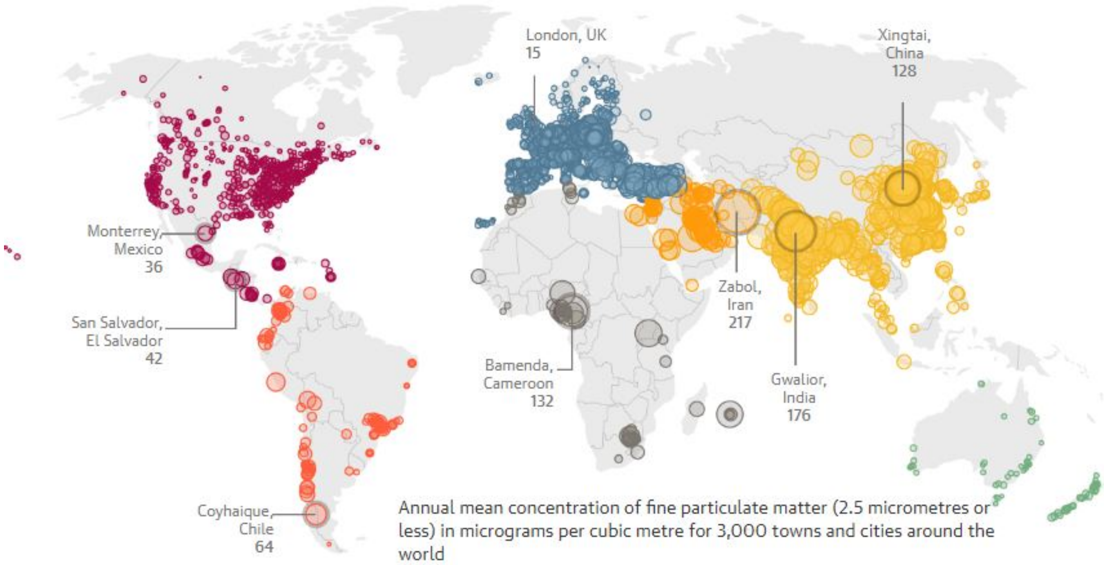

premature deaths a year. So in this scenario becomes incredibily important to exploit all the sources of renewable energy. More over, there are all those problems connected to the increase of the global temperature and of the CO_2 levels. Both of these trends are represented in figure 1.2.

For these reasons among the aims of the *Paris Agreement* there are the goal of limiting global temperature increase to well below two degrees Celsius and the obbligation for the developed countries to build clean, climate-resilient futures.

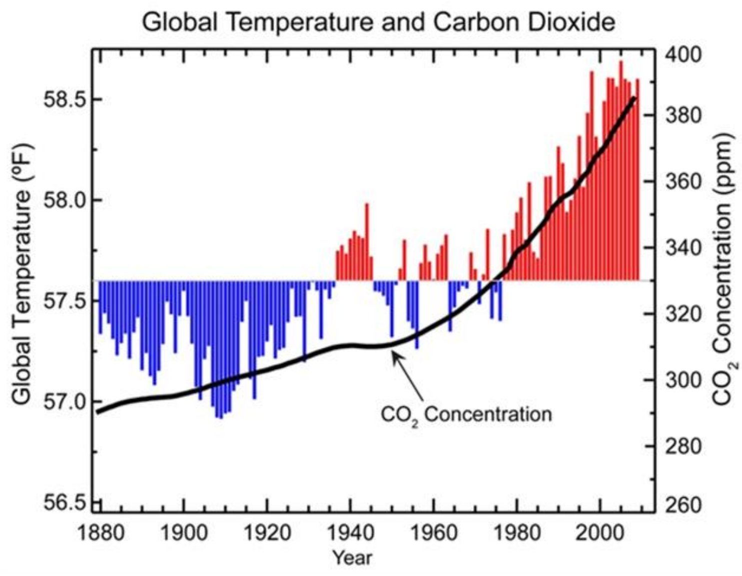

Figure 1.2: Trend of CO_2 level and global temperature

1.2 Wave energy conversion systems

The first attempt to recover energy from the ocean waves dates back to 1799. During the oil crisis of the seventies was done a big effort from the mayor universities in order to develop an efficient system to convert a large amount of energy from the wave power. Today, there are more than 340 different patents divided in these following main groups [2],[3]:

- Attenuator : *is a floating device which operates parallel to the wave direction and effectively rides the waves. These devices capture energy from the relative motion of the two arms as the wave passes them.*

- Point absorber : *is a floating structure which absorbs energy from all directions through its movements at/near the water surface. It converts the motion of the buoyant top relative to the base into electrical power. The power take-off system may take a number of forms, depending on the configuration of displacers/reactors.*

- Oscillating wave surge converter : *extracts energy from wave surges and the move-*

ment of water particles within them. The arm oscillates as a pendulum mounted on a pivoted joint in response to the movement of water in the waves.

- Oscillating water column : *is a partially submerged, hollow structure. It is open to the sea below the water line, enclosing a column of air on top of a column of water. Waves cause the water column to rise and fall, which in turn compresses and decompresses the air column. This trapped air is allowed to flow to and from the atmosphere via a turbine, which usually has the ability to rotate regardless of the direction of the airflow. The rotation of the turbine is used to generate electricity.*

- Overtopping/Terminator device : *captures water as waves break into a storage reservoir. The water is then returned to the sea passing through a conventional low-head turbine which generates power. An overtopping device may use 'collectors' to concentrate the wave energy.*

- Submerged pressure differential : *is typically located near shore and attached to the seabed. The motion of the waves causes the sea level to rise and fall above the device, inducing a pressure differential in the device. The alternating pressure pumps fluid through a system to generate electricity.*

- Bulge wave : *consists of a rubber tube filled with water, moored to the seabed heading into the waves. The water enters through the stern and the passing wave causes pressure variations along the length of the tube, creating a 'bulge'. As the bulge travels through the tube it grows, gathering energy which can be used to drive a standard low-head turbine located at the bow, where the water then returns to the sea.*

- Rotating mass : *two forms of rotation are used to capture energy by the movement of the device heaving and swaying in the waves. This motion drives either an eccentric weight or a gyroscope causes precession. In both cases the movement is* *attached to an electric generator inside the device.*

The purpouse of this master thesis is to design the hull of an inertial ocean wave energy converter (IOWEC) that we can insert in the last one of the categories listed above. The principle of operation and technology are equal to its younger brother ISWEC (Inertial Sea Wave Energy Converter) developed by *Wave for Energy*, a company born in Turin thanks to which this project was realized.

1.2.1 Europe needs ocean energy

The size of the prize for commercializing ocean energy is huge. In Europe alone, the ocean energy industry plans to deploy 100GW of production capacity by 2050, meeting 10% of electricity demand. That's enough to meet the daily electricity needs of 76 million households. Deploying 100GW of ocean energy will also mean creating a new industrial sector based firmly in Europe, and 400,000 skilled jobs all along the supply chain. Today, European companies are the clear global leaders in ocean energy, accounting for 66% of tidal energy patents and 44% of wave energy patents globally. Most projects developed outside Europe, in Canada and South-East Asia, use European technology. This puts our european companies in prime position to capture a global market estimated to be worth € 53 billion annually in 2050. Over the past decade, Ocean Energy Europe members have invested over € 1 billion in research and development activities. These investments have created the base of world leading knowledge and expertise needed to build an industry. In 2016, the world's first tidal power farms hit the water in the UK, Netherlands, and France. Pre-commercial wave energy, OTEC and salinity gradient farms will soon follow across Europe. Farms are also underway in Canada, Japan, Indonesia, Chile, all with EU technology. Industry take-off is underway [4].

1.3 Iswec

The energy production of ISWEC is due to the combination of a pitching movement induced by the waves and the rotation of the flywheel of a gyroscope that is connected through a driveshaft to the power generator (PTO)[5]. This model is schematized in the figure 1.3 [6].

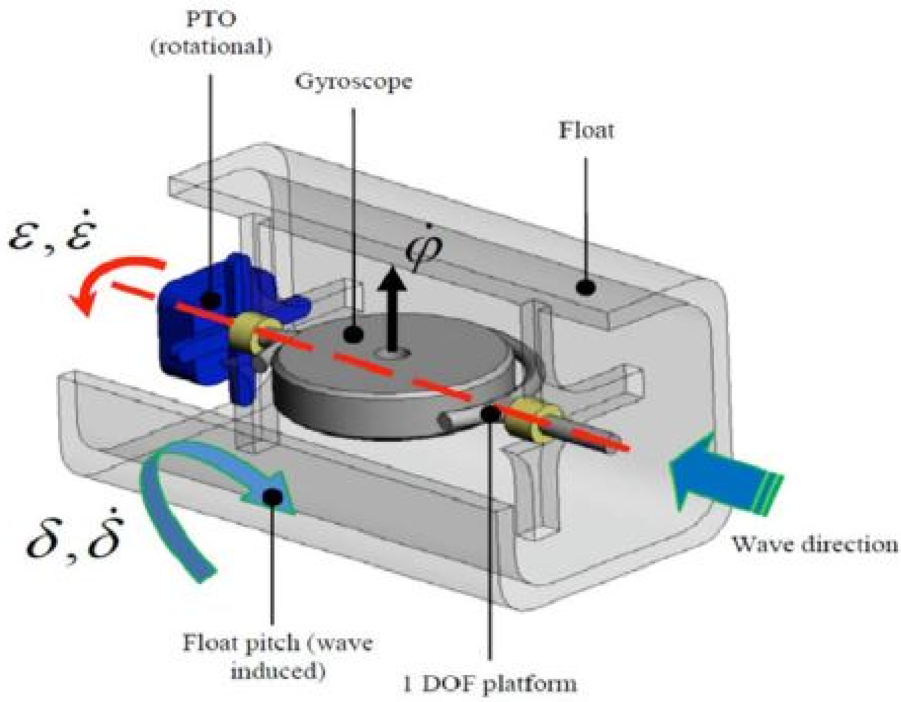

Figure 1.3: Operating scheme of a gyroscopic group in ISWEC

Figure 1.4: Hull of Iswec

The system has overall dimensions of 8 m width, 15 m length and 4.5 m height. Dimensions are designed in proper ways : the length choosed depends on the most common wave length, respecting the relation $L = \lambda/3$ in order to have the best pitch possible while the width must guarantee a certain roller stability and regards the magnitude of the energy production, infact the wave power is mesaured as W/m.

The nominal power of the system is about 100 kW. It has some exclusive characteristics that make it really competitive in the WEC world. First of all, it presents a **sealed hull**. This means firstly an high reliability of the device because all of its components are protected from the marine environment and secondly a reduced enviromental impact. More over it doesn't need for rigid links with the sea bed and so together with a smooth running it doesn't interfere with the marine flora and fauna. Then there is an intelligent **dynamic control** that uses a weather-wave forecasting

Figure 1.5: Iswec operating at a 800 m from the shore of the northwest side of Pantelleria island

algorithm to adapt the flywheel speed to the long-term ocean conditions an the PTO to the next incoming wave. Another point of strength is its **scalability**, it's possible to satisfy several power sizes and it's easy to industrialize.

CHAPTER 2

Installation Site

An extremely important point in the design of a wave energy converter is the localization of the installation site that has to respect some characteristics. First of all, the presence of the WEC must not affect the flora and fauna of the ocean and obviously it has not to occupy areas of maritime traffic both commercial and tourist. Usually are selected a couple of different sites in a certain area and then, after the characterization of the most important wave parameters and a deep study on the occurrency of the waves, a specific site is chosen.

In order to understand the study on the characterization of the sites, some theories about the waves will be introduced.

2.1 Linear wave theory

Linear wave theory is the core theory of ocean surface waves used in ocean and coastal engineering and naval architecture. As a first approach waves are considered in their easiest way, that is **regular gravity waves** on the surface of a fluid, in our case, the surface of water. For gravity waves, gravitation constitutes the restoration force, that is the force that keep the waves going. This applies to waves with wavelengths larger than a few centimeters. For shorter surface waves capillary forces come into action, but this is not the case. The *sine* or *cosine* function defines a regular wave (Figure

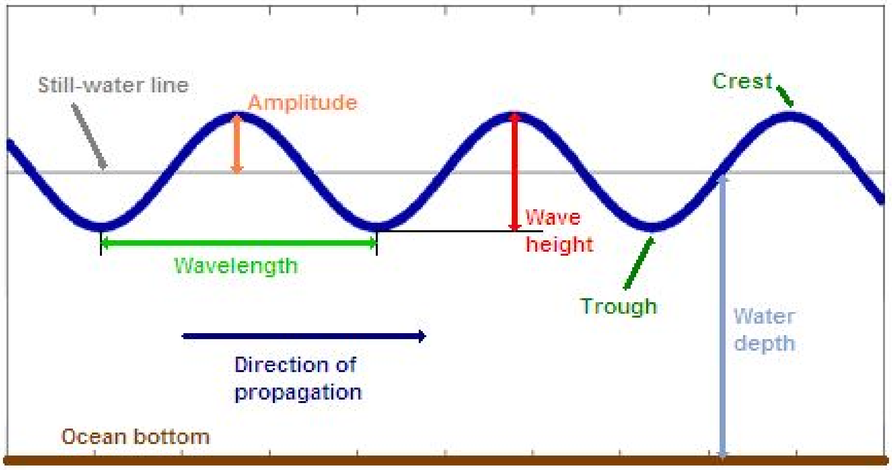

Figure 2.1: Representation of a regular wave

2.1). It is cheracterized by these factors [7]:

- wavelength - λ [m]: distance over which the wave's shape repeats
- period - T [s]: time interval corresponding to the wavelength
- amplitude - a [m]: maximum distance from the mean level

  And secondly there are:

- height - H [m]: displacement of a crest with respect to the previous trough
- phase velocity - c [m/s]: speed with which a wave phase propagates, $c = \dfrac{\lambda}{T}$

So the wave η, function of the time t and of the space x results:

$$\eta(x,t) = asin(\frac{2\Pi}{T}t - \frac{2\Pi}{\lambda}x) \tag{2.1}$$

Where the quantity $2\pi/\lambda$ is called *wavenumber* and is usually denoted by the letter k $[rad/m]$ while the factor $2\pi/T$ normally denoted with ω $[rad/s]$ is called *angular frequency*. These dimensions will be very important in the design of the hull.

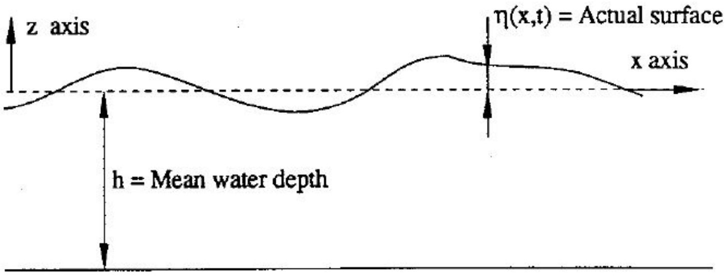

Figure 2.2: Waves in a two-dimensional space

2.1.1 Equations of the surface motion

Deriving the equations to describe the dynamic of the waves on the water surface is rather difficult, so for simplicity let's consider the problem two-dimensional (2.2).

Wave motion is governed by the fluid mechanical laws, as instance all the *conservation laws.* The goal now is to find out how the wavelength and the period of the waves can be expressed in terms of water depth, acceleration of gravity and so on. At any point the water has a certain velocity, defined by the equation 2.2:

$$v(x,z,t) = u\mathbf{i} + w\mathbf{k} \tag{2.2}$$

Where $\mathbf{i}$ and $\mathbf{k}$ are the unit vectors along x-axis and z-axis while u and w represent x- and the z-components of the velocity. Water is very hard to compress, so is possible to assume water to be *incompressible.* It means that the velocity satisfies at each point the equation:

$$\frac{\partial u}{\partial x} + \frac{\partial v}{\partial y} + \frac{\partial w}{\partial z} = 0 \tag{2.3}$$

named *equation of continuity.* Water is considered to be also *irrotational* so the velocity ca be expressed in terms of *velocity potential* ϕ in the following way:

$$u = \frac{\partial \phi}{\partial x} \tag{2.4}$$

$$v = \frac{\partial \phi}{\partial y} \tag{2.5}$$

$$w = \frac{\partial \phi}{\partial z} \tag{2.6}$$

These concepts and the derivation of their equations are treated in many fluid mechanics textbooks, such as [8]. Introducing the velocity potential in the equation of continuity, neglecting the y-term due to the simplified case considered, we obtain:

$$\frac{\partial^2 \phi}{\partial x^2} + \frac{\partial^2 \phi}{\partial z^2} = 0 \tag{2.7}$$

That is a partial differential equation called *Laplace equation*. This equation defines all about the water motion away from the boundaries and the surface. Therefore, to define completely the problem we have to find the *boundary conditions*. The bottom of the considered control volume is not permeable to the water so here the vertical component of the velocity must be zero always:

$$w(x, z = -h, t) = \frac{\partial \phi}{\partial z}(x, z = -h, t) = 0 \tag{2.8}$$

And this is the first boundary condition. At the surface the analysis is a little bit harder. It has been observed that the fluid paricles near the surface remain near the surface during the wave motion as long as the motion is smooth. So one of the boundary conditions at the free surface consists of stating this property in mathematical terms, and it is represented by the following equation:

$$\frac{\partial \eta}{\partial t} + u\frac{\partial \eta}{\partial x} = w \tag{2.9}$$

This is the mathematical formulation of the physical condition that a fluid particle at the surface should remain at the surface at all times. It tells you something about the motion of the surface and is therefore called the *kinematic boundary condition*. The other condition regards the pressure p, infact it must be equal to the atmospheric pressure, supposed to be constant. The equation that represents this fact in mathematical terms is the *Bernoulli's equation*, widely described in several fluid mechanic textbooks, that is for an irrotational fluid:

$$\frac{p}{\rho} + \frac{\partial \phi}{\partial t} + \frac{1}{2}(u^2 + w^2) + gz = C(t) \tag{2.10}$$

The function $C(t)$ can be set to a convinient constant. If we consider $C(t) = \dfrac{p_{atm}}{\rho}$ for the free surface it will be:

$$\frac{\partial \phi}{\partial t} + \frac{1}{2}(u^2 + w^2) + g\eta = 0 \tag{2.11}$$

This condition, dealing with the force on the surface, is usually called the *dynamic boundary condition*. All together, these equations define the mathematical problem that describes the fluid motion of the surface.

$$\begin{cases} \dfrac{\partial^2 \phi}{\partial x^2} + \dfrac{\partial^2 \phi}{\partial z^2} = 0 \\ w(x, z = -h, t) = \dfrac{\partial \phi}{\partial z}(x, z = -h, t) = 0 \\ \dfrac{\partial \eta}{\partial t} + u\dfrac{\partial \eta}{\partial x} = w \\ \dfrac{\partial \phi}{\partial t} + \dfrac{1}{2}(u^2 + w^2) + g\eta = 0 \end{cases} \tag{2.12}$$

2.1.2 The dispersion relation

Recalling the equation 2.1 for a regular wave we have $\eta(x,t) = asin(\omega t - kx)$ where the wavenumber k and the frequency ω are connected by the *dispersion relation* $\omega^2 = gktanh(hk)$. For a given k, there are two solutions Fig.2.3:

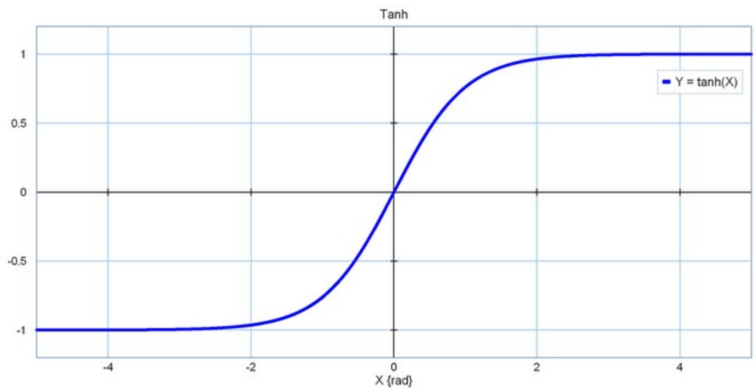

Figure 2.3: The hyperbolic tangent

$$\omega = \pm\sqrt{gktanh(hk)} \tag{2.13}$$

Let us focus on the argument of the hyperbolic tangent, kh. By expressing the wavenumber in funcion of the wavelenght we obtain $kh = \frac{2\pi}{\lambda}h$, recalling that h is the water depth. It is clear that If kh is small, then $h << l$, that is, the water depth is much smaller than the wavelength. This corresponds to *shallow water*. Conversely, if kh is large, this corresponds to *deep water*. Therefore:

- Shallow water: $tanh(kh)$ may be replaced by kh. Thus

$$\omega = \pm k\sqrt{gh} \tag{2.14}$$

- Deep water: $tanh(kh) = 1$ and so

$$\omega = \sqrt{gk} \tag{2.15}$$

There is a zone in which the water is neither shallow nor deep but as a *rule of thumb* is possible to say that:

- Deep water if $h > \frac{\lambda}{2}$
- Shallow water if $h < \frac{\lambda}{20}$

Relation between λ and T

Is possible to derive the relation between the wavelength λ and the wave period T from the equations 2.14 and 2.15. Making the necessary substitutions we find:
Shallow water:

$$\lambda = T\sqrt{gh} \tag{2.16}$$

Deep water:

$$\lambda = \frac{gT^2}{2\Pi} \tag{2.17}$$

From the last expressions is clear that period and wavelength are strickly connected and this means that is very important to find an installation site with an appropriate depth in order to exploit as much as possible the longest and most energetic waves.

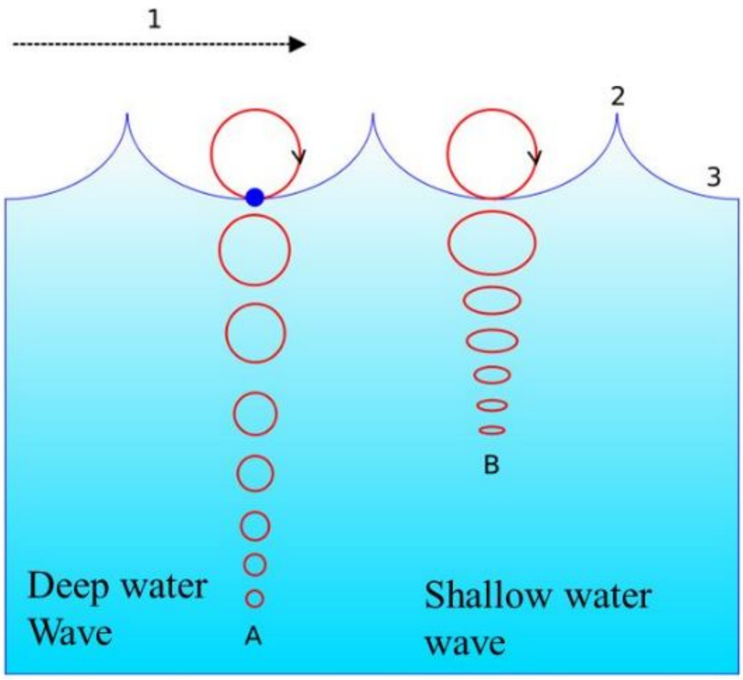

Figure 2.4: Particle trajectories associated with linear waves

The water depth affects not only the wavelength but also the shape of the trajectory traced by the particles during the wave motion. The reader may refer to [9] for the complete treatment of the phenomenon. As is possible to see in Figure 2.4, for the shallow water the trajectory is elliptic. This is due to the fact that the wave "feels" the bottom and so its shape is consequently modified.

2.2 Irregular wave theory

The waves treated until now were regular, useful to understand the basical concepts but too ideal for a real case. Infact, if we watch the sea in a windy day, the waves are far from being regular. The only waves that can be almost regular are the *swell* ones generated by a distant storm. Nevertheless, we can consider the irregular wave theory as the regular wave theory described in the previous part put in a probabilistic setting. The most important tool necessary in case of random waves is the *wave spectrum*. It gives all the important properties about the waves and defines the **sea state**.

2.2.1 Irregular waves

In the open ocean is impossible to distinguish each individual wave, due to the fact that the sea surface is a set of many regular waves [10]. So using the superposition principle (Fig. 2.5), is possible to find a first definition for the random model:

$$\eta(x,t) = \sum_{n=1}^{N} a_n sin(\omega_n t - k_n x + \phi_n) \tag{2.18}$$

This is only the starting point. To arrive at the final form all statistical variables must be calculated, like the variance or the standard deviation. The whole explication can be found in [12]. All these datas allow to produce the wave spectrum. There are many different types of spectra, for the simulations in this thesis was used the *JONSWAP spectrum* with a γ equal to 3.3.

Short term statistics

Under normal conditions the wave spectrum and hence the sea state is likely to be constant over, say, half an hour. The properties of the sea for a constant sea state is covered by what is denoted short term wave statistics. Short term wave statistics deals with the properties of the individual waves, typically the probability distributions of wavelength, period, height and so on (Fig. 2.6). The data can be recorded by a buoy or a similar device.

Long term statistics

For time periods longer than a few hours, the sea state is likely to vary. Variations in the sea states are covered by a random theory and described by long term wave statistics. This deals with the statistical properties of wave parameters like significant wave height, peak period etc. Recall that within short term wave statistics, these parameters were considered to be constant. This is therefore a change in viewpoint:

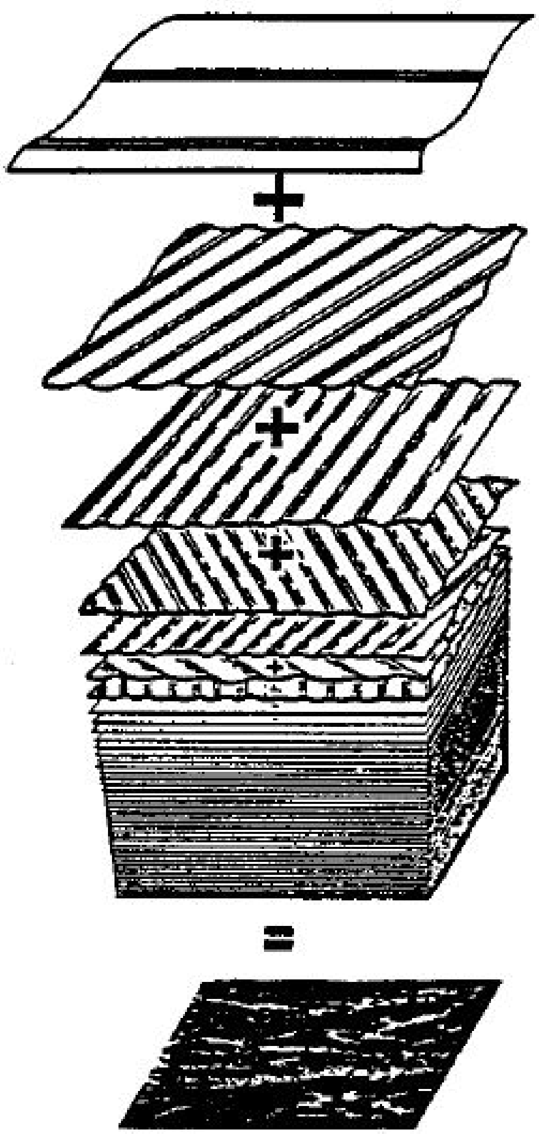

Figure 2.5: Superposition of regular waves

We are considering the properties of the sea with respect to long term variations, i.e. seasonal or yearly variations. To do it are used occurrence tables and scatter plots. In the next chapters will be possible to watch the ones relative to the installation site.

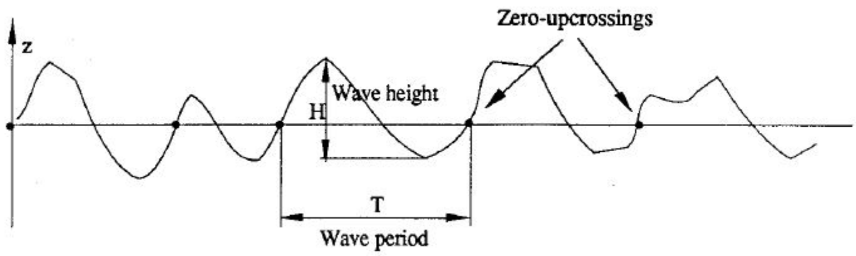

Figure 2.6: Example of wave record in short term statistic

Extreme wave statistics

For coastal and ocean engineering, it is very important to know how rough conditions the structures are likely to encounter during their lifetime, and this part of the long term statistics is treated by extreme wave statistics. Extreme wave statistics provides methods to estimate how rough conditions are likely to happen at a given location over a time span of, say 100 years.

2.3 Study of the sites

For the installation of IOWEC are been proposed two places: Easter island, a Chilean island in the southeastern Pacific Ocean, at the most southeastern point of the Polynesian Triangle in Oceania and the Robinson Crusoe island, the second largest of the Juan Fernández Islands, situated 670 km west of San Antonio, Chile, in the South Pacific Ocean. The *Wave for Energy* team decided for the second one, Robinson Crusoe island. The study is very detailed and nothing is left to chance but here below will be described only the most important ocean features that regard the design of the hull.

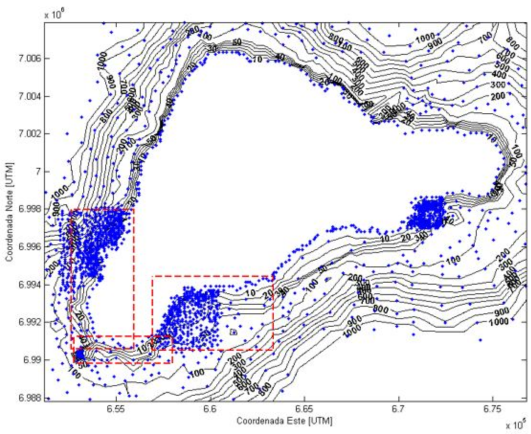

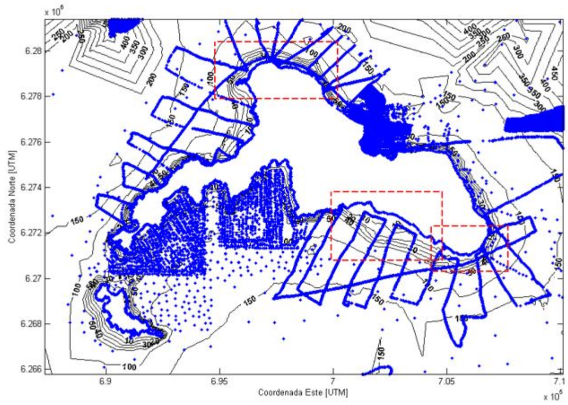

Figure 2.7: Bathymetric maps of Easter island and Robinson Crusoe island

2.3.1 Power density

Each wave has a certain amount of energy. In case of deep water the wave energy flux per unit of wave-crest length is

$$P = \frac{\rho g^2}{64\pi} H_{m0}^2 T \tag{2.19}$$

Where H_{m0} (or H_s) is the significant wave height (Fig. 2.8), defined as as the mean wave height (trough to crest) of the highest third of the waves ($H_{1/3}$). Nowadays it is usually defined as four times the standard deviation of the surface elevation – or equivalently as four times the square root of the zeroth-order moment (area) of the wave spectrum.

Around the Robinson Crusoe island are been selected five different points, as is possible to see in Figure 2.9. All these points have a mean power density about $40kW/m$ and everyone respct the conditions described at the beginning of this chapter but only one is situated with a sufficient distance from the shore and consequently with an appropriate depth in order to exploit the *deep water* condition even with the longest waves. It is the point number **three**.

Looking at the wave height map (Fig. 2.10) we can observe as the third point is the best one for this feature as well.

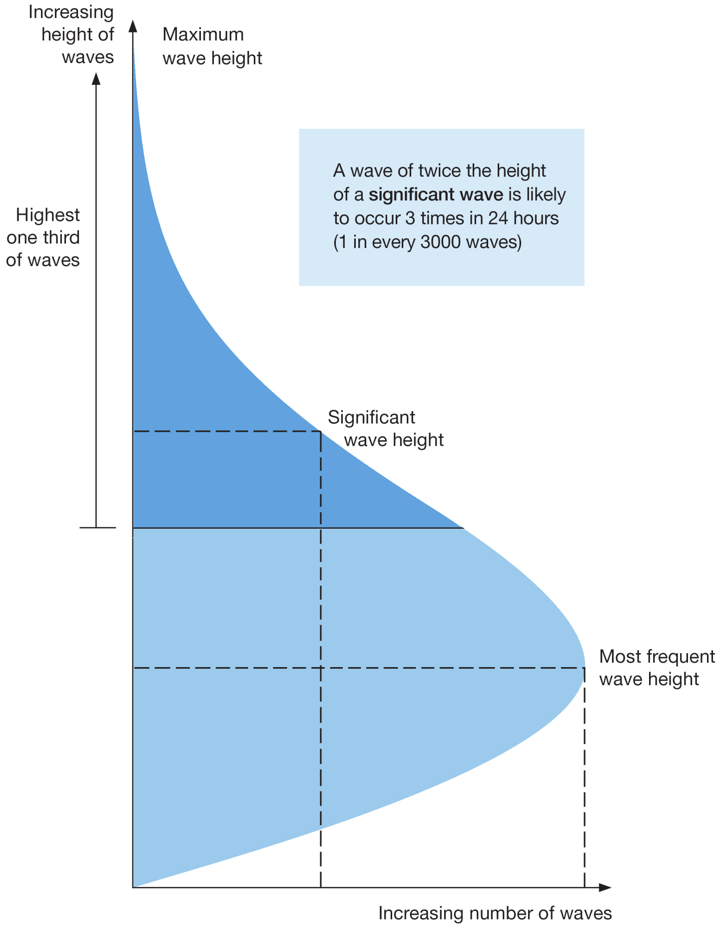

Figure 2.8: Statistical distribution of ocean wave heights

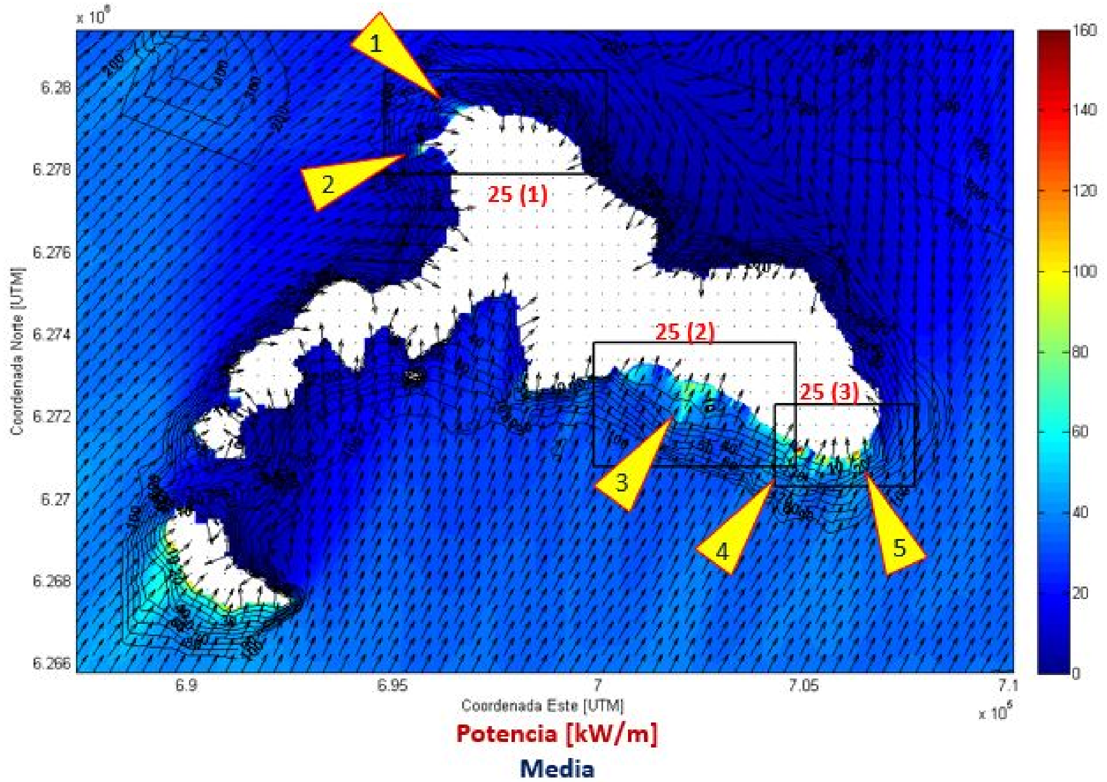

Figure 2.9: Power density map of Robinson Crusoe island

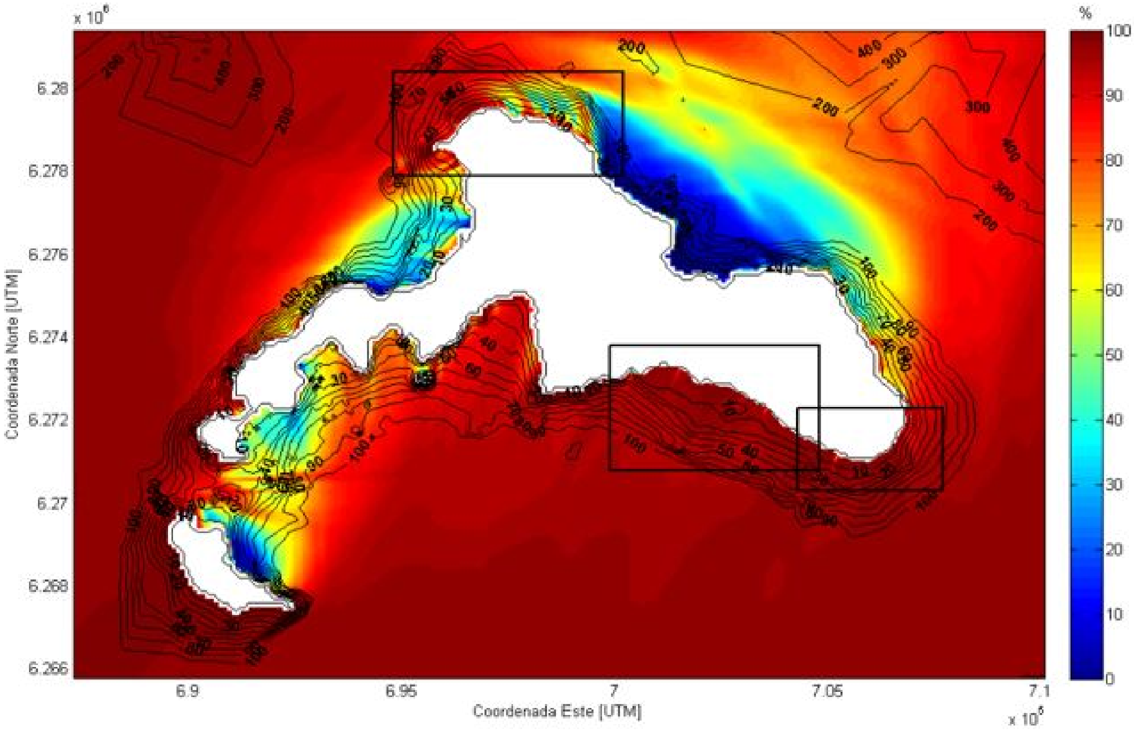

Figure 2.10: Percentage of time in which the wave height is higher than 1 meter

2.3.2 Wave period

As described in the section about the *Linear Wave Theory* the wave period is the the time required for two successive wave crests to pass a fixed point, or the time for a single wave crest to travel a distance equal to the length of the wave. Looking at the equation 2.19 we note that power is proportional to the period too. Therefore waves with a longer period lead to an higher energy amount that is possible to extract.

In the Figure 2.11 the mean wave period is graphically represented. It settles around $11s$.

Zoom of the site number three

Below are reported the magnifications of the previous images regarding the point three.

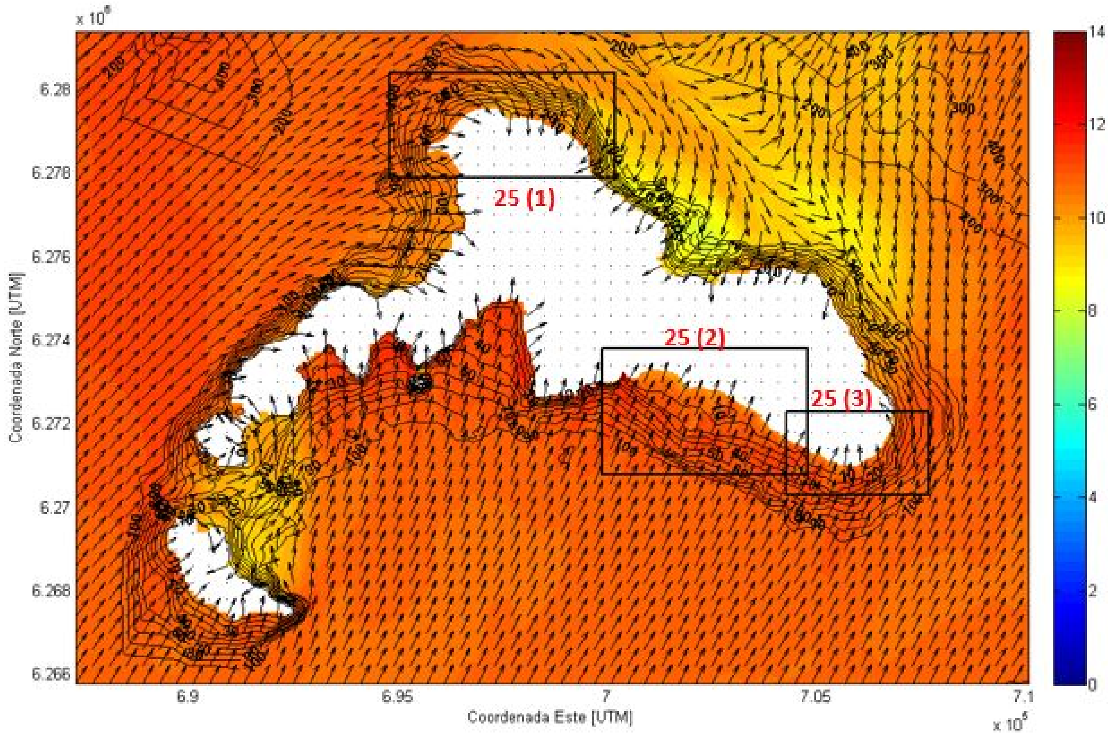

Figure 2.11: Wave period map

Scatter of waves - site N3

Here in Table 2.1 is reported the percentage of the occurrences for each wave in a year. Is possible to observe that the most frequent and the most energetic waves have a period from 10 to 12 seconds.

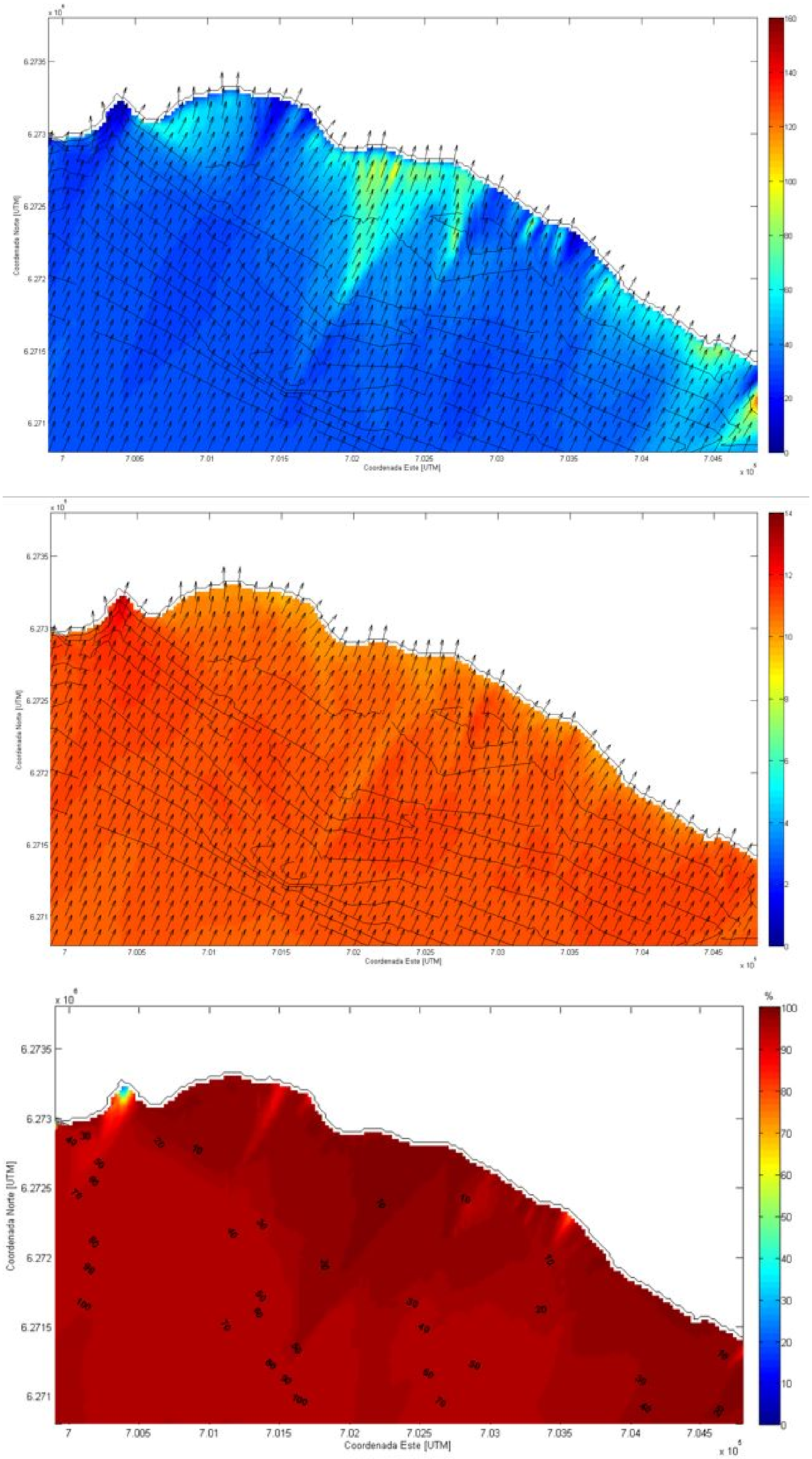

Figure 2.12: Magnifications of the site 3

		Periodo energético [s]															
		4 a 5	5 a 6	6 a 7	7 a 8	8 a 9	9 a 10	10 a 11	11 a 12	12 a 13	13 a 14	14 a 15	15 a 16	16 a 17	17 a 18	% Rel	% Acum
Altura significativa [m]	0 a 0,5	–	–	–	–	–	–	–	0,00	–	–	–	–	–	–	0,00	0,00
	0,5 a 1	–	0,00	0,00	0,04	0,30	0,49	0,33	0,10	0,02	0,00	–	–	–	–	1,28	1,28
	1 a 1,5	–	–	0,02	0,47	1,68	2,67	2,59	1,35	0,48	0,09	0,02	–	–	–	9,37	10,65
	1,5 a 2	–	–	0,01	0,67	2,12	4,63	5,38	3,65	1,59	0,37	0,09	0,01	–	–	18,52	29,17
	2 a 2,5	–	–	0,00	0,47	2,31	4,63	6,34	5,70	2,67	0,86	0,20	0,04	–	–	23,22	52,39
	2,5 a 3	–	–	–	0,14	1,48	2,95	4,74	5,18	3,26	1,23	0,36	0,04	0,00	–	19,38	71,77
	3 a 3,5	–	–	–	0,02	0,53	1,32	2,57	3,78	3,29	1,40	0,28	0,07	0,00	–	13,26	85,03
	3,5 a 4	–	–	–	–	0,13	0,54	1,05	1,94	2,24	1,40	0,45	0,08	0,00	–	7,83	92,86
	4 a 4,5	–	–	–	–	0,01	0,18	0,40	0,90	1,22	0,86	0,34	0,06	0,01	–	3,98	96,84
	4,5 a 5	–	–	–	–	0,00	0,05	0,22	0,41	0,44	0,49	0,21	0,05	0,01	–	1,88	98,72
	5 a 5,5	–	–	–	–	–	0,00	0,06	0,12	0,20	0,22	0,11	0,02	0,01	–	0,74	99,46
	5,5 a 6	–	–	–	–	–	0,00	0,04	0,04	0,07	0,07	0,06	0,01	–	–	0,29	99,75
	6 a 6,5	–	–	–	–	–	–	0,01	0,02	0,03	0,04	0,02	0,01	–	–	0,13	99,88
	6,5 a 7	–	–	–	–	–	–	0,00	0,02	0,01	0,02	0,02	0,00	–	–	0,07	99,95
	7 a 7,5	–	–	–	–	–	–	0,00	0,00	0,01	0,01	0,00	0,00	–	–	0,02	99,97
	7,5 a 8	–	–	–	–	–	–	0,01	–	0,01	–	0,00	–	–	–	0,02	99,99
	8 a 8,5	–	–	–	–	–	–	0,00	–	0,00	–	–	–	–	–	0,00	99,99
	8,5 a 9	–	–	–	–	–	–	–	–	–	–	–	–	–	–	0,00	99,99
	Mayor a 9	–	–	–	–	–	–	–	–	0,00	–	–	0,00	–	–	0,00	100,0
	% Rel	0,00	0,00	0,03	1,81	8,56	17,46	23,74	23,21	15,54	7,06	2,16	0,39	0,03	0,00		
	% Acum	0,00	0,00	0,03	1,84	10,40	27,86	51,60	74,81	90,35	97,41	99,57	99,96	100,0	100,0		

Table 2.1: Spectrum of site N3

CHAPTER 3

Design of the Hull

In this chapter will be described the structural design phase of the IOWEC hull. The concepts previously described are the theoretical foundations used to develop this project.

3.1 Pre-Project conditions

The installation site, as described in the previous chapter, is the third one (N3) of the *Robinson Crusoe* island. In the Table 3.1 are summarized the main characteristics of the most recurrent wave and of the most energetic one [11].

Here are reported some graphics about the recurrences and the energy of the site N3 (Figure 3.1):

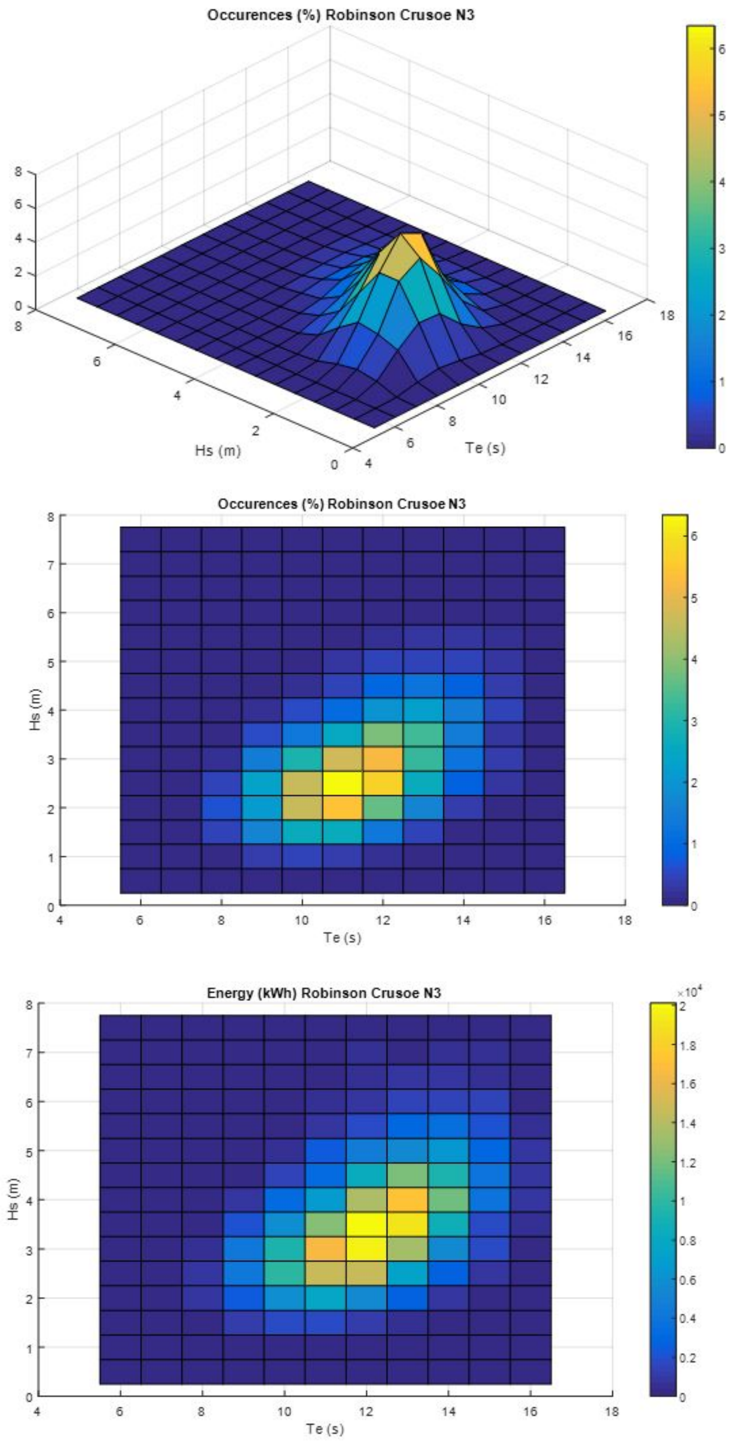

Figure 3.1: Scatter plots of the site N3

Site Data: Most recurrent wave
wave height [m]: 2,25
wave period [s]: 10,5
wave lenght [m]: 172
wave steepness max [deg]: 2,4
power density [kW/m]: 50,9
Site Data: Most energetic wave
wave height [m]: 3,25
wave period [s]: 11,5
wave lenght [m]: 206
wave steepness max [deg]: 2,8
power density [kW/m]: 116,3

Table 3.1: Wave characteristics of the site N3

3.2 First design attempt

The starting point of this thesis is the hull studied in [14]. This first step involves some hypothesis:

- Hull length = wavelength/3 to maximize the pitch
- Hull width = 25 m in order to produce 1 MW of nominal power
- Hull height = 18 m
- Draft percentage = 68%. Therefore displacement and total mass are defined due to the Archimede law 3.1

$$\rho\nabla = m \tag{3.1}$$

Where:

- ρ = water density $[Kg/m^3]$

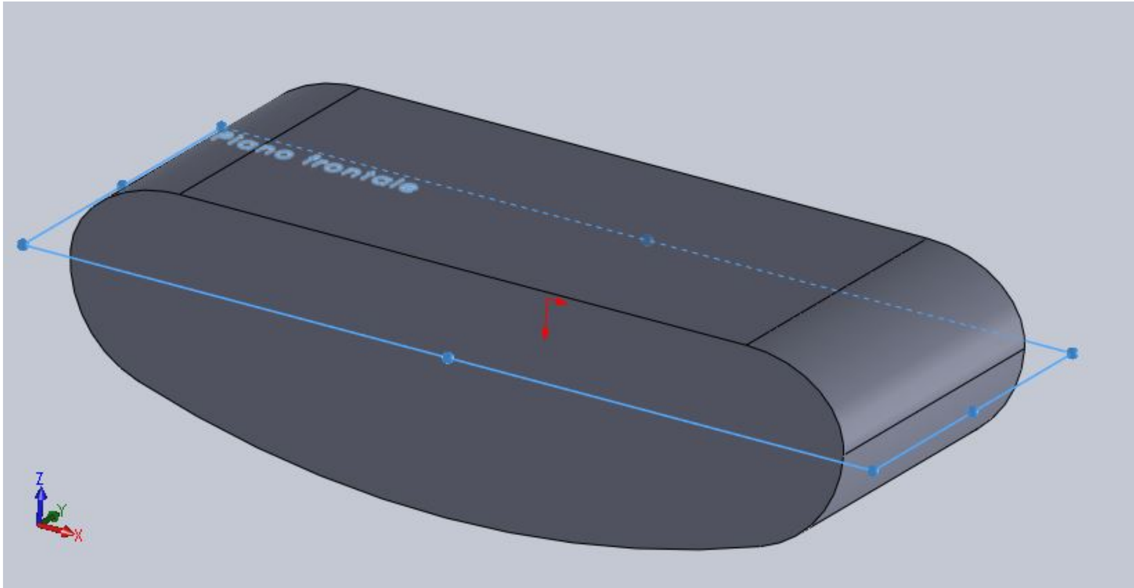

Figure 3.2: First hull and its water plane

- ∇ = displacement $[m^3]$
- m = total mass of the device $[Kg]$

Now for the design is possible to follow two strategies: tuning the resonance period of the hull with the *most recurrent wave* or with the *most energetic wave*. Both the strategies will be analyzed and the results will be compared. To understand the structural cheanges done to achieve these goals we have to study the motion and the mathematical model of the system.

3.2.1 Floating structure

The inertial ocean wave energy converter is a floating body and consequently has six degrees of freedom, as is shown in the Figure 3.3. Where, considering the reference frame fixed at the center of gravity:

- 1 - Heave
- 2 - Sway

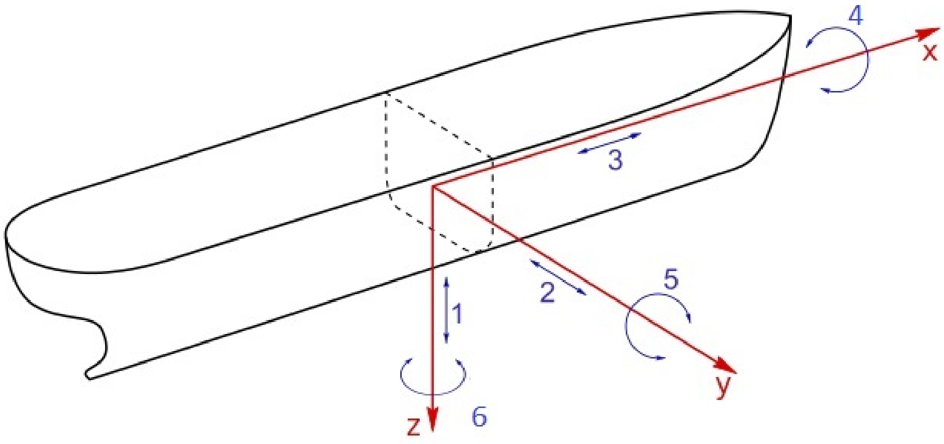

Figure 3.3: Scheme of the reference frame of the system

- 3 - Surge
- 4 - Roll
- 5 - Pitch
- 6 - Yaw

This is the **body-bound** reference frame and it is used to define the mathematical model of the system. It is a second-order system and takes into the interation among the masses, the intertias and the external forces. To have a better understanding of the last ones is possible to look at [20]. The system is considered at a *zero forward speed*, it means that the body is moored but the forces generated by the mooring tool are not considered yet. Below is reported the equation of motion, exhaustively described in [13].

$$\sum_{j=1}^{6}[(m_{i,j}+a_{i,j}(\omega_e))\cdot\ddot{x}_j(\omega_e,t)+b_{i,j}(\omega_e)\cdot\dot{x}_j(\omega_e,t)+c_{i,j}\cdot x_j(\omega_e,t)] = F_{\omega a_i}(\omega_e)\cdot cos(\omega_e t+\varepsilon_i(\omega_e)) \tag{3.2}$$

Where:

$$m = \begin{bmatrix} \rho\nabla & 0 & 0 & 0 & 0 & 0 \\ 0 & \rho\nabla & 0 & 0 & 0 & 0 \\ 0 & 0 & \rho\nabla & 0 & 0 & 0 \\ 0 & 0 & 0 & I_{44} & 0 & -I_{46} \\ 0 & 0 & 0 & 0 & I_{55} & 0 \\ 0 & 0 & 0 & -I_{64} & 0 & I_{66} \end{bmatrix} \tag{3.3}$$

$$a = \frac{c - \frac{F_a}{z_a} cos\varepsilon F_z}{\omega^2} - m \tag{3.4}$$

a is the *added mass*, that is the inertia added to a system because an accelerating or decelerating body must move (or deflect) some volume of surrounding fluid as it moves through it [15]. Added mass is a common issue because the object and surrounding fluid cannot occupy the same physical space simultaneously.

$$b = \frac{\frac{F_a}{z_a} sin\varepsilon F_z}{\omega} \tag{3.5}$$

$$c = \rho g A_w \tag{3.6}$$

Now, similarly at a mass-spring system, we divide the equation 3.2 by the mass and we find the angular fraquency of the system. Therefore is possible to evaluate the changes to do in order to tune it with the frequency (and hence with the period) of the most occurrent or the most energetic wave. So:

$$\omega^2 = \frac{c}{m+a} = \frac{\rho g A_w}{m+a} \tag{3.7}$$

from 3.7 is clear what can be modified to regulate the frequency of the system: mass and spring coefficient.

Response Amplitude Operator

The instrument used to evaluate the performance of each hull is the response amplitude operator (RAO). It is the ratio between the motion of the component and the amplitude of the wave. There is a RAO for each DOF but the most important for us is the one relative to the pitch (RAO 55). It is defined in this way: $\frac{\theta_{55}}{a}$ $[°/m]$ (note that "a" is the amplitude of tha wave, see eq. 2.1).

3.3 The hulls

Below are reported the different hulls realized. At the end of the chapter are reported the results of the simulations for each hull.

3.3.1 V1

The first step was to increase the ballast mass on the sides of the hull in order to increase the inertia of the system. In Figure 3.4 are represented the hull with the ballasts(Red) and the gyroscope groups(green). The number of gyroscopes is kept constant. All the studies about them can be found in [14]. The shape is a little bit different with respect to the first attempt (Fig. 3.2). Obviously the draft percentage is kept constant, so the same quantity of mass added at the external sides was removed from the internal ones. The sketch in which are represented the dimensions is the drawing of the *water plane area*. It is very important for the frequency of the system, infact as is shown in the equation 3.6, we can modify the spring coefficient by changing the area of the waterplane. This concept is quite important in naval engineering and it is represented by its *coefficient of fineness*.

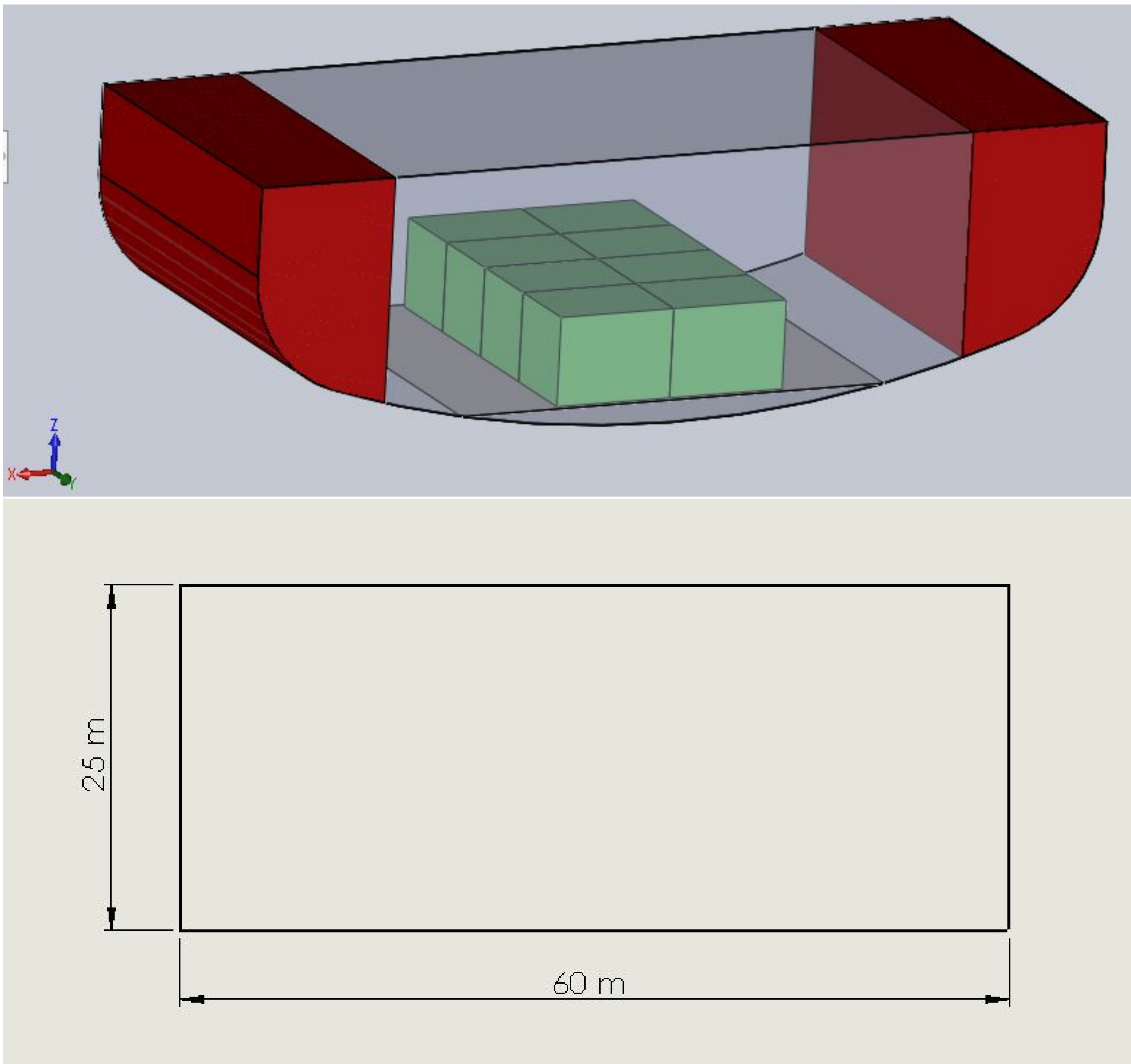

Figure 3.4: IOWEC Hull: version 1

Coefficients of Fineness

A table of offsets, although accurately defining the hull shape, does not provide an immediate feel of the main characteristics of that shape. There are some "coefficients" which can be obtained for the underwater hull which provide clues as to its general nature and its likely behaviour. They are derived by relating certain areas and volumes to their circumscribing rectangles or prisms. These coefficients are known as the coefficients of fineness. Looking at the Figure 3.5 :

- **V** = volume of displacement

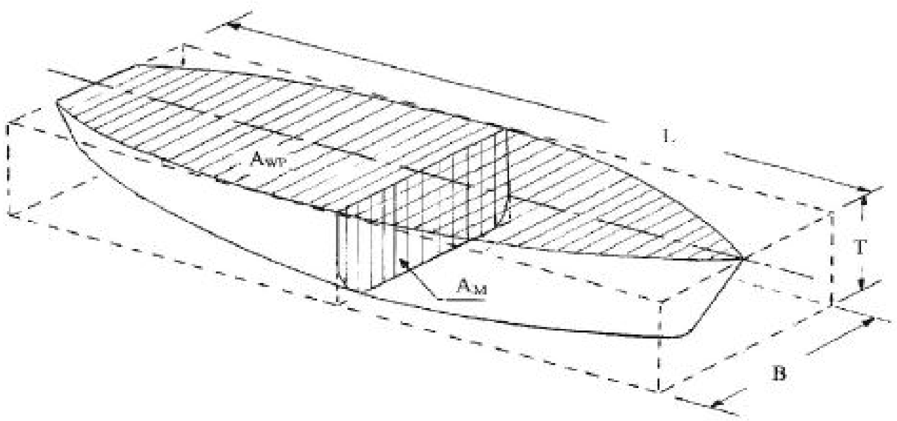

Figure 3.5: Represetation of the most important fineness coefficients

- A_{WP} = waterplane area
- A_M = underwater area of the midship section
- **L, B, T** = length, beam, draught

Considering these magnitudes, is possible to define the fineness coefficients:

- $C_B = \dfrac{V}{LBT}$ - block coefficient
- $C_{WP} = \dfrac{A_{WP}}{LB}$ - waterplane coefficient
- $C_M = \dfrac{A_M}{BT}$ - midship area coefficient
- $C_{VP} = \dfrac{V}{A_{WP}T}$ - vertical prismatic coefficient

3.3.2 V2

As announced in the previous section, the next modification regards the waterplane area. We reduced it by the 10% ; therefore the waterplane coefficiente will be equal to 0,9. The hull changes in this way (Fig. 3.6): Reducing the waterplane also the volume and mass are reduced and consequently the ballast mass is adjusted.

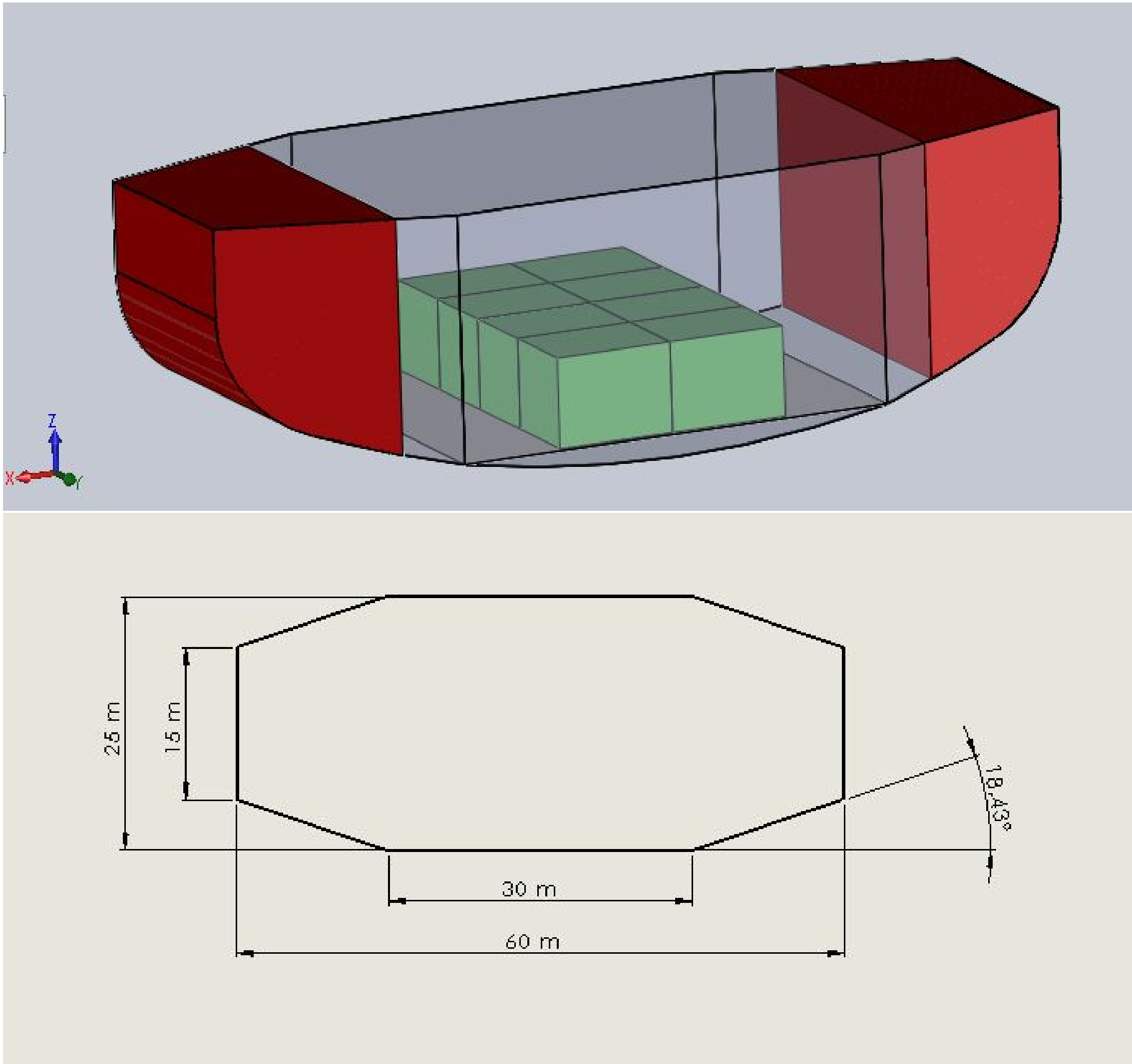

Figure 3.6: IOWEC hull: version 2

3.3.3 V3

In order to find a trend, in the third version the waterplane was reduced by 10% more, for a total with respect to the V1 of 20% . As previously said, reducing the waterplane means decreasing the mass as well. So, looking at the equation 3.7, is clear the these two things have an opposite effect on the frequency of the system. Therefore the version 3 was created in order to evaluate how the system responds (Fig. 3.7).

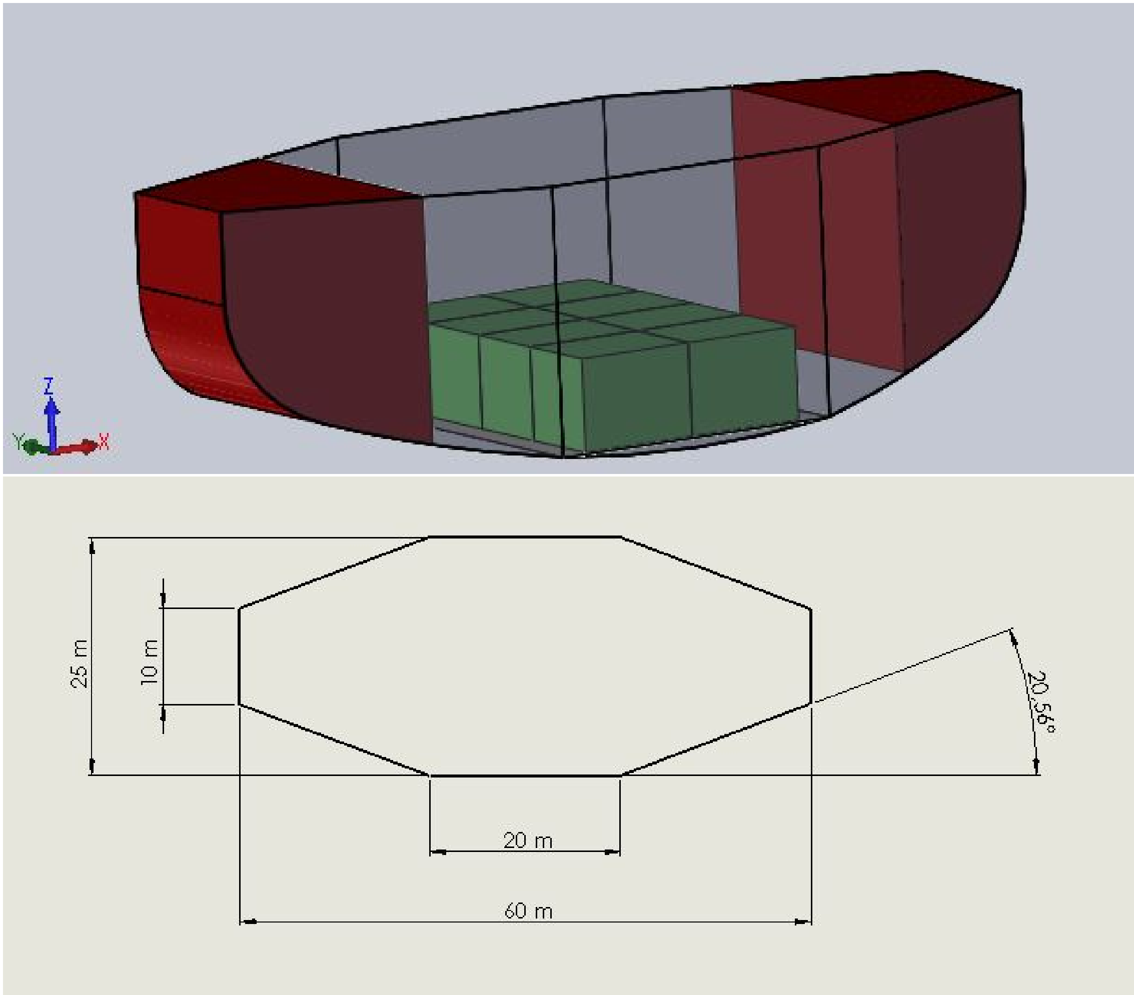

Figure 3.7: IOWEC hull: version 3

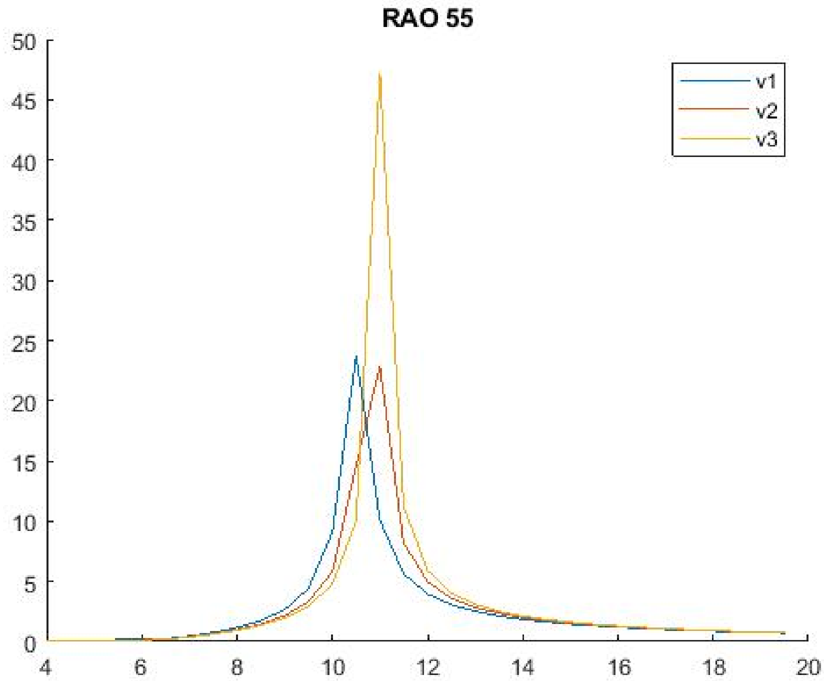

Figure 3.8: RAO of the hulls V1, V2, V3

	V2/V1	V3/V1
Mass	6,81%	17,29%
K55	22,60%	39,68%

Table 3.2: Percentages of reduction with respect to V1

3.4 Comparison of the hulls

The first tool to compare the hulls is the RAO, previously described. In the Figure 3.8 we can see the curves: From this plot, we note immediately two things. Firstly, the peak of resonance of the versions V2 and V3 is "more to the right" and it means that they exploit longer and more energetic waves. Secondly, the hull V3 has an amplitude remarkably high but it's probably a "too theoretical" result. To deduce it, we can look at the trend of the *added mass* (Fig. 3.9) and to the variations regarding the masses and stiffness of the hulls (Tab 3.2).

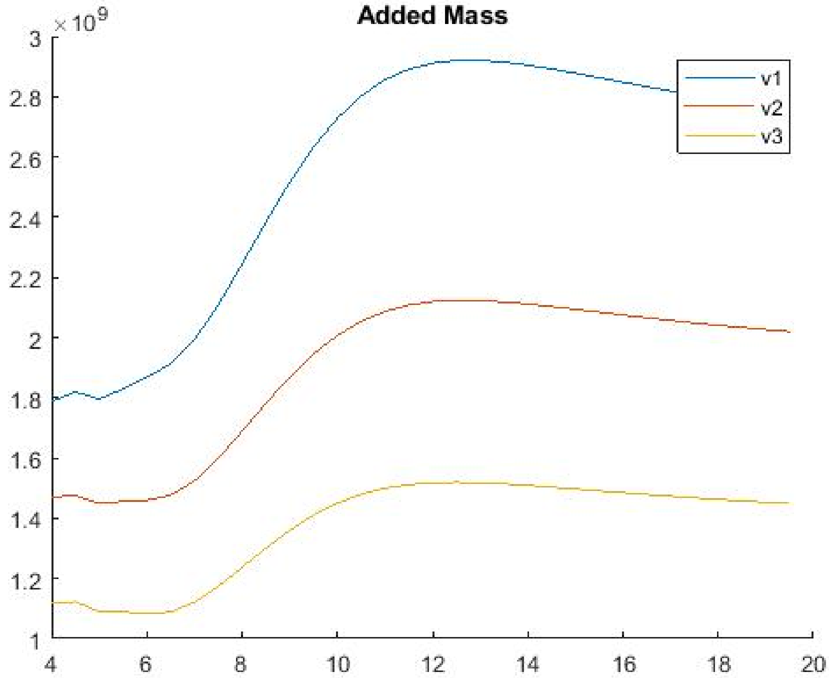

Figure 3.9: Trend of the added masses

Looking at the Table 3.2 is immediate to see that comparing the version V3 with the first one the stiffness decrease much more with respect to the mass and so, recalling the equation 3.7 the high peak in the RAO is justified. Also the added mass follows a similar trend. The hulls must be compared also with a lot of others characteristics. They are listed in the Table 3.3 . Considering the *metacetric heights* (GMX) the V3 presents a problem, because this magnitude is too small. It leads to the *roll instability*. This issue will be analyzed later on.

The considerations made until now concern only the amplitude of the pitching movement of the hulls in regular waves with a fixed amplitude equal to one meter. The most important magnitude to be considered is the annual energy production evaluated with the design wave and with the whole wave scatter of the site chosen.

	V1	V2	V3
Mass[Kg]	1,52E+07	1,42E+07	1,26E+07
COG[m]	-1,37	-1,66	-1,95
LPV	12	12	12
COB[m]	-5,16	-5,26	-5,34
WP_area[m^2]	1500	1350	1200
CWP	1	0,90	0,80
BG[m]	3,79	3,60	3,39
GMX[m]	1,54	0,83	0,42
GMY[m]	26,93	22,43	19,22
BMX[m]	5,33	4,43	3,81
BMY[m]	30,72	26,03	22,62
MX[Nm/°]	3,97E+06	1,98E+06	9,05E+05
MY[Nm/°]	6,92E+07	5,36E+07	4,17E+07
K55[Nm/°]	3,97E+09	3,07E+09	2,39E+09
K44[Nm/°]	2,27E+08	1,13E+08	5,18E+07

Table 3.3: Hydrostatic datas

3.5 Productivity

The matlab code [16] used to compute the annual productivity optimizes some parameters of the entire system like the flywheel speed, PTO damping coefficient and so on to maximize the productivity (Tab. 3.4). The mathematical model contains the equations: 3.2, (4.12 only when the Prtt is present) and finally the equation relative to the gyroscope 3.8.

$$I\ddot{\varepsilon} + c\dot{\varepsilon} + k\varepsilon = J\dot{\varphi}\dot{\delta} \tag{3.8}$$

Therefore the final model used is:

$$[(M + A)(\omega)]\ddot{X_{sys}} + [B(\omega)]\dot{X_{sys}} + [K(\omega)]X_{sys} = F_w(j\omega) \tag{3.9}$$

where:

$$X_{sys} = \begin{bmatrix} x \\ z \\ \delta \\ \varepsilon \\ \tau \end{bmatrix} \tag{3.10}$$

$$[M + A] = \begin{bmatrix} (M_{11} + A_{11}) & 0 & (M_{15} + A_{15}) & 0 & 0 \\ 0 & (M_{33} + A_{33}) & 0 & 0 & 0 \\ (M_{51} + A_{51}) & 0 & (M_{55} + A_{55}) & 0 & a_{5\tau} \\ 0 & 0 & 0 & I_{gyro} & 0 \\ 0 & 0 & a_{\tau 5} & 0 & a_{\tau\tau} \end{bmatrix} \tag{3.11}$$

$$[B] = \begin{bmatrix} B_{11} & 0 & B_{15} & 0 & 0 \\ 0 & 0 & 0 & 0 & 0 \\ B_{51} & 0 & B_{55} & -J\dot{\varphi} & b_{5\tau} \\ 0 & 0 & J\dot{\varphi} & c_{gyro} & 0 \\ 0 & 0 & b_{\tau 5} & 0 & b_{\tau\tau} \end{bmatrix} \tag{3.12}$$

$$[K] = \begin{bmatrix} K_{11} & 0 & K_{15} & 0 & 0 \\ 0 & K_{33} & 0 & 0 & 0 \\ K_{51} & 0 & K_{55} & 0 & c_{\tau 5} \\ 0 & 0 & 0 & K_{gyro} & 0 \\ 0 & 0 & c_{5\tau} & 0 & c_{\tau\tau} \end{bmatrix} \tag{3.13}$$

Note that, the terms $a_{\tau\tau}; b_{\tau\tau}; c_{\tau\tau}$ are equal to zero in this part due to the fact that the "pitch resonance tuning tank" are not installed yet. They will appear in the chapter 4.

These parameters are set up considering the design wave, that is the most energetic among the most recurrent. It has a period of 11,5 seconds and an height of 3,25 meters. Then the system is simulated with the whole spectrum of irregular waves of the site in order to obtain the parameters "weighed" on the scatter, so in this way comparing the weighed results with the optimal ones is possible to verify the avarage behaviour (Tab. 3.5).

Recalling the Figure 1.3 is possible to understand the meaning of the angles δ, ε and of the speed φ. These operational parameters are very important in order to evaluate the efficency of the machine. Infact, looking at them in the two tables is possible to observe that δ and ε are higher in the V2 than the other two either with the design wave or with the whole annual scatter of the waves. It leads to the higher energy production.

Design wave results	V1	V2	V3
Phid [rpm]	302,7	260,8	220,8
c [Nms/rad]	463519	498432	412715
Tot_Power_Net [kW]	502	553	474
Tot_Power_Gross [kW]	668	679	572
Tot_Power_Lost [kW]	166	126	98
δ_Max [deg]	10,6	13,0	12,9
δ_Rms [deg]	3,2	4,0	4,0
ε_Max [deg]	114,3	114,1	113,9
ε_Rms [deg]	35,0	34,5	35,3
T_PTO_Max [Nm]	25695	27534	22596
T_PTO_Rms [Nm]	8032	8399	7013
Vel_Max [rpm]	214	208	211
Vel_Rms [rpm]	66,2	64,4	64,9
Annual Net Productivity [MWh/y]	2508	2647	2127
Annual Gross Productivity [MWh/y]	3322	3262	2603
Te [s]	11,5	11,5	11,5
Hs [m]	3,25	3,25	3,25

Table 3.4: Productivity and main parameters for the design wave

Weighted results	V1	V2	V3
Phid [rpm]	213	175	151
c [Nms/rad]	290817	283778	245760
ε_Rms [deg]	31,0	32,1	30,9
ε_Max [deg]	102,5	102,6	98,9
δ_Rms [deg]	2,5	3,0	3,0
δ_Max [deg]	8,4	9,9	9,7
T_PTO_Rms [Nm]	4719	4610	3811
T_PTO_Max [Nm]	15903	15247	12617
Vel_Rms [rpm]	60,3	61,4	58,4
Vel_Max [rpm]	200,5	196,8	187,2
Annual Gross Productivity [MWh/y]	3322	3262	2603
Annual Net Productivity [MWh/y]	2509	2647	2127

Table 3.5: Productivity and main parameters weighed on the scatter

Graphical representation of the energy production

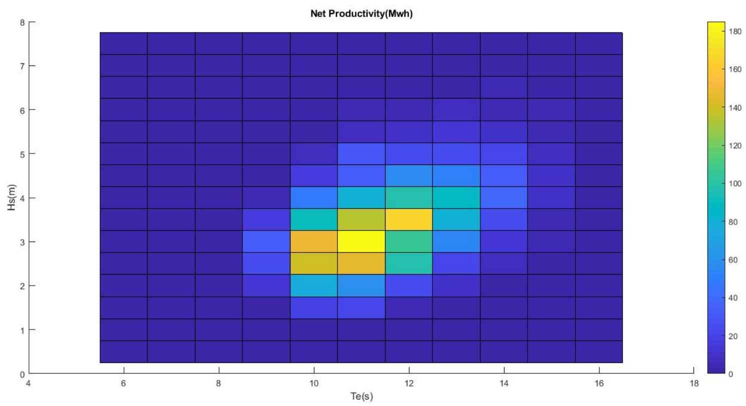

Figure 3.10: Energy production scatter - V1

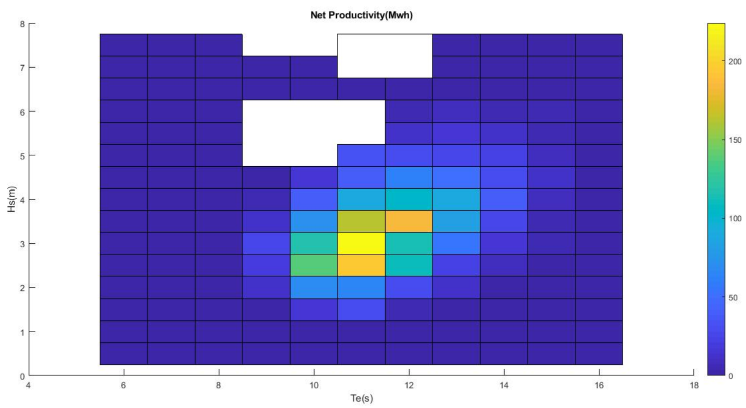

Figure 3.11: Energy production scatter - V2

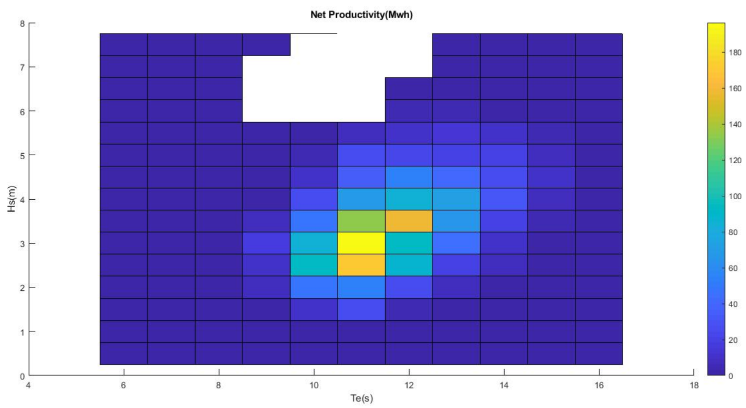

Figure 3.12: Energy production scatter - V3

The "holes" in the energy scatters, such as in Figure 3.12, are due to the inexistence of those waves because are too high and too short, therefore they break up.

CHAPTER 4

Pitch Resonance Tuning Tank

The PRTT is a U-tube passive tank filled by water. It works for the hull like a dynamic damper, it means that the system passes from the second to the fourth order introducing another resonance peak and enlarging the frequency spectrum covered. They are been installed in all three hulls, below in Figure 4.1 is reported the V2.

4.1 Mathematical model of a U-tank

The reference system is the same used for the hulls [17]. The water level into the reservoirs is described through the angular coordinate τ, with positive direction given by the clockwise rotation. It is represented in Figure 4.2.

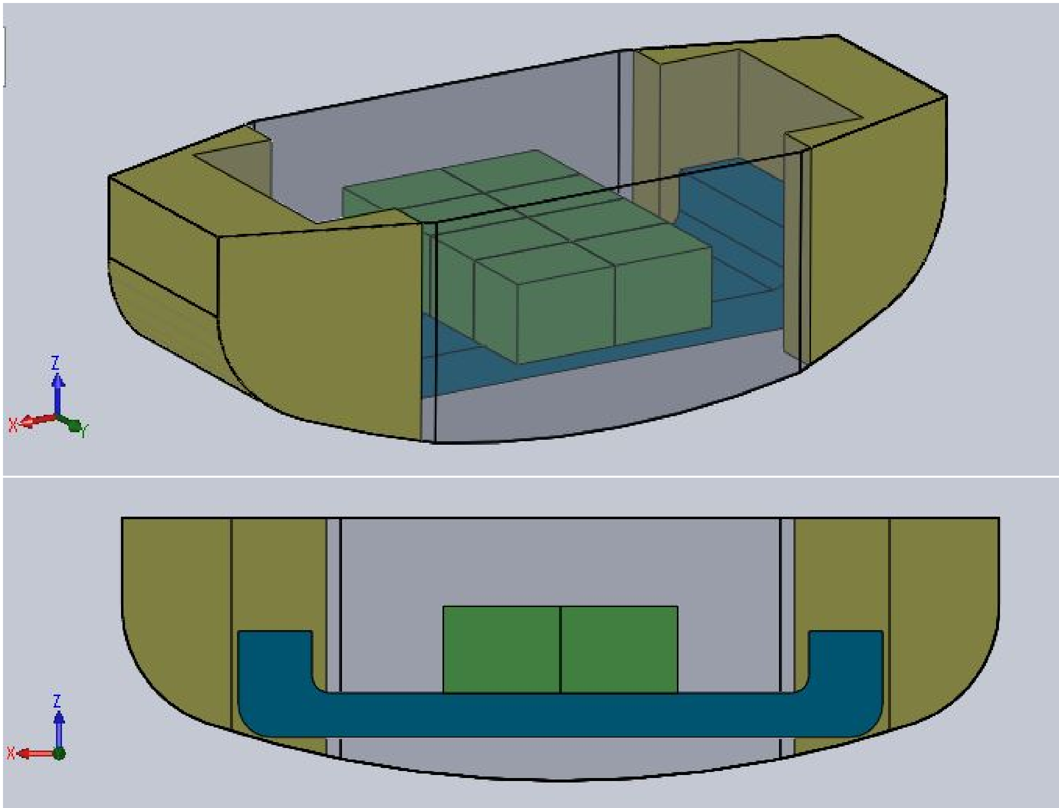

Figure 4.1: Example of PRTT installation - V2

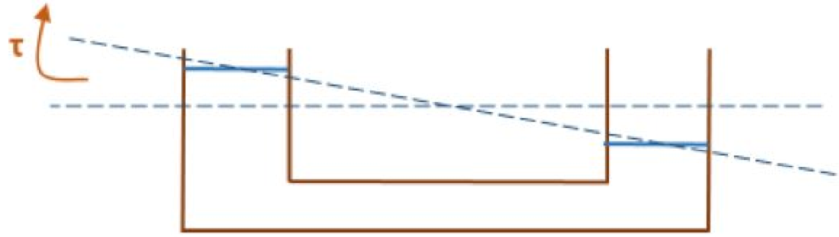

Figure 4.2: PRTT coordinate system

Here below is given a schematic representation of the U-tube system (Fig. 4.3) in order to have a better understanding of the equations. It is made up of two vertical reservoirs connected by a central duct.

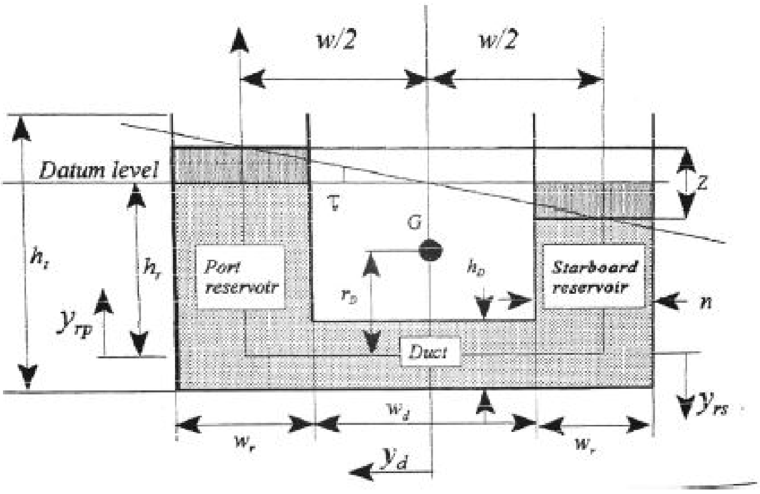

Figure 4.3: PRTT dimensions

The model includes the following assumptions:

- The motion of the water inside the U-tank is one-dimensional
- Only the pitch motion couples with the tank motion
- The response of the tank due to a sinusoidal motion is also sinusoidal
- The system response is linear
- No flow in the n direction

4.1.1 Euler's equation

Let's start from Euler's equation, by integrating it along the y-axis is possible to find the velocity and the tank angle. For the one dimensional problem the equation is:

$$\frac{\partial \nu}{\partial t} + \nu \frac{\partial \nu}{\partial y} = Y - \frac{1}{\rho_t} \frac{P}{\partial y} \tag{4.1}$$

where Y is the external force per unit mass. Considering that the cross section is always constant, is possible to assume that:

$$\frac{\partial \nu}{\partial y} = 0$$

and tehrefore the Euler's equation becomes:

$$\frac{\partial \nu}{\partial t} = Y - \frac{1}{\rho_t} \frac{P}{\partial y} \tag{4.2}$$

4.1.2 Continuity equation

Considering the continuity equation already presented in the second chapter (Eq. 2.3) and taking into account the dimensions represented in Figure 4.3 the fluid velocity into the reservoirs is:

$$v_r = \frac{d}{dt}(\frac{z}{2}) = \frac{w}{2}\dot{\tau} = \frac{w_r + w_d}{2}\dot{\tau} \tag{4.3}$$

Therefore the velocity at any point of the tank is given by the following equation:

$$(1 \cdot n)v = (1 \cdot w_r)v_r \Rightarrow v = \frac{w_r v_r}{n} = \frac{w_r w}{2n}\dot{\tau} \tag{4.4}$$

4.1.3 External forces

The contributions to the external forces are:

- Acceleration applied to the tank
- Frictional forces arising from valve losses, wall friction, etc.

Therefore they are:

1. Component due to the gravity
$$Y_g = -gcos\phi_1 \tag{4.5}$$
2. Component relative to the pitch acceleration
$$Y_\delta = -r\ddot{\delta}cos(\phi_2 - \frac{\Pi}{2}) = -r\ddot{\delta}sin\phi_2 \tag{4.6}$$
3. Components due to the surge acceleration for the duct and the reservoirs
$$Y_{x,duct} = \ddot{x}cos\delta \cong \ddot{x} \tag{4.7}$$
$$Y_{x,res} = \ddot{x}sin\delta \cong 0 \tag{4.8}$$
4. Frictional damping forces
$$Y_d = -\frac{qv}{n} \tag{4.9}$$
where q is the damping coefficient.

4.1.4 Final equation of the system

Putting all the expressions shown until now into the Bernoulli's equation we obtain:
$$\frac{d}{dt}(\frac{w_r w}{2n}\dot{\tau}) = gcos(\phi_1) - r\ddot{\delta}sin\phi_2 + \ddot{x} - \frac{q}{n}(\frac{w_r w}{2n}\dot{\tau}) = -\frac{1}{\rho_t}\frac{P}{dy} \tag{4.10}$$
Now integrating this equation with respect to y we compute the motion of the fluid as a function of the pressure difference in the reservoirs. Because of the level of water changes continuously the solution is an approximation. The result of the integration between the datum levels is:
$$\frac{\rho_t w_r w l_1}{2}\ddot{\tau} + \frac{\rho_t q w_r w l_2}{2}\dot{\tau} + \rho_t g l_3 + \rho_t \ddot{\delta} l_4 = P_s - P_p \tag{4.11}$$
with:
$$P_s = -P_p = -\rho_t g \frac{w}{2}\tau$$
So the equation of motion of the tuning tank is:
$$a_{\tau\tau}\ddot{\tau} + b_{\tau\tau}\dot{\tau} + c_{\tau\tau}\tau = a_{5\tau}\ddot{\delta} + c_{5\tau}\delta \tag{4.12}$$
where:

- $\tau = \frac{h}{\frac{w_d + w_r}{2}}$ is the tank angle
- $a_{\tau 5} = Q_t(r_d + h_r)$ is the inertial coupling coefficient between hull and U-tank
- $c_{5\tau} = c_{\tau\tau} = Q_t g$ is the restoring coupling coefficient between hull and U-tank
- $a_{\tau\tau} = Q_t w_r (\frac{w}{2h_d} + \frac{h_r}{w_r})$ is the U-tank inertial coefficient
- $b_{\tau\tau} = Q_t q w_r (\frac{w}{2h_d^2} + \frac{h_r}{w_r^2})$ is the U-tank damping coefficient
- $Q_t = \frac{\rho w_r w^2 x_t}{2}$ is the U-tank restoring coefficient

The damping term can be also rewritten as a function of the damping coefficient q, which is usually defined experimentally:

$$b_{\tau\tau} = 2qQ_t \sqrt{g w_r (\frac{w}{2h_d} + \frac{h_r}{w_r})} \tag{4.13}$$

The natural frequency of the system is:

$$\omega_n = \sqrt{\frac{c_{\tau\tau}}{a_{\tau\tau}}} = \sqrt{\frac{2g}{2h_r + \frac{w_r w}{h_d}}} \tag{4.14}$$

4.2 Coupling the hulls with the U-tube tank

Coupling the hull with the pitch resonance tuning tank the problem becomes of the fourth order and it is represented by the following system:

$$\begin{cases} I_{55}\ddot{\delta} + B_{55}\dot{\delta} + K_{55}\delta = F_{w,5} + a_{5\tau}\ddot{\tau} + c_{5\tau}\tau \\ a_{\tau\tau}\ddot{\tau} + b_{\tau\tau}\dot{\tau} + c_{\tau\tau}\tau = a_{5\tau}\ddot{\delta} + c_{5\tau}\delta \end{cases} \tag{4.15}$$

For simplicity of treatment it was used the model with one degree of freedom (1 DoF). In order to have a sensible effect on the dynamic of the hulls, it has been estimated that the mass of the water in the U-tube tank must be around the 20% of the total mass. In the Table 4.2 are reported the relations among the masses of the system.

Connection duct height [m]	Hd	3
Connection duct length [m]	Wd	34
Reservoir total height [m]	Ht	10
Reservoir length [m]	Wr	5
Reservoir width [m]	Xt	15
Reservoir distance [m]	W	44
Water level height [m]	Hr	5,5
Water mass [Kg]	Mw	2,59E+06
Vertical distance between the COG of the hull and the centerline of the duct [m]	rd	5,47 (V1) - 5,33 (V2) - 4,1 (V3)

Table 4.1: Dimensions of U-tube tank

Mass relations	V1	V2	V3
$PRTT/M_{tot}$	$17,4\%$	$18,4\%$	$20,8\%$
$Ballast/M_{tot}$	$62,7\%$	$61,6\%$	$45,6\%$
$Gyroscopes/M_{tot}$	$12,8\%$	$13,6\%$	$15,4\%$
$Metalsheets/M_{tot}$	$7,1\%$	$6,4\%$	$18,3\%$

Table 4.2: Mass of the components with respect to the total mass

4.2.1 V2 with PRTT

The hull V2 equipped with the U-tank is represented in Figure 4.1. Apparently it has not remarcable differences with the original version, only the presence inside of the tuning device. Obviously the hydrostatic datas will change, they are reported in the Table 4.3.

The metacentric height is sufficient to ensure a good roll stability while the center of gravity and the stiffness are increased and this will decrease the pitch amplitude. In the graph reported in Figure 4.5 is possible to observe the RAO with the U-tank activated ($with - prtt$) or disabled ($no - prtt$). As expected, the response presents

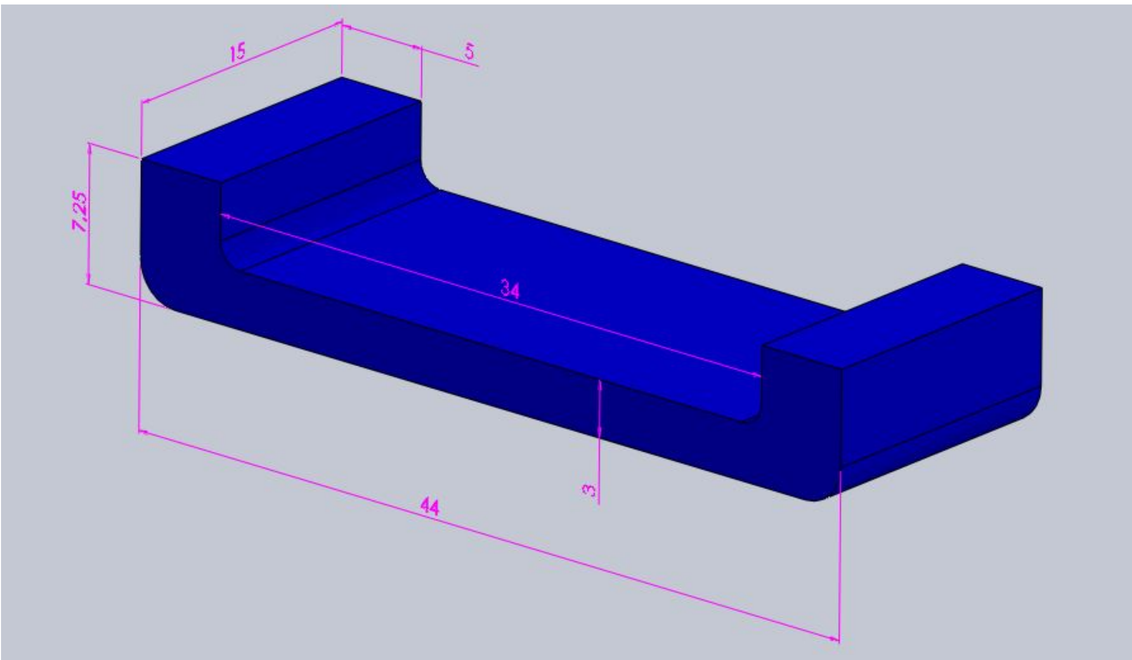

Figure 4.4: Representation of the dimensions in Tab. 4.1

Mass[Kg]	1,41E+07
COG[m]	-2,17
LPV	12
COB[m]	-5,26
WP_area[m^2]	1350
BG[m]	3,09
GMX[m]	1,34
GMY[m]	22,94
BMX[m]	4,43
BMY[m]	26,03
MX[Nm/deg]	3,20E+06
MY[Nm/deg]	5,48E+07
K55[Nm/deg]	3,14E+09
K44[Nm/deg]	1,83E+08

Table 4.3: Hydrostatic datas V2 with PRTT

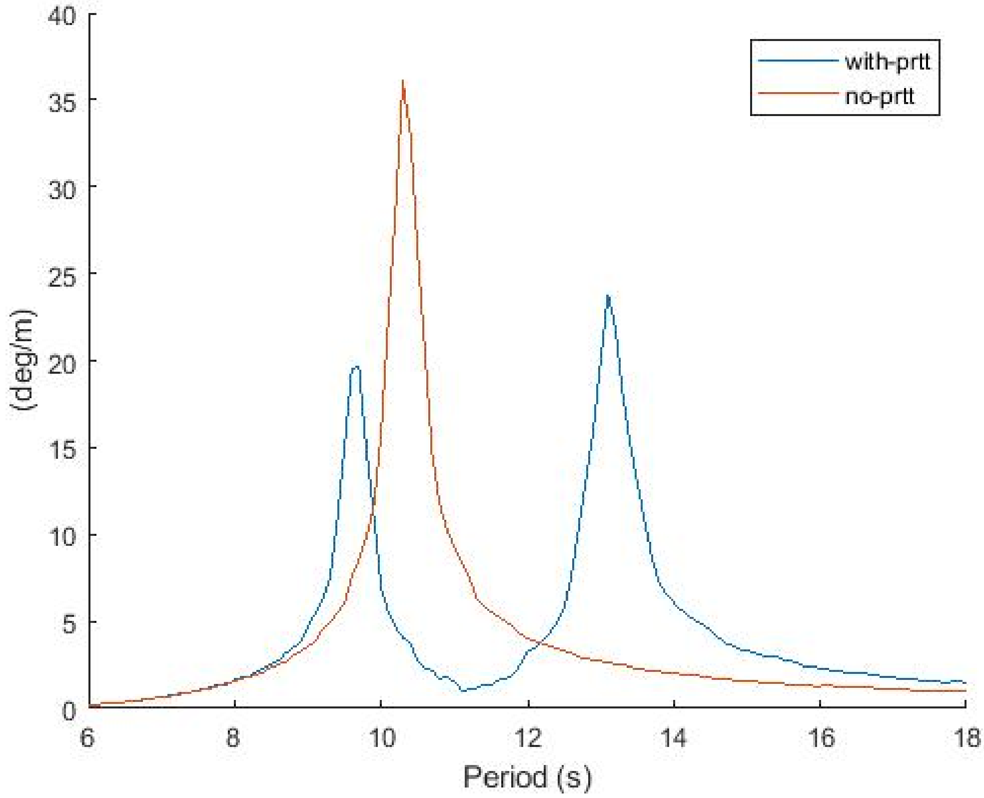

Figure 4.5: Response of the V2 with PRTT

two resonance peaks and one anti-resonance peak. With the PRTT activated the pitch amplitude is lower but the spectrum covered is bigger. Therefore, activating and disabling the U-tube tank it will be possible to maximize the energy production. The analysis of productivity starts with the simulation in a regular spectrum of both cases: with PRTT On and Off. After that, it will be used an irregular wave spectrum with an algorithm that will choose to activate or disable the U-tank in order to improve the energy production.

Productivity with PRTT On

Now are reported the graphs to evaluate the performance of the whole system. Then a table with the summary of the datas (Tab. 4.4) and the scatter of the energy production (Fig. 4.10).

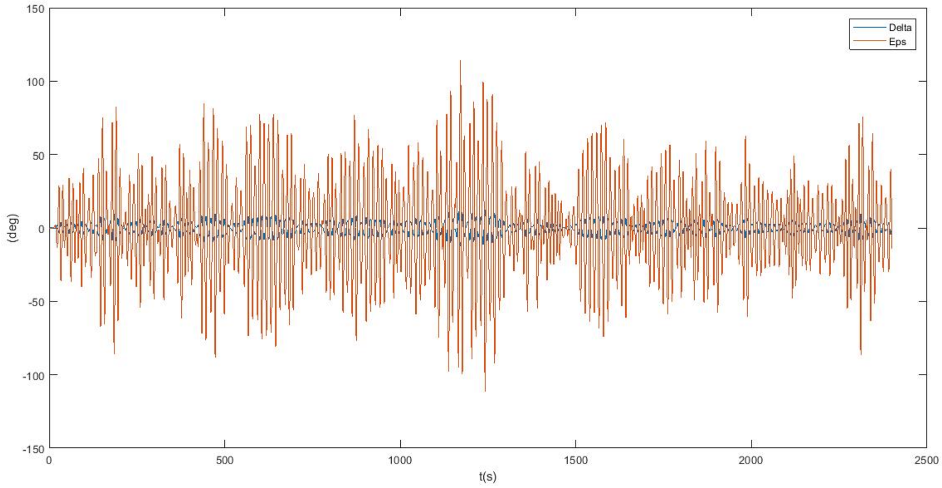

Figure 4.6: Overlap between δ and ε - V2 - PRTT On

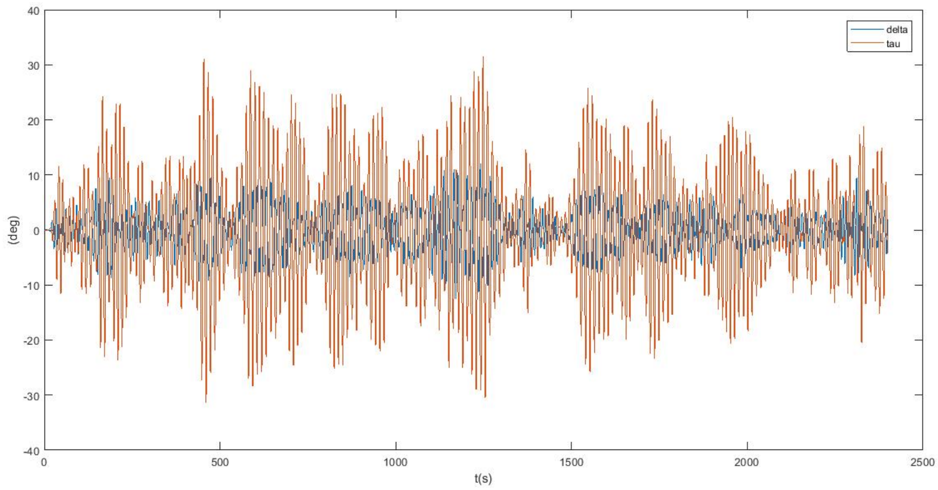

Figure 4.7: Overlap between δ and τ - V2 - PRTT On

Comparing the Table 4.4 with the one of the V1 in appendix A reporting the productivity of V1 in the same condition, we can observe how in V2 the net power is slightly higher and the gross lower. It means that the efficency of the machine is increased.

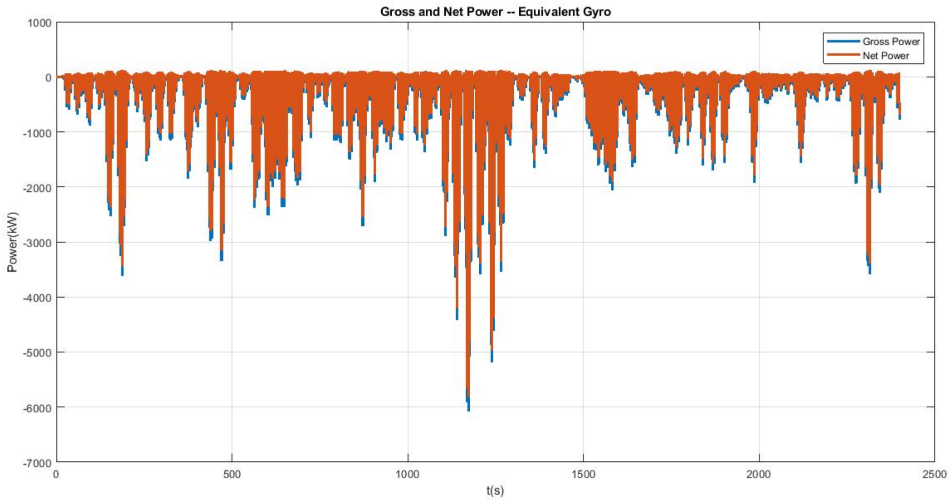

Figure 4.8: Gross and net productivity - V2 - PRTT On

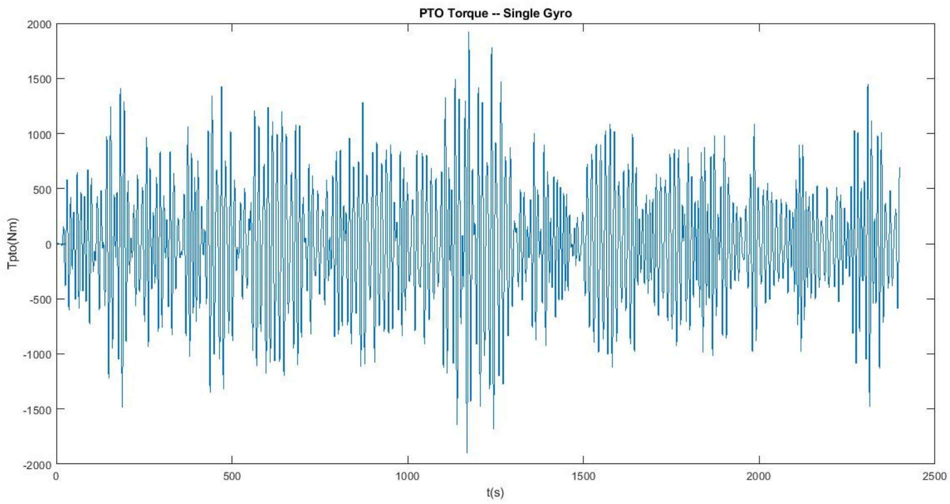

Figure 4.9: Torque transmitted to the PTO - V2 - PRTT On

Phid (rpm)	219
c (Nms/rad)	379209
TotPowerNet (kW)	378
TotPowerGross (kW)	475
TotPowerLost (kW)	97
DeltaMax (deg)	12,7
DeltaRms (deg)	3,7
EpsMax (deg)	114
EpsRms (deg)	35,1
TptoMax (Nm)	21483
TptoRms (Nm)	6128
VelMax (rpm)	206
VelRms (rpm)	62
Annual Net Productivity (MWh/y)	1932
Annual Gross Productivity (MWh/y)	2527
Te (s)	11,5
Hs (m)	3,25

Table 4.4: Production and main parameters - V2 - PRTT On

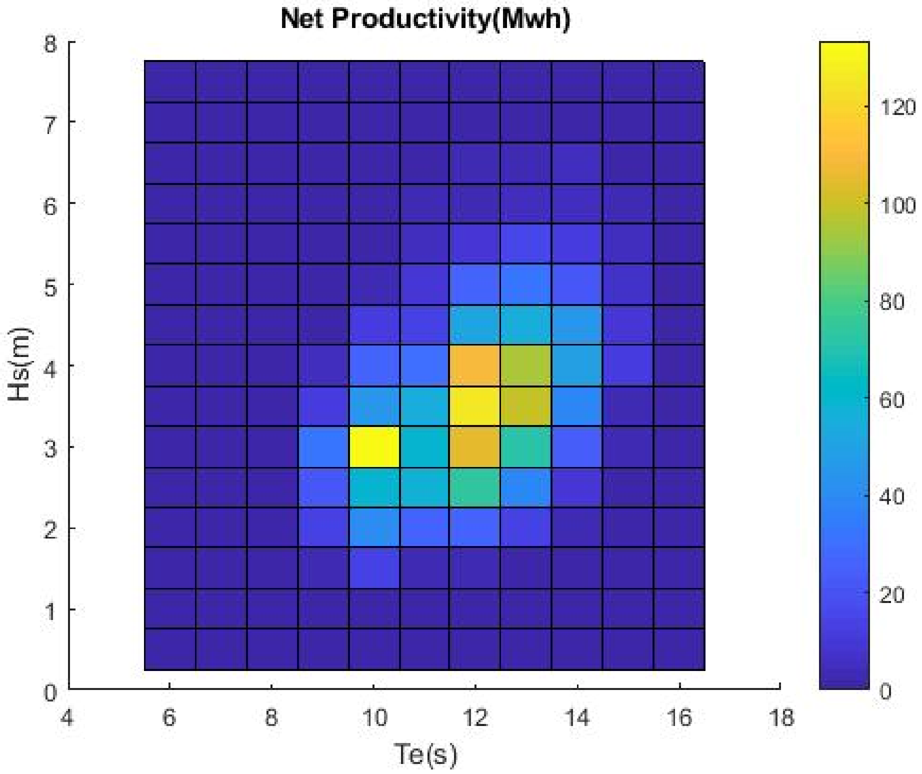

Figure 4.10: Production scatter - V2 - PRTT enabled

Productivity with PRTT Off

Here below follow the tables and graphs relative to the V2 with the U-tube passive tank disabled.

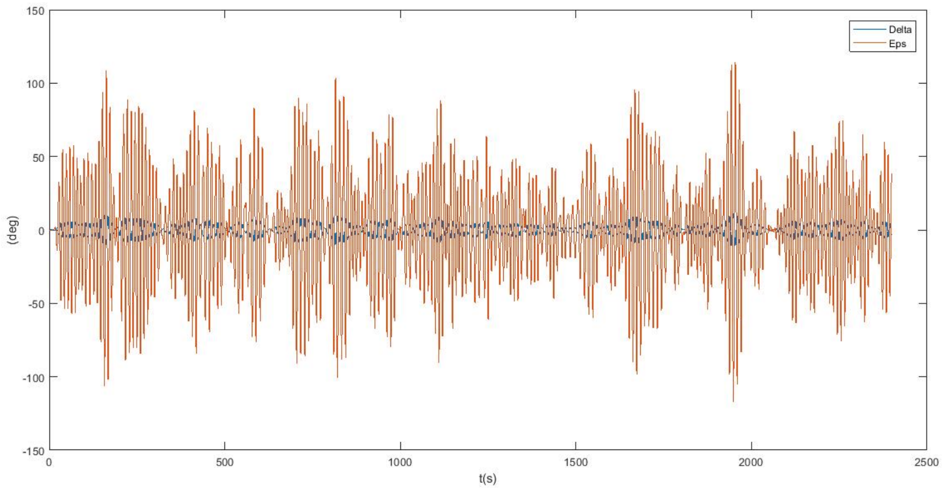

Figure 4.11: Overlap between δ and ε - V2 - PRTT Off

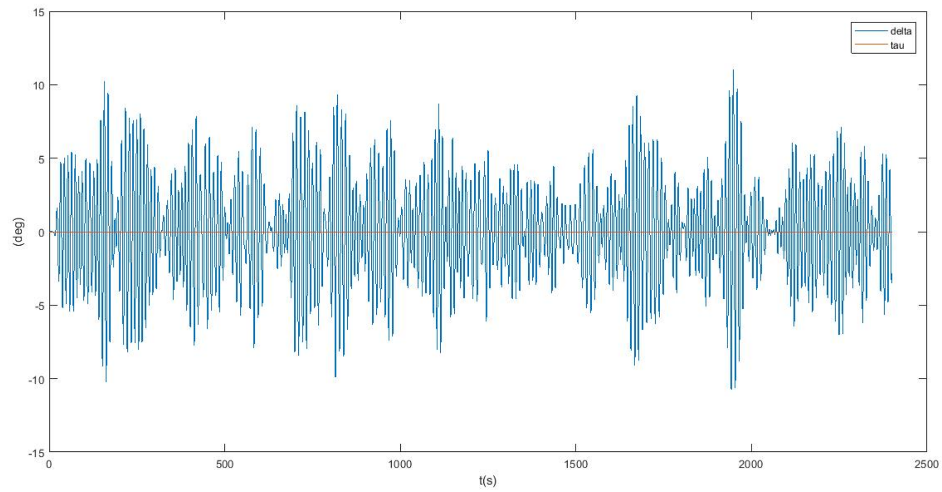

Figure 4.12: Overlap between δ and τ - V2 - PRTT Off

Looking at the Table 4.5 emerges that the production with the U-tank disabled is quite higher respect to the case with the device enabled. It could significate a lower utility of the tank with this hull. To verify it we have to mix the configuration and

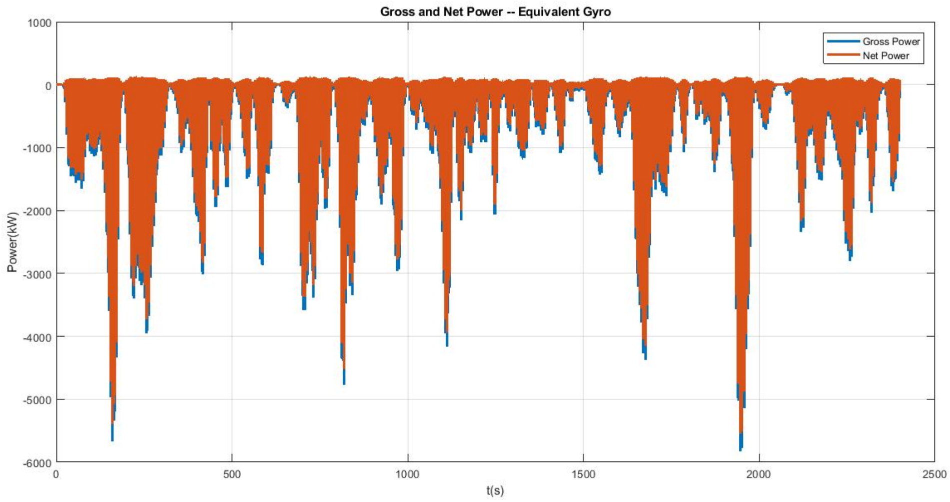

Figure 4.13: Gross and net productivity - V2 - PRTT Off

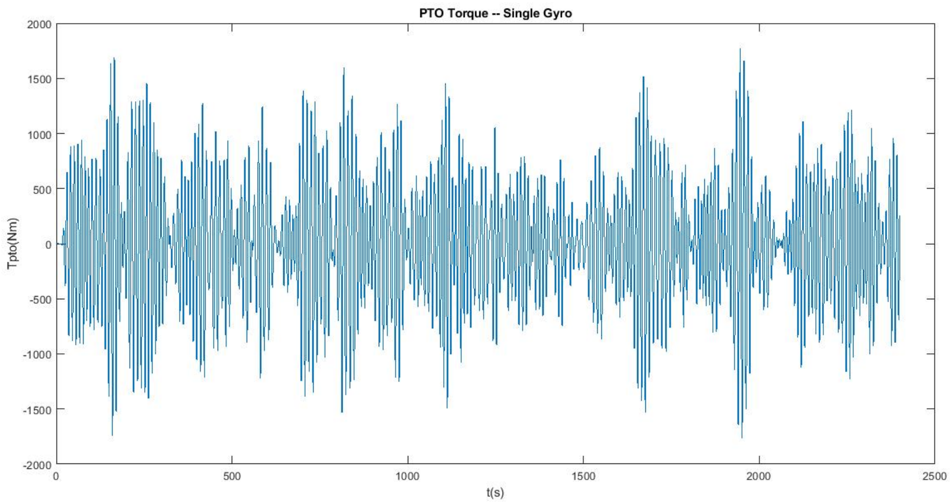

Figure 4.14: Torque transmitted to the PTO - V2 - PRTT Off

Phid (rpm)	240
c (Nms/rad)	372891
TotPowerNet (kW)	461
TotPowerGross (kW)	579
TotPowerLost (kW)	118
DeltaMax (deg)	10,97
DeltaRms (deg)	3,36
EpsMax (deg)	113,9
EpsRms (deg)	35,7
TptoMax (Nm)	21286
TptoRms (Nm)	6708
VelMax (rpm)	217
VelRms (rpm)	69
Annual Net Productivity (MWh/y)	2513
Annual Gross Productivity (MWh/y)	3123
Te (s)	11,5
Hs (m)	3,25

Table 4.5: Production and main parameters - V2 - PRTT Off

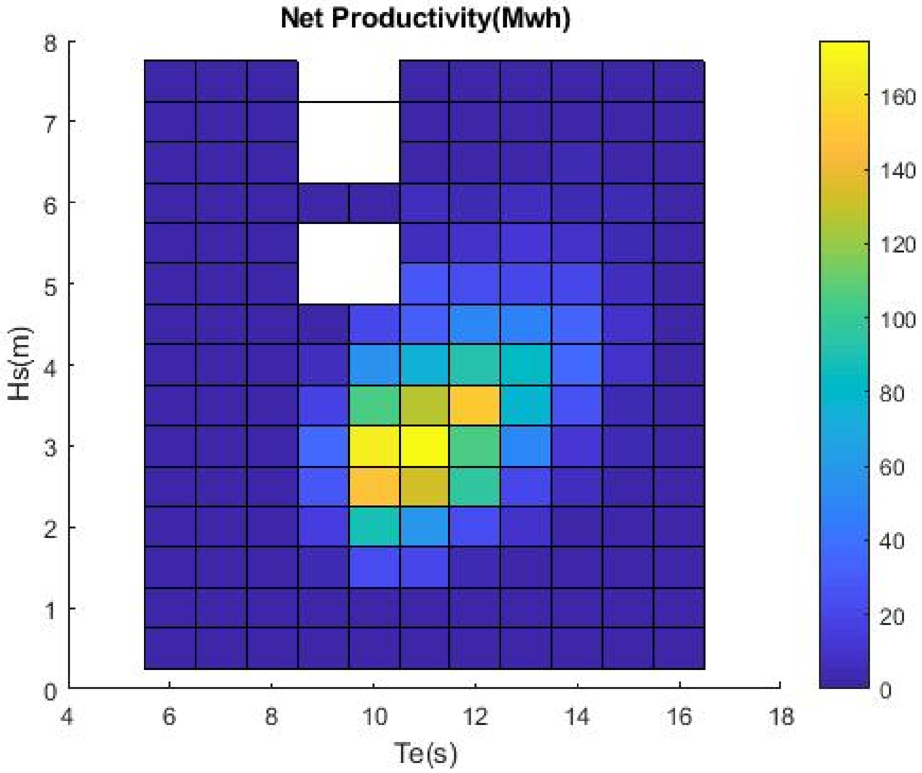

Figure 4.15: Production scatter - V2 - PRTT disabled

compute the productivity. It will be compared with the productivity of the V2 hull of the prevoius chapter.

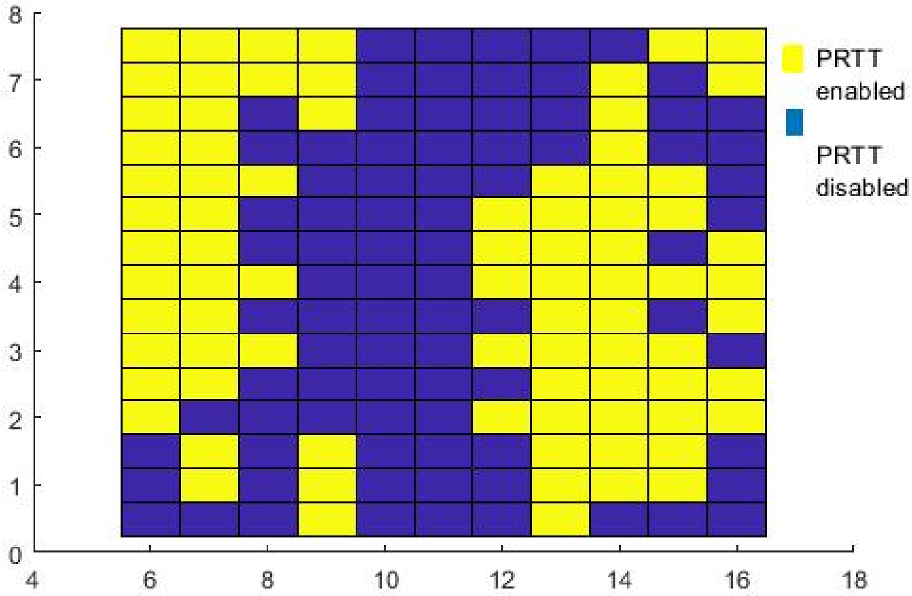

Figure 4.16: Utilization of the U-tank in dependence of the waves - V2

Optimization of the productivity

Also this time, mixing together the two configurations, the productivity results higher than the cases with the U-tube tank always enabled or disabled. It is equal to 2694 MWh/y. Here are reported the graphs relative to the optimization.

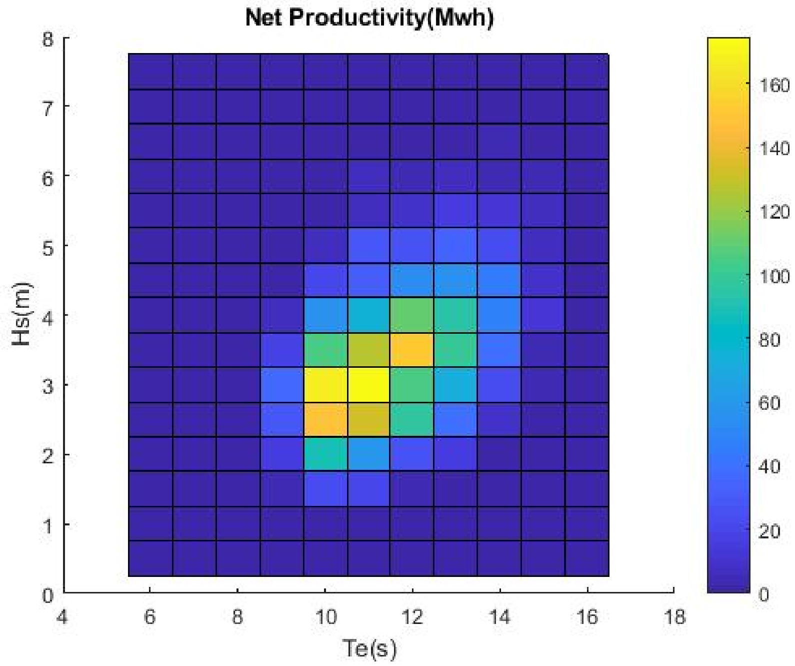

Figure 4.17: Production scatter of V2 with the optimal use of the U-tank

4.2.2 V1 and V3 with PRTT

The hulls V1 and V3 seem to be negatively affected by the installation of the U-tube tank. Probably because the masses are badly distributed and this is reflected on the inertia of the system. Therefore the productivity of both the hulls diminishes (4.8). All the graphs and tables that regard the performance of the hulls V1 and V3 are contained in the **appendix A**.

4.2.3 Summary of the hulls productivity

Looking at the production scatter of the three hulls the V2 seems to be the one that exploit more the U-tube passive tank. In fact, is the one with the best productivity. All the values are reported in the table 4.8.

From these datas we can make two observations. The first one is that with and without the pitch resonance tuning tank the best hull is the V2. The second regards the effectiveness of the U-tank. In fact, this device does not seem to bring benefits in

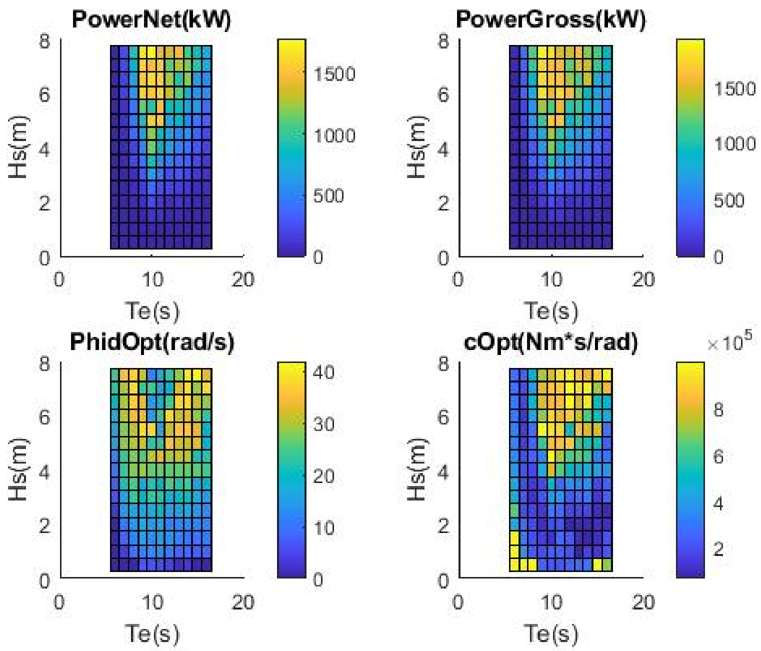

Figure 4.18: Performance graphs - V2 - group 1

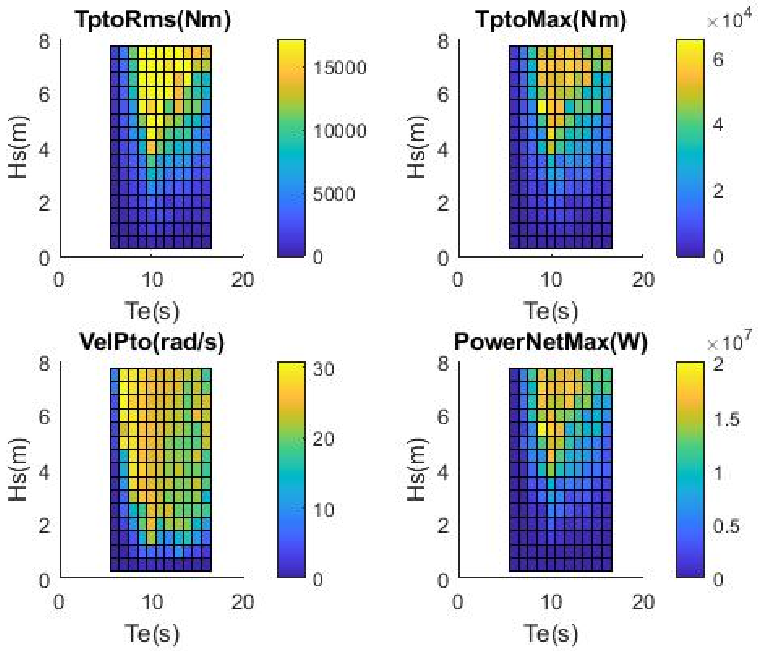

Figure 4.19: Performance graphs - V2 - group 2

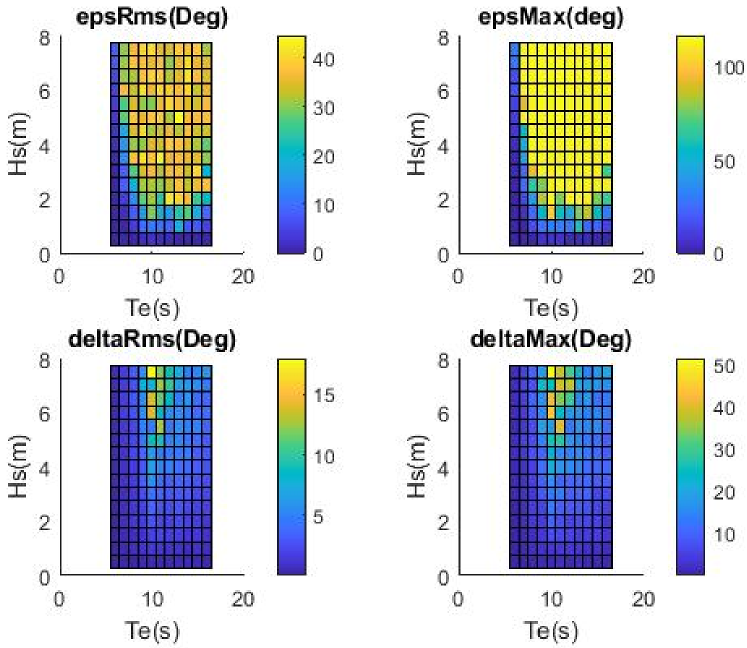

Figure 4.20: Performance graphs - V2 - group 3

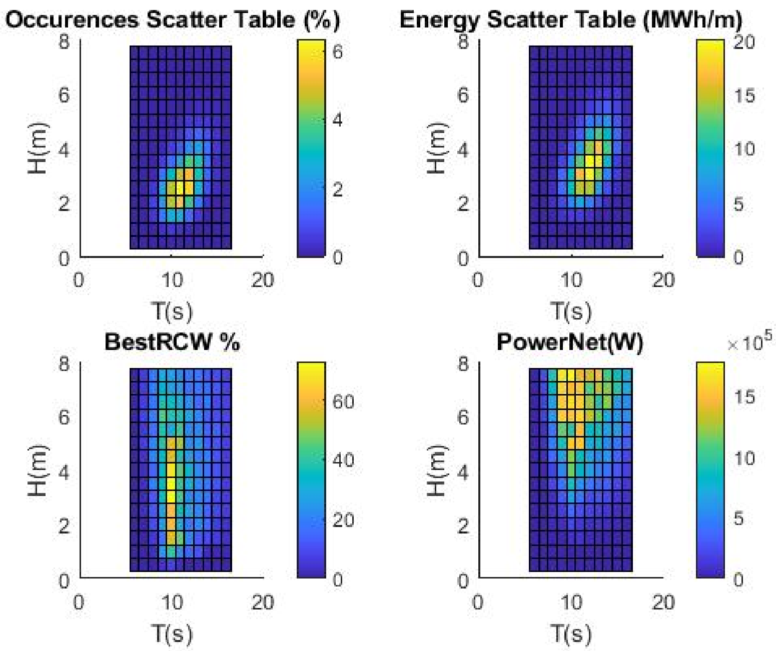

Figure 4.21: Performance graphs - V2 - group 4

	V2	V2 - Prtt - OFF	V2 - Prtt - ON
Phid (rpm)	261	240	219
c (Nms/rad)	498432	372891	379209
TotPowerNet (kW)	553	460	378
TotPowerGross (kW)	679	579	475
TotPowerLost (kW)	126	118	97
DeltaMax (deg)	13	11	12,7
DeltaRms (deg)	4	3,4	3,7
EpsMax (deg)	114	114	114
EpsRms (deg)	34,5	35,7	35
TptoMax (Nm)	27534	21286	21483
TptoRms (Nm)	8399	6708	6128
VelMax (rpm)	209	217	205
VelRms (rpm)	64,4	68,7	61,7
Annual Net Productivity (MWh/y)	2647	2513	1932
Annual Gross Productivity (MWh/y)	3262	3123	2527
Te (s)	11,50	11,50	11,50
Hs (m)	3,25	3,25	3,25

Table 4.6: Performance parameters of all V2 versions for the design wave

	V2	V2 - Prtt - optimized	V2 - Prtt - OFF	V2 - Prtt - ON
Phid_Weighted (rpm)	175	184	179	177
c_Weighted (Nms/rad)	283778	292258	271424	253069
Eps_RmsWeighted (deg)	32	32,4	30,3	30,3
Eps_MaxWeighted (deg)	102,5	103,9	101,3	97,3
Delta_RmsWeighted (deg)	3	3	2,8	2,6
Delta_MaxWeighted (deg)	9,9	9,8	9,4	8,3
T_ptoRmsWeighted (Nm)	4611	4757	4408	3807
T_ptoMaxWeighted (Nm)	15247	15433	14825	12284
Vel_RmsWeighted (rpm)	61,5	61	60	56
Vel_MaxWeighted (rpm)	197	197,5	201	182,5
Gross_Productivity (MWh)	3262	3354	3123	2527
Net_Productivity (MWh)	2647	2694	2513	1932

Table 4.7: Performance parameters of all V2 versions weighed on the scatter

Hull	Net productivity [MWh/y]
V1	2509
V2	2647
V3	2127
V1 - PRTT	2437
V2 - PRTT	2694
V3 - PRTT	1985

Table 4.8: Productivity of all the hulls

the V1 and V3. But in the V2 it improves the performance. Probably this result is due to the fact that the hull V2 has the correct characteristics to suit the installation of the PRTT.

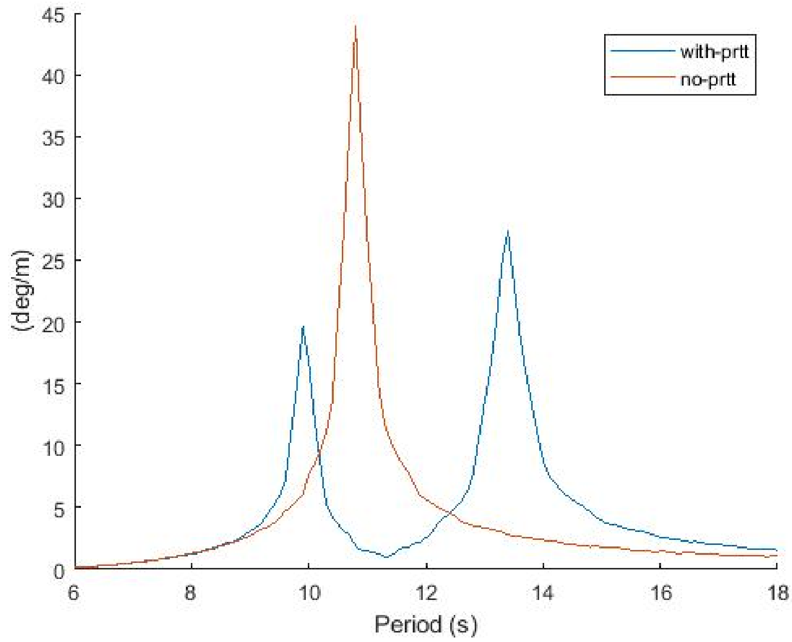

Figure 4.22: Response amplitude operator of the V2 with the rised deck

4.2.4 V2: Rised Deck

In addition to the hulls described in this thesis, there are others hulls realized but rejected due to their poor performance. However, they were useful to understand some trends. One of these regards the height of the COG, in fact the higher is the COG and the higher is the RAO. To rise the COG was rised the deck of the hull by 2 meters and in Figure 4.22 is possible to see the effect. The second and the third peaks are remarcably higher than the ones of the V2 in the prevoius section (Fig. 4.5). Now is interesting to see if also the productivity results improved.

Looking at Table 4.9 the metacentric height GMX results too small, but is possible to fix oe reduce this problem using some devices, for example the *bilge keel*.

Productivity

Here are reported the tables about the productivity of this hull. All the performance graphs are contained in the appendix A. This hull was realized only in the version with

Mass[Kg]	1,42E+07
COG[m]	-1,21
LPV	12
COB[m]	-5,26
WP_area[m2]	1350
BG[m]	4,05
GMX[m]	0,38
GMY[m]	21,97
BMX[m]	4,43
BMY[m]	2,60E+01
MX[Nm/°]	9,03E+05
MY[Nm/°]	5,25E+07
K55[Nm/°]	3,01E+09
K44[Nm/°]	5,17E+07

Table 4.9: Hysrostatic datas of V2 - rised deck

	V2 - RD - Prtt - OFF	V2 - RD - Prtt - ON
Phid (rpm)	249	215
c (Nms/rad)	465694	432232
TotPowerNet (kW)	517	345
TotPowerGross (kW)	634	430
TotPowerLost (kW)	118	85
DeltaMax (deg)	12,7	12,3
DeltaRms (deg)	3,9	3,9
EpsMax (deg)	114	114
EpsRms (deg)	34,4	32,2
TptoMax (Nm)	25710	22518
TptoRms (Nm)	7844	6225
VelMax (rpm)	209	199
VelRms (rpm)	64	55
Annual Net Productivity (MWh/y)	2489	2009
Annual Gross Productivity (MWh/y)	3070	2526
Te (s)	11,5	11,5
Hs (m)	3,25	3,25

Table 4.10: Performance parameters of the hull V2 - RD for the design wave

the PRTT.

With this configuration the net productivity is increased by the 7% with respct to the original hull V2.

Phid_Weighted (rpm)	170
c_Weighted (Nms/rad)	307922
Eps_RmsWeighted (deg)	32,7
Eps_MaxWeighted (deg)	102,8
Delta_RmsWeighted (deg)	3,44
Delta_MaxWeighted (deg)	11
T_ptoRmsWeighted (Nm)	4931
T_ptoMaxWeighted (Nm)	15919
Vel_RmsWeighted (rpm)	60,5
Vel_MaxWeighted (rpm)	191
Gross_Productivity (MWh)	3427
Net_Productivity (MWh)	2839

Table 4.11: Productivity and main parameters weighed on the scatter - V2 RD

4.3 Considerations about the productivity

Looking at the Table 4.8 the increase of the production due to the adoption of the Prtt is very small and does not justify the economic investment to realize a test bench, other studies and so on. However, it's possible to do two important considerations. Firstly, the IOWEC is an ensemble of devices and all of these must be tuned, above hull the gyroscope that is probably the most important element of the machine but it is not a target of this thesis. Secondly, we can make a deeper inspection considering four particular waves of the spectrum. Two are the most energetic ones with the period more similar to the resonance period of the hull with the U-tank disabled and enabled(in this case the second peak) and two are the ones with the period exactly equal to the two periods of the hull previously considered in order to evaluate its potential. The all waves have an height equal to $2,75m$. In Table 4.12 are reported the Welch's method parameters used for the PSD calculation. To pass from energy frequency to peak

Samples	Window samples	Mean elements	Percentage of overlap	Window NFFT	Frequancy resolution [Hz]
16384	2521	12	50	4096	1,67E-03

Table 4.12: Welch's method parameters used in the PSD estimation

	Prtt OFF	Prtt ON
Tnat [s]	10,3	13,1

Table 4.13: Natural frequencies of the hull

frequency of the wave in the Jonswap spectrum was used the relation 4.16 with a γ equal to 3.3.

$$f_e = \frac{f_p}{(0,8255 + 0,03852\gamma - 0,005537\gamma^2 + 0,0003154\gamma^3)} \tag{4.16}$$

In Tables 4.13; 4.14; 4.15 are reported respectively the natural frequencies of the hull, the most important parameters of the waves chosen and finally avarage pitch of the hull for each case study.

Examining the Figure 4.23 we can observe how almost half of the most energetic wave is unexploited (even consideration un eventual use of the U-tube tank) and this can partially justify the lack in the power prodution expectations. Considering a wave with the peak period equal to the resonance of the hull (Fig. 4.24) is possible to observe that potentially the productivity can be much higher.

Practically the same considerations can be made with the resonance peak of the Prtt and observed in the Figures 4.25 and 4.26. Therefore, from these considerations

	Tp[s]	Te[s]	Hs[m]	Power[W/m]
1	11,6	10,5	2,75	39
2	10,5	9,5	2,75	35
3	13,8	12,5	2,75	46,2
4	12,7	11,5	2,75	42,5

Table 4.14: Main parameters of the waves used for the frequency analisys

	δ Rms [Deg] - Prtt On	δ Rms [Deg] - Prtt OFF
1	2	3,6
2	3,8	4
3	3,3	2,2
4	3	2,8

Table 4.15: Avarage pitch amplitude of the four case studies

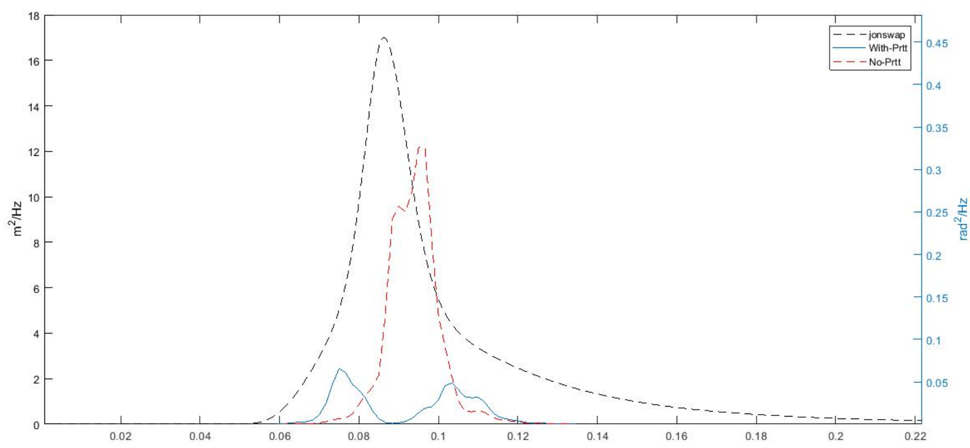

Figure 4.23: Comparison between the wave and the hull - Case study 1

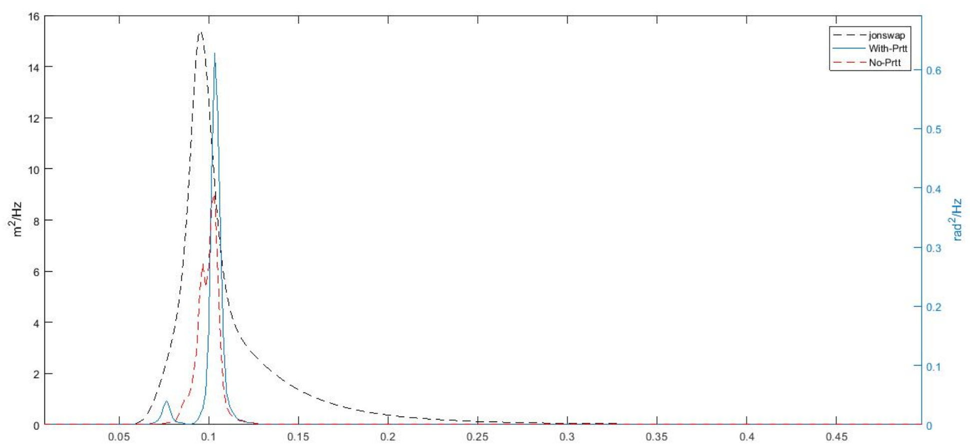

Figure 4.24: Comparison between the wave and the hull - Case study 2

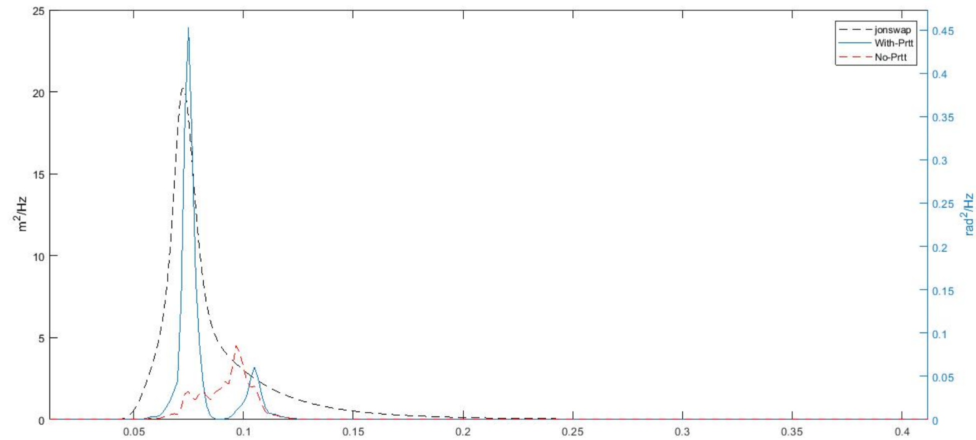

Figure 4.25: Comparison between the wave and the hull - Case study 3

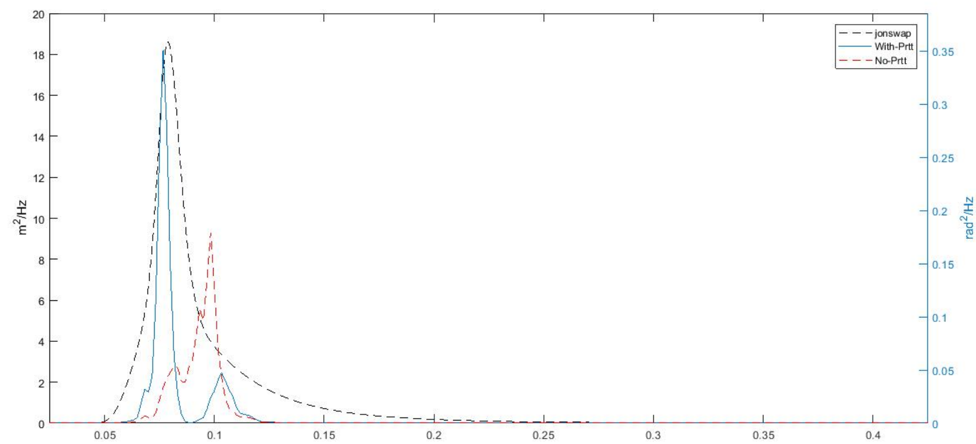

Figure 4.26: Comparison between the wave and the hull - Case study 4

we can try to modify some geometrical parameters of the Prtt and evaluate the effects.

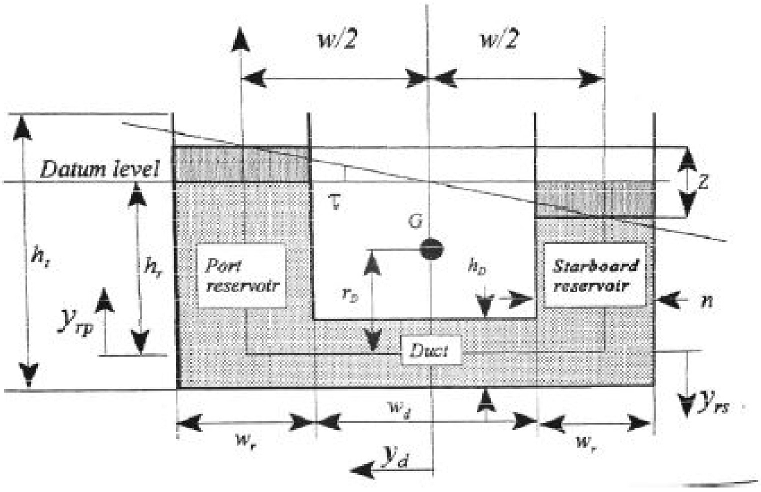

Figure 4.27: PRTT dimensions

	Hr	3,5	5,5	7,5
Hd				
2		2516	2514	2515
3		2767	2694	2698
5		3489	3410	3319

Figure 4.28: Map of the productivity

4.3.1 Geometrical variations of the Prtt

In order to have a better understanding let's recall the natural frequency equation of the Prtt and the geometrical parameters:

$$\omega_n = \sqrt{\frac{c_{\tau\tau}}{a_{\tau\tau}}} = \sqrt{\frac{2g}{2h_r + \dfrac{w_r w}{h_d}}}$$

To simplify the analisys the COG of the hull is considered constant. The goal is to find a trend that could give more sense to the adoption of the U-tank. The parameters analyzed are the height of the central duct h_d and the water level in the lateral reservoirs h_r. These allow to consider the results obtained with the COG fixed as a good approximation. In Table 4.28 is contained the power production with the starting point in the middle.

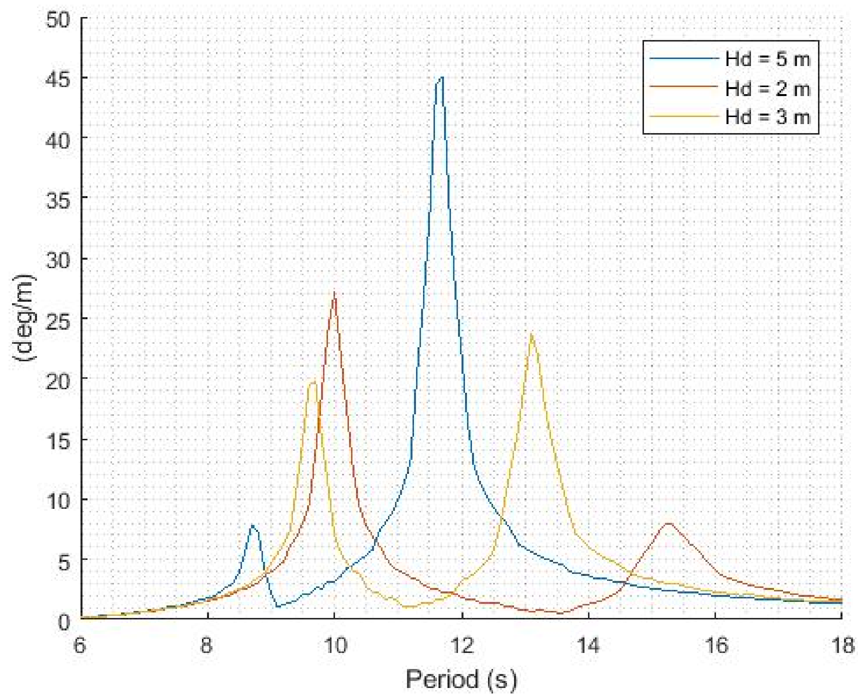

Figure 4.29: RAO with $h_r = 5,5m$

Is immediately clear that the most important parameter is the connection duct height h_d. By increasing it the water velocity is increased and it allows a faster and higher response of the device that is translated in an higher productivity. Observing the RAO of the system (Fig. 4.29) the case with $h_d = 5m$ can be considered a "lucky" case because the resonance of the system is aligned with the period of the most energetic wave of the whole scatter. Nevertheless, the importance of the conclusion remains.

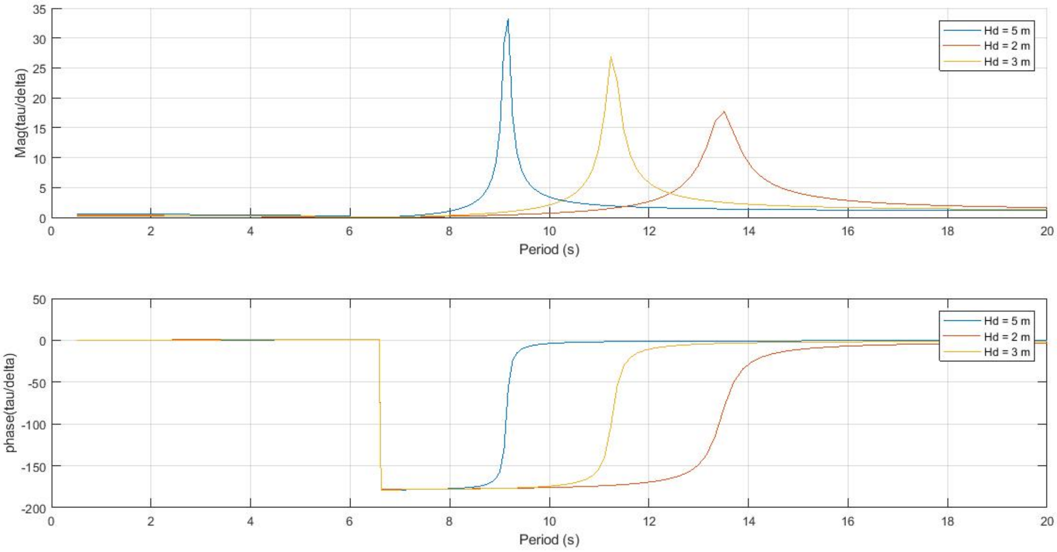

Figure 4.30: Ratio τ/δ with $h_r = 5,5m$

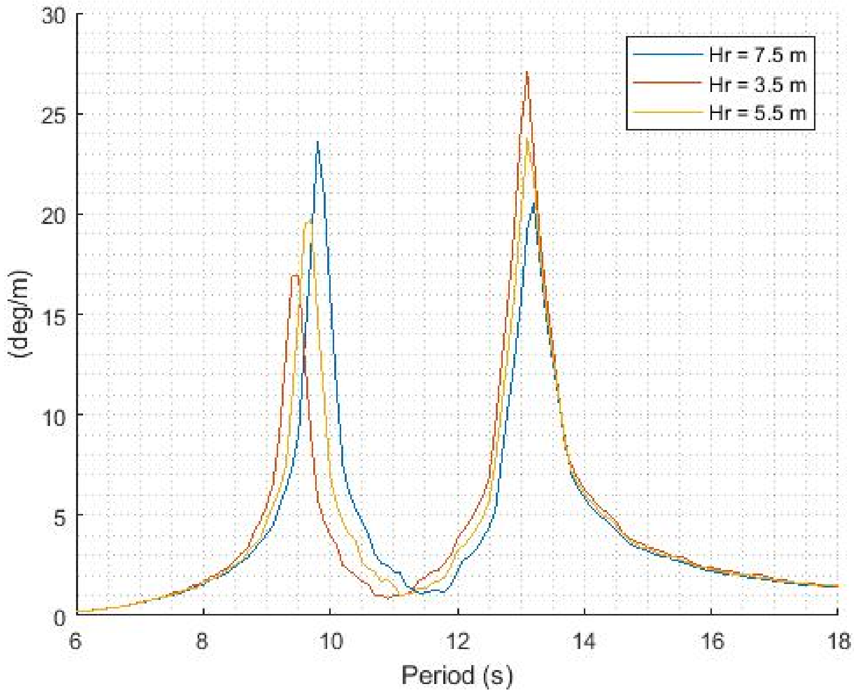

Figure 4.31: RAO with $h_d = 3m$

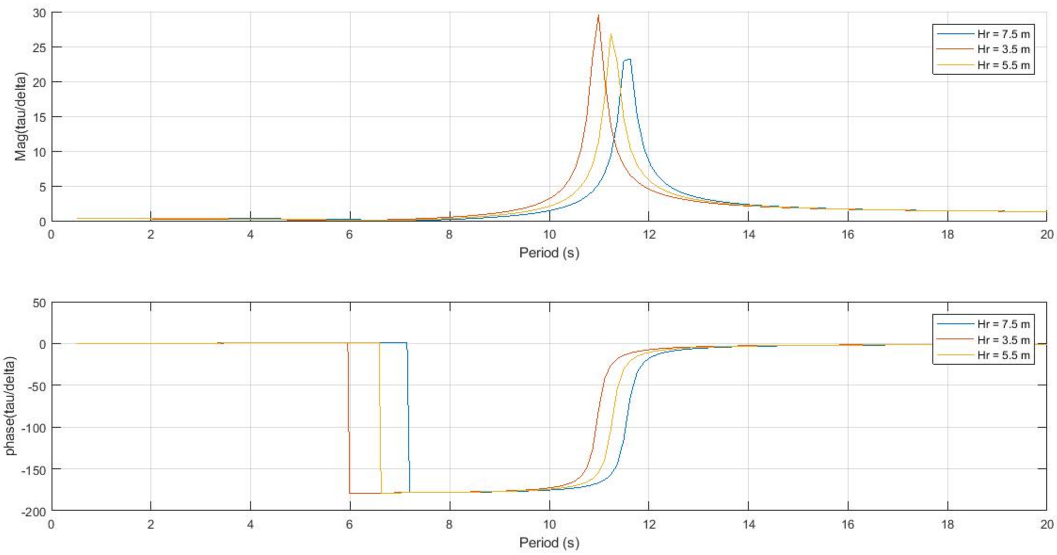

Figure 4.32: Ratio τ/δ with $h_d = 3m$

CHAPTER 5

Initial Stability

The stability of a floating body depends on two main aspects :

- The position of the center of gravity
- The shape of the body

The equilibrium of a floating body is due to the compensation between the **weight force** and the **buoyant force** (Archimedes' principle). In the rest position these are on the same line action, so there is not momentum (Fig. 5.1). If the body, in our case the hull, starts to rotate due to an external force, the center of buoyancy (point B) changes its position. The shift of the point B depends on the shape of the hull and the relative position between the center of gravity G and B determines the type of

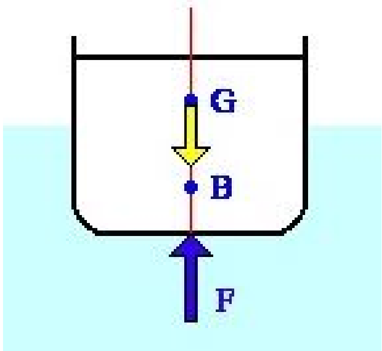

Figure 5.1: Initial position

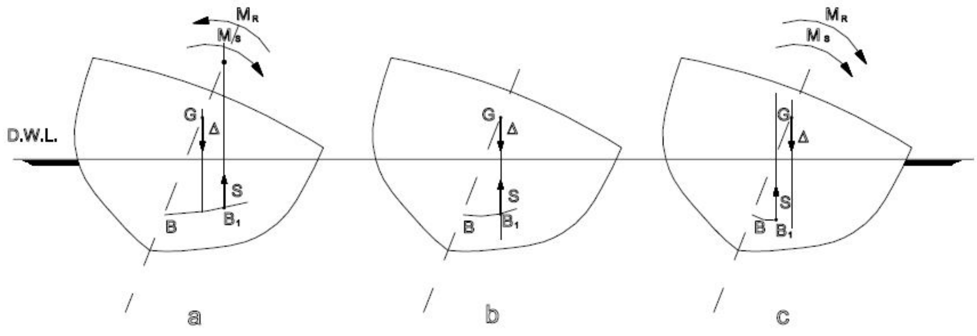

Figure 5.2: Equilibrium conditions in dependence of B

equilibrium. There are three possible cases [18]:

a) Stable equilibrimu

b) Neutral equilibrium

c) Unstable equilibrium

In Figure 5.2 are represented these cases. The moment can be *righting* (Fig. 5.2 a) or *heeling* (Fig.5.2 c). If the equilibrium is neutral there is no momentum. The position of the point G is foundamental, considering the *Metacentric height.*

Let's consider an hull in the initial equilibrium position that rotates of an angle α. For small angles ($<10°$) is possible to approximate the curve from B to B1 as a circumference arc with the center of curvature in M, that it the *transverse metacentre.* Looking at the Figure 5.3 is clear that M must stay over G to have the stable equilibrium and that the higher is the distance between them (r) and the higher in the righting moment. With reference to the Figure 5.3 the righting moment is:

$$M_\alpha = \Delta b = \Delta \cdot \overline{GH} = \Delta \cdot \overline{GM} sen(\alpha) = \Delta(r - a) sen(\alpha) \tag{5.1}$$

where Δ is the portion of the hull under the water plane. The value of "r-a" is called *index of initial stability* and gives an idea about the capability of the hull to react against the heeling forces. Therefore the higher is this value and the higher is the

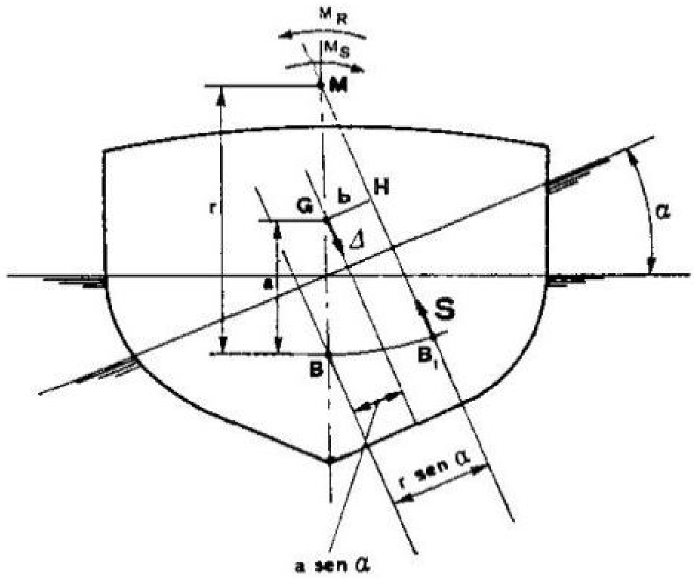

Figure 5.3: Geometrical representation of the relation among B, G, M

stability of the hull. To have an idea of how long is this parameter, here are reported some intervals:

- military ships = 0.8 - 1.2 m
- sailing ships = 0.6 - 0.8 m
- sailboats = 2.0 - 2.5 m
- motosailer = 0.6 - 0.8 m
- planed hulls = 0.3 - 0.6 m

Obviously in the ships of the examples is considered the comfort of the passengers. In fact, an high metacentric height means also continous longitudinal and transversal movements and accelerations that could be dangerous for people

Rolling stability for angles >10°

For inclination higher than 10°is not possible to consider the shifting of the center of buoyancy as a circumference arc with center in M, because it is a series of arcs

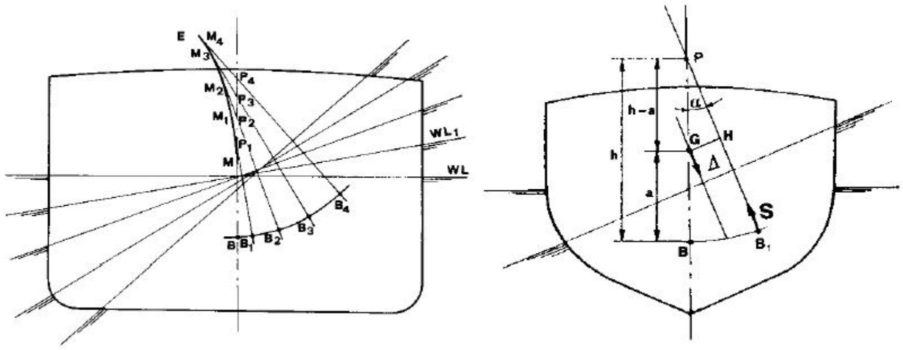

Figure 5.4: Metacentric involute for $\alpha > 10$

with different radius centered in M_1, M_2, M_3... The trajectory described by the different centers of curvature is named *metacentric involute*. The moment is equal to the previous one (eq. 5.1) but to compute the quantity $\overline{GH}$ is better to refer to the points P_1, P_2, P_3...called *false metacenters* (Fig. 5.4). Therefore the momentum will be:

$$M_\alpha = \Delta \cdot \overline{GH} = \Delta \cdot \overline{GP} sen(\alpha) = \Delta(h - a) sen(\alpha) \tag{5.2}$$

To analyze the stability of a ship or a hull is used the *stability giagram*.

5.1 Stability Diagram

The stability curve represents the momentum in function of the rotation angle α computed trough the equation 5.2. There are two equilibrium position, at $\alpha = 0$ and at $\alpha = \alpha_c$ in which appear the *statical overturning*; for $\alpha > \alpha_c$ the momentum becomes heeling (negative). The curve is influenced by several parameters, the most important ones are:

- height of the tack
- shape of the tack
- position of the center of gravity G
- beam of the hull

In Figure 5.5 are reported some examples of the influence of these parameters.

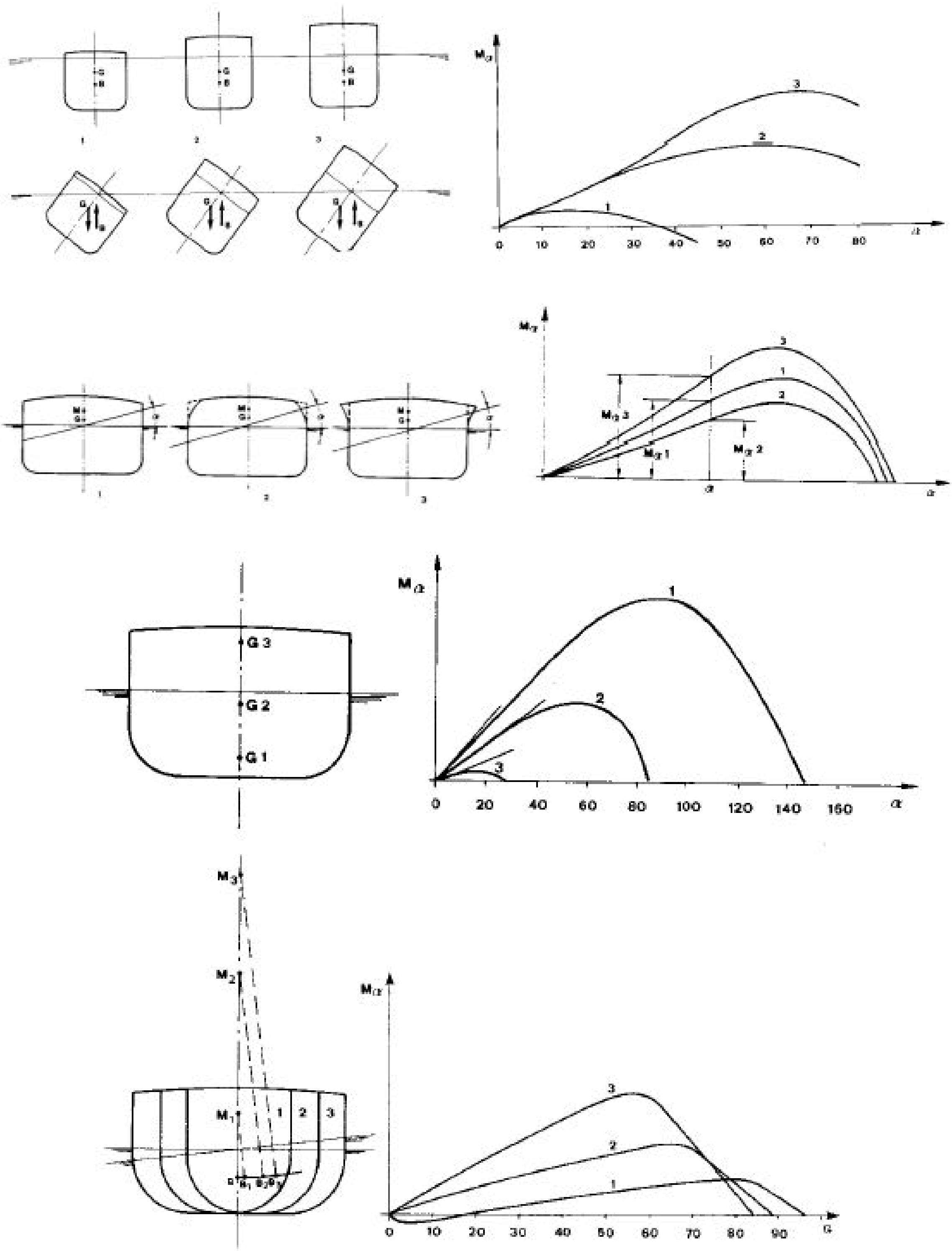

Figure 5.5: Relations among the characteristics of the hull and the stability curve

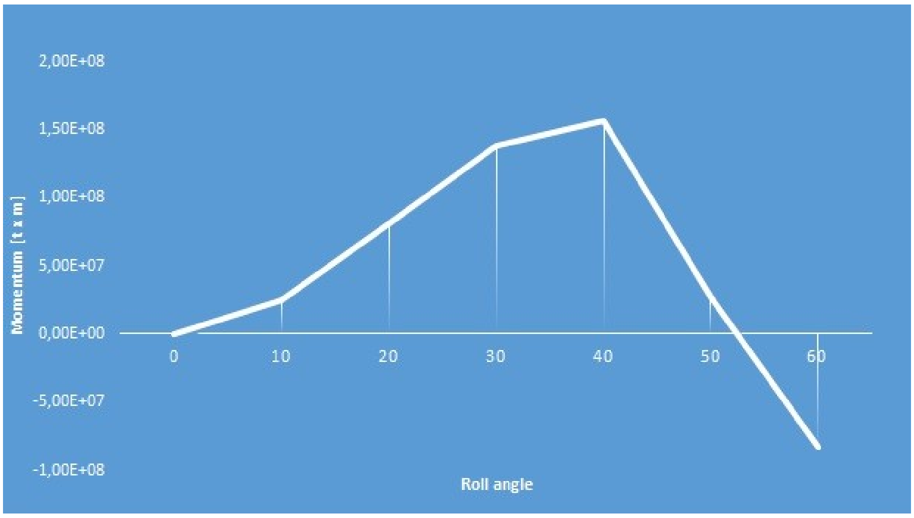

Figure 5.6: Stability curve - hull V2

5.1.1 Stability curve of the hull V2

To have a better idea of the behavoiur of the hull V2 its stability curve was calculated. The first step was to determine the metacetric height in order to compute the arm of the restoring force to be used in the equation 5.2. So the quantity $\overline{BM}$ is equal to:

$$\overline{BM} = \frac{I_x}{\nabla} \tag{5.3}$$

the demonstration of this expression can be found in several books, like [19]. The inertia of the water plane must be recalculated for each inclination angle, and this was done by using SolidWorks. The volume ∇ is always the same because depends only on the mass that is constant obviously. Finally subtracting the distance $\overline{GB}$ from $\overline{BM}$ and substituting all the values in the equation 5.2 is possible to find the value of the moment. Repeating it for many angles α is possible to produce the whole curve (Fig. 5.6).

CHAPTER 6

Conclusions

All the work contained in this thesis represents almost a "finish line" for some aspects and a starting point for new evolutions. The most important target achieved is the validation of a 3 Dof model that represents a step forward with respect to the previous 1 Dof model. In fact, the last one probably overestimates the productivity of the whole system. Now is possible to work with a more precise and reliable model. Different hull geometries have been realized and tested in order to find the best solution and, at the moment, it seems to be the V2 which is the one that was equipped with the pitch resonance tuning tank. For the first time this device was installed on a wave energy converter of this type as IOWEC, and obviously this brought some troubles but the way followed seems to be the right one. The frequency study realized and resumed in the Tables 4.14 ans 4.15 shows the potential of this device that will be developed working either on the U-Tank geometry or the dynamic controls. Also the stability of the machine was verified in order to have a complete design of the hull. There were a lot of other design attempts, mistakes and wrong ways taken and then left that are not contained in this dissertation for obvious reasons. There is still so much to do, but the way is the right one for the rising of a new technological and sustainable sector.

Appendix A

Mass[Kg]	1,49E+07
COG[m]	-1,78
LPV	12
COB[m]	-5,15
WP_area[m^2]	1500
BG[m]	3,38
GMX[m]	1,95
GMY[m]	27,3
BMX[m]	5,33
BMY[m]	30,72
MX[Nm/deg]	5,02E+06
MY[Nm/deg]	7,03E+07
K55[Nm/deg]	4,03E+09
K44[Nm/deg]	2,88E+08

Table 1: Hydrostatic datas of V1 with the PRTT

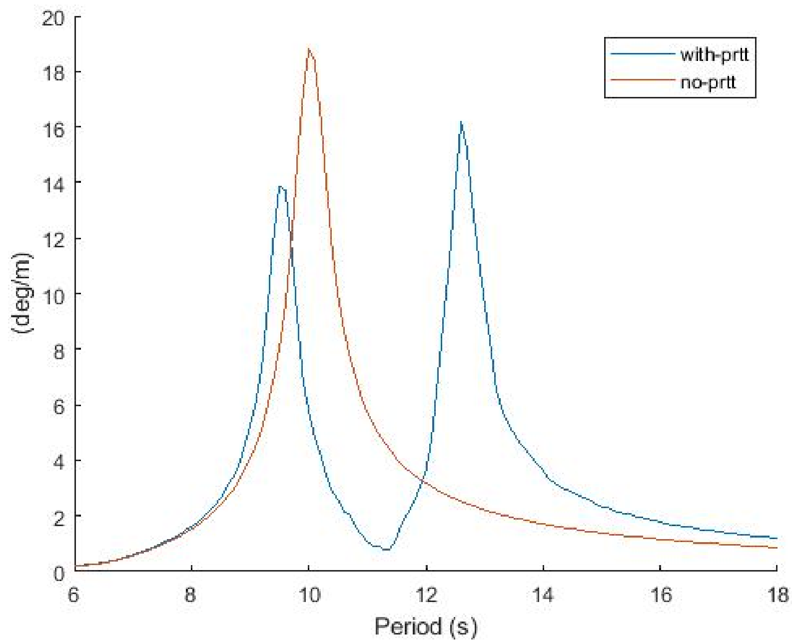

Figure 1: Response of the V1 with the PRTT

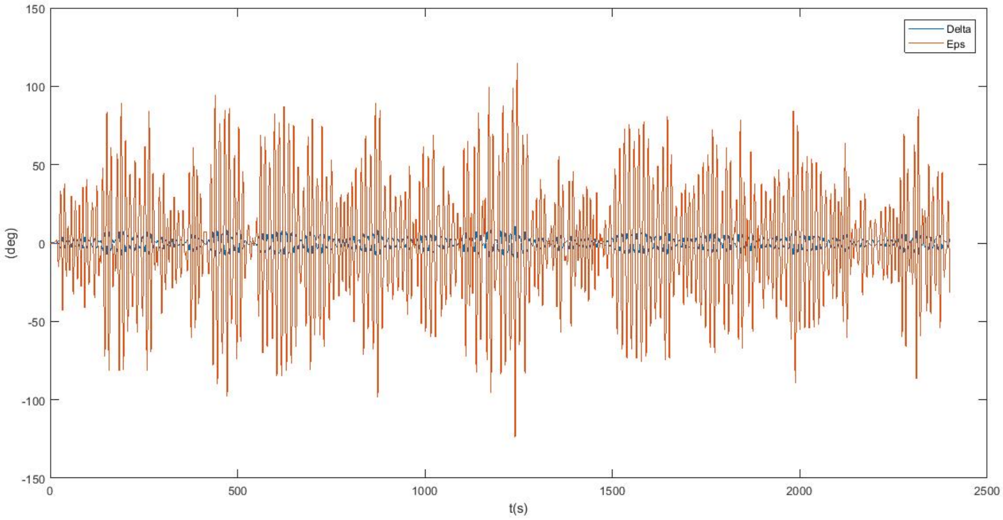

Figure 2: Overlap between δ and ε - V1 - PRTT On

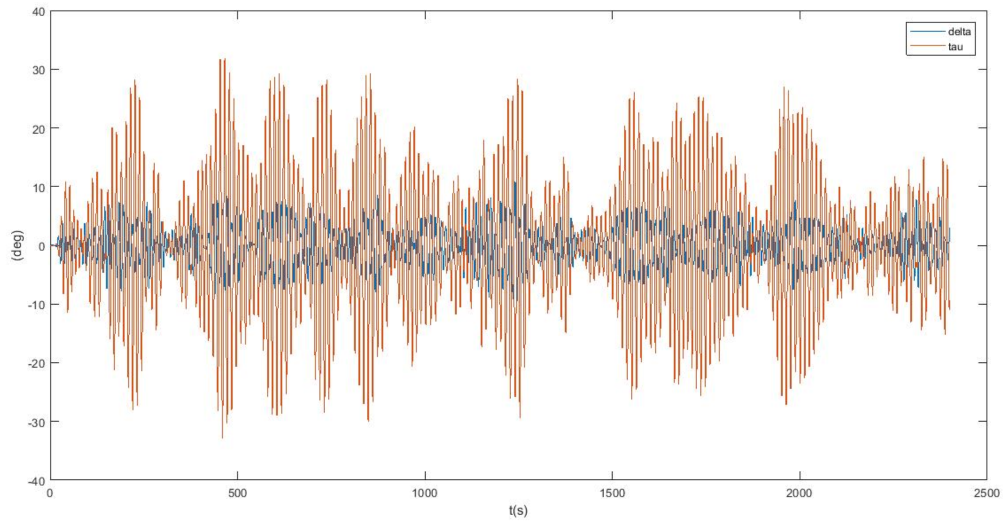

Figure 3: Overlap between δ and τ - V1 - PRTT On

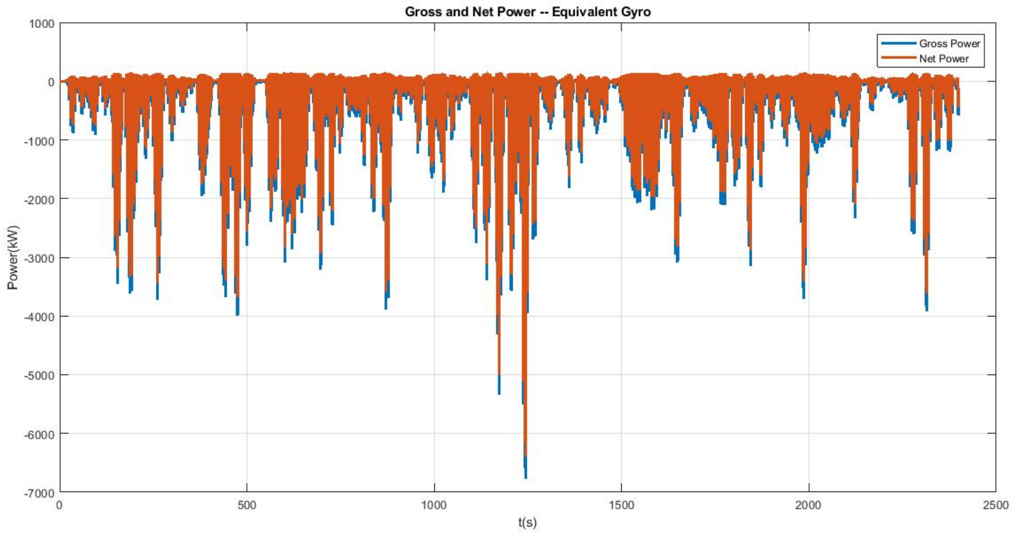

Figure 4: Gross and net productivity - V1 - PRTT On

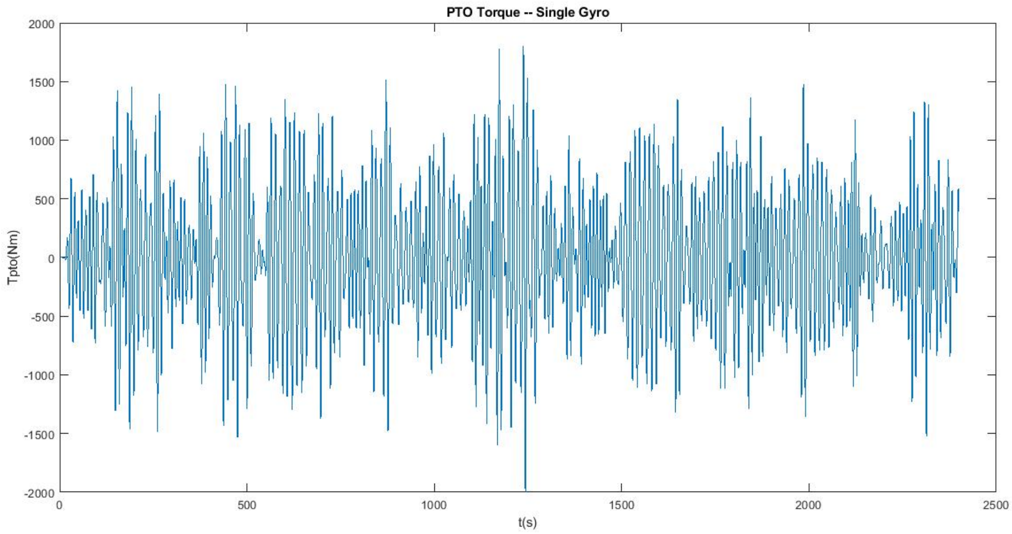

Figure 5: Torque transmitted to the PTO - V1 - PRTT On

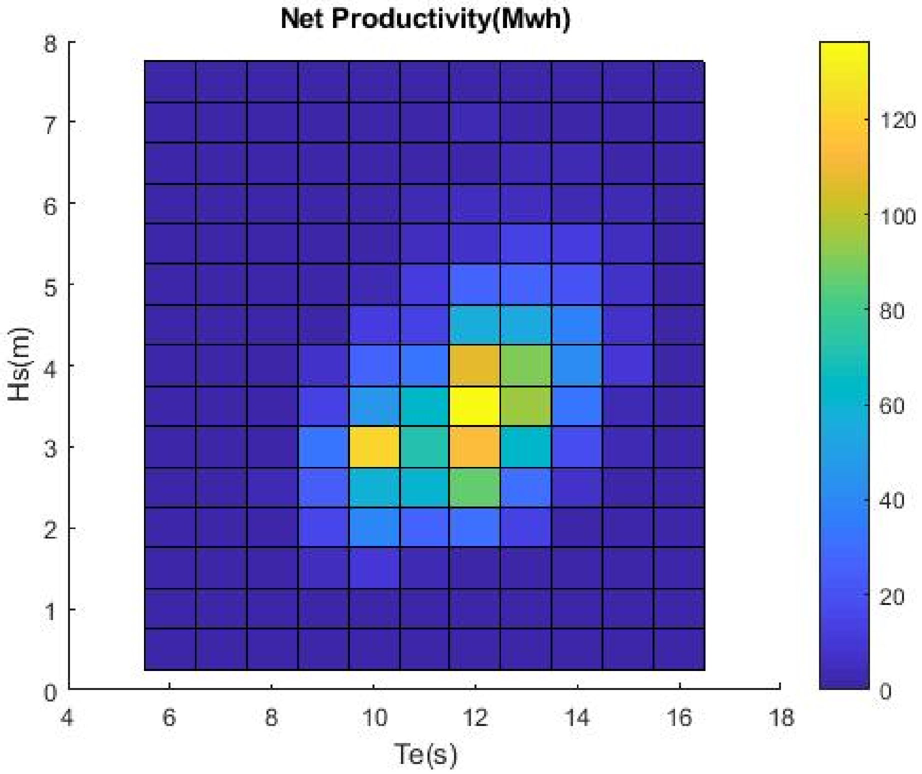

Figure 6: Production scatter of V1 with PRTT activated

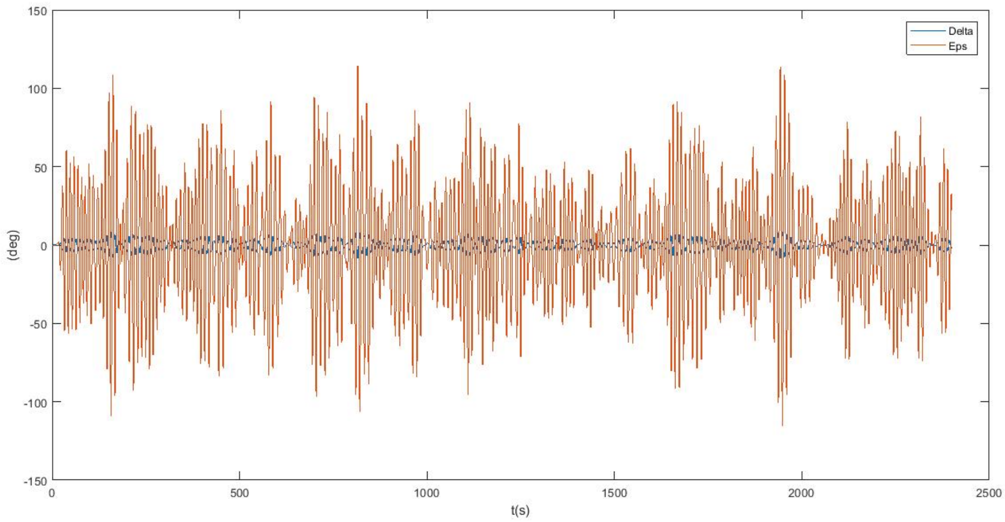

Figure 7: Overlap between δ and ε - V1 - PRTT Off

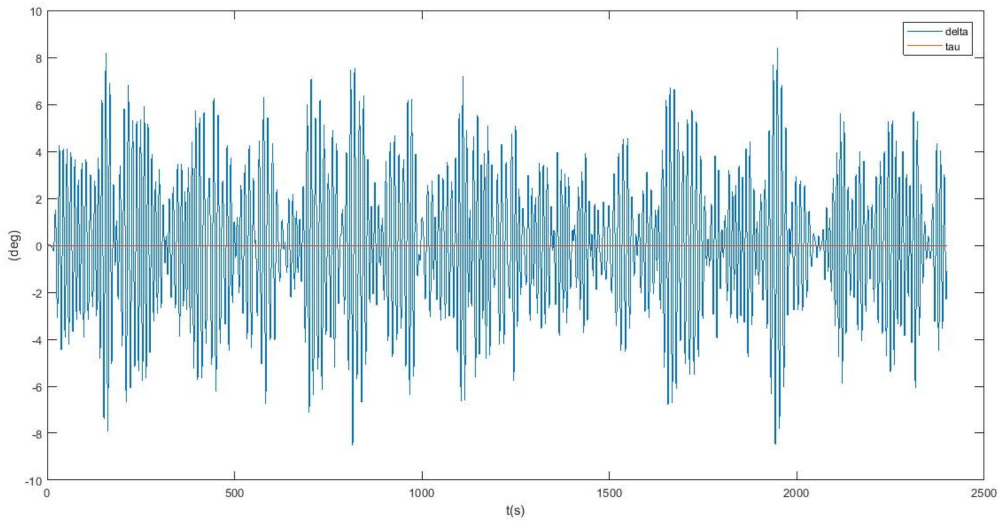

Figure 8: Overlap between δ and τ - V1 - PRTT Off

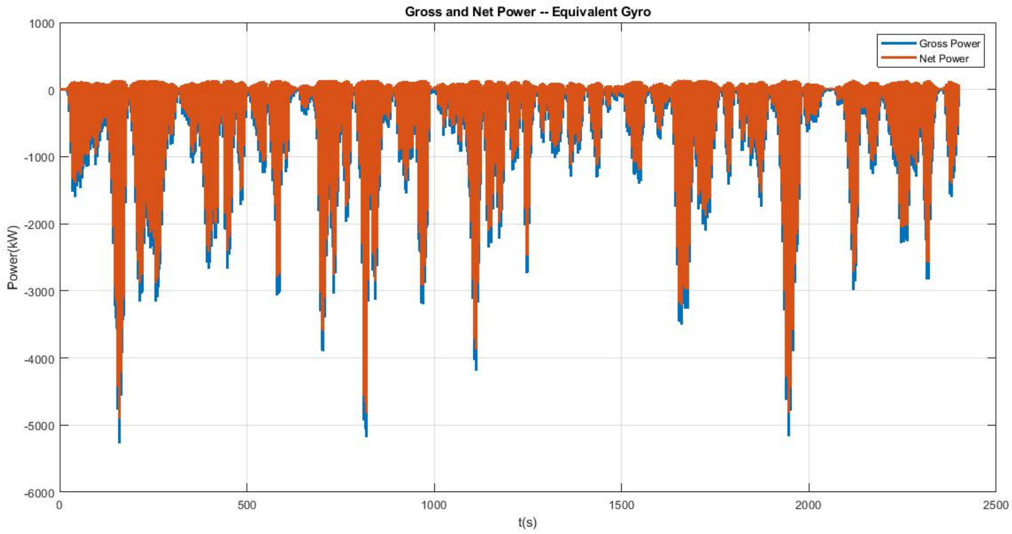

Figure 9: Gross and net productivity - V1 - PRTT Off

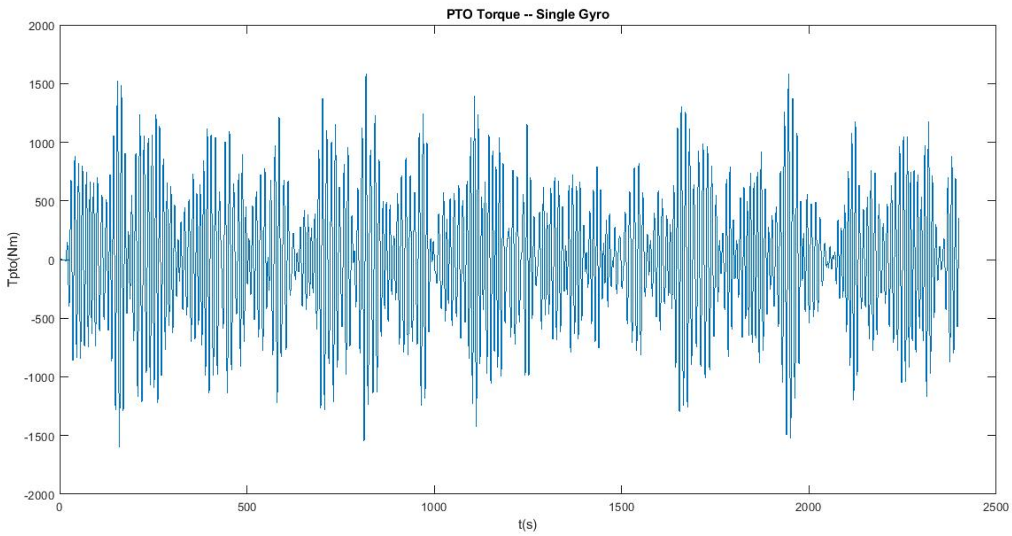

Figure 10: Torque transmitted to the PTO - V1 - PRTT Off

	V1	V1 - Prtt - OFF	V1 - Prtt - ON
Phid (rpm)	302,74	273,63	281,89
c (Nms/rad)	463518,90	334000,03	409942,52
TotPowerNet (kW)	502,50	406,72	412,12
TotPowerGross (kW)	668,11	558,39	561,08
TotPowerLost (kW)	165,62	151,67	148,96
DeltaMax (deg)	10,62	8,43	10,93
DeltaRms (deg)	3,22	2,73	3,15
EpsMax (deg)	114,29	114,10	114,26
EpsRms (deg)	34,97	36,76	36,03
TptoMax (Nm)	25694,61	18949,57	21643,28
TptoRms (Nm)	8032,27	6233,34	6922,37
VelMax (rpm)	214,51	211,24	224,01
VelRms (rpm)	66,19	71,29	64,50
Annual Net Productivity (MWh/y)	2508,89	2202,21	1929,37
Annual Gross Productivity (MWh/y)	3322,81	2986,52	2701,32
Te (s)	11,5	11,5	11,5
Hs (m)	3,25	3,25	3,25

Table 2: Performance parameters of all V1 versions for the design wave

	V1	V1 - Prtt - optimized	V1 - Prtt - OFF	V1 - Prtt - ON
Phid_Weighted (rpm)	212,93	110,39	212,33	209,26
c_Weighted (Nms/rad)	290817,65	144245,48	267001,19	264829,51
Eps_RmsWeighted (deg)	30,95	15,17	29,21	30,07
Eps_MaxWeighted (deg)	102,55	50,59	99,04	96,65
Delta_RmsWeighted (deg)	2,49	1,22	2,23	2,24
Delta_MaxWeighted (deg)	8,36	4,07	7,56	7,34
T_ptoRmsWeighted (Nm)	4719,37	2322,81	4268,19	4026,42
T_ptoMaxWeighted (Nm)	15903,03	7701,37	14399,06	13085,38
Vel_RmsWeighted (rpm)	60,31	31,28	58,51	56,31
Vel_MaxWeighted (rpm)	200,46	102,91	197,02	184,71
Gross_Productivity (MWh)	3322,81	3295,64	2986,52	2701,32
Net_Productivity (MWh)	2508,89	2437,40	2202,21	1929,37

Table 3: Performance parameters of all V1 versions weighed on the scatter

Mass[Kg]	1,25E+07
COG[m]	-3,61
LPV	12
COB[m]	-5,34
WP_area[m^2]	1200
BG[m]	1,73
GMX[m]	2,08
GMY[m]	20,88
BMX[m]	3,81
BMY[m]	22,62
MX[Nm/deg]	4,51E+06
MY[Nm/deg]	4,54E+07
K55[Nm/deg]	2,60E+09
K44[Nm/deg]	2,58E+08

Table 4: Hydrostatic datas - V3 - PRTT

	V3	V3 - Prtt - OFF	V3 - Prtt - ON
Phid (rpm)	220,75	203,80	187,68
c (Nms/rad)	412714,73	249533,12	307357,90
TotPowerNet (kW)	474,31	320,90	276,77
TotPowerGross (kW)	572,07	416,40	350,20
TotPowerLost (kW)	97,76	95,50	73,44
DeltaMax (deg)	12,93	8,27	11,10
DeltaRms (deg)	3,97	2,76	3,30
EpsMax (deg)	113,87	113,52	113,68
EpsRms (deg)	35,31	36,52	33,28
TptoMax (Nm)	22595,70	13928,72	16098,58
TptoRms (Nm)	7013,42	4652,63	4735,45
VelMax (rpm)	211,06	213,23	213,72
VelRms (rpm)	64,91	71,22	58,85
Annual Net Productivity (MWh/y)	2127,38	1792,06	1422,65
Annual Gross Productivity (MWh/y)	2603,45	2299,85	1893,05
Te (s)	11,5	11,5	11,5
Hs (m)	3,25	3,25	3,25

Table 5: Performance parameters of all V3 versions for the design wave

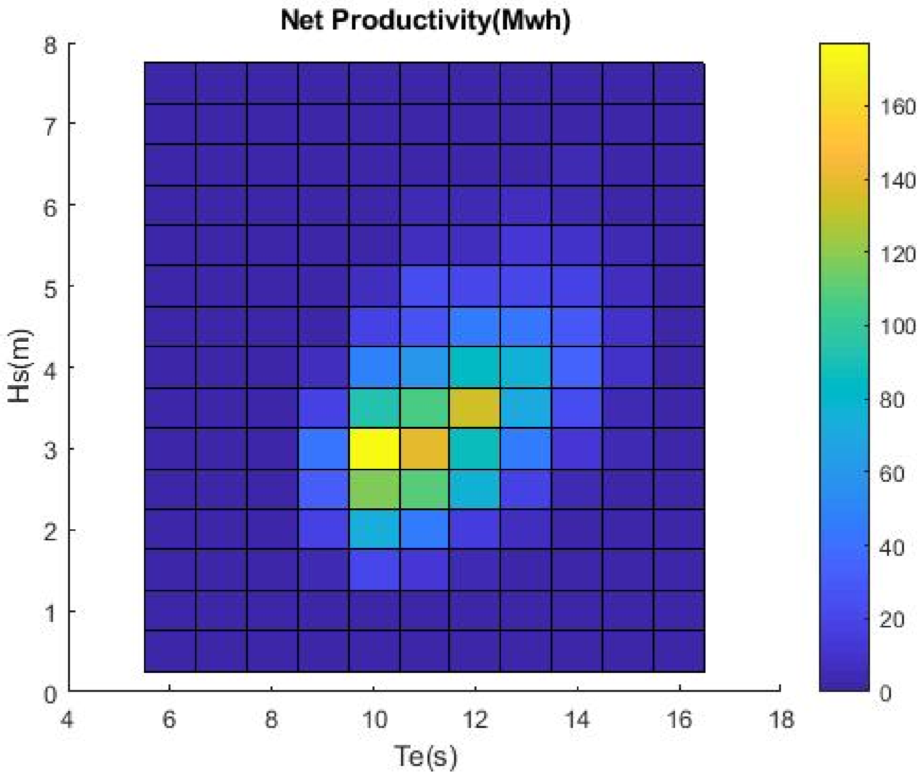

Figure 11: Production scatter of V1 with PRTT disabled

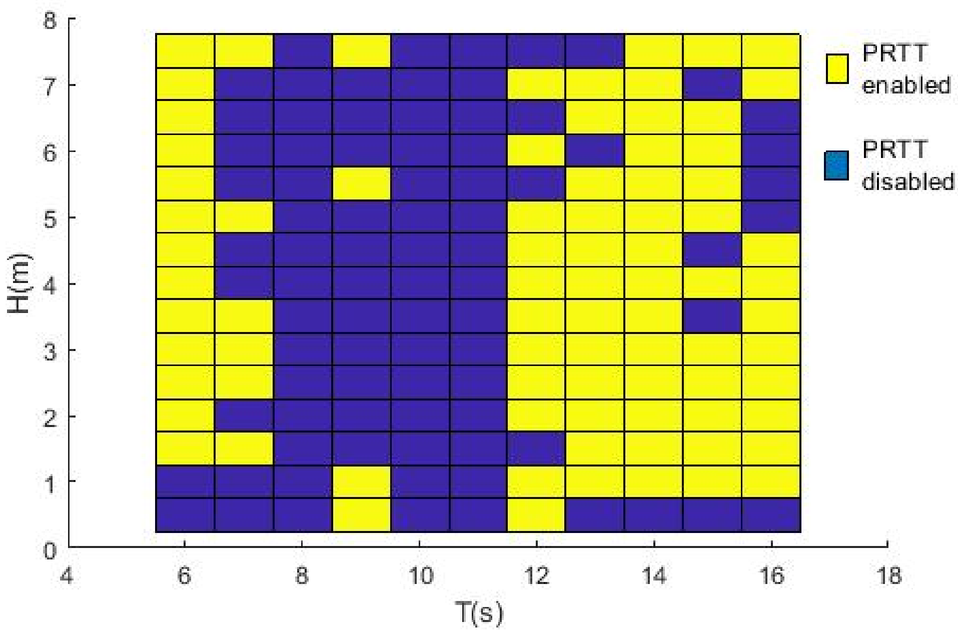

Figure 12: Utilization of the U-tank in dependence of the waves - V1

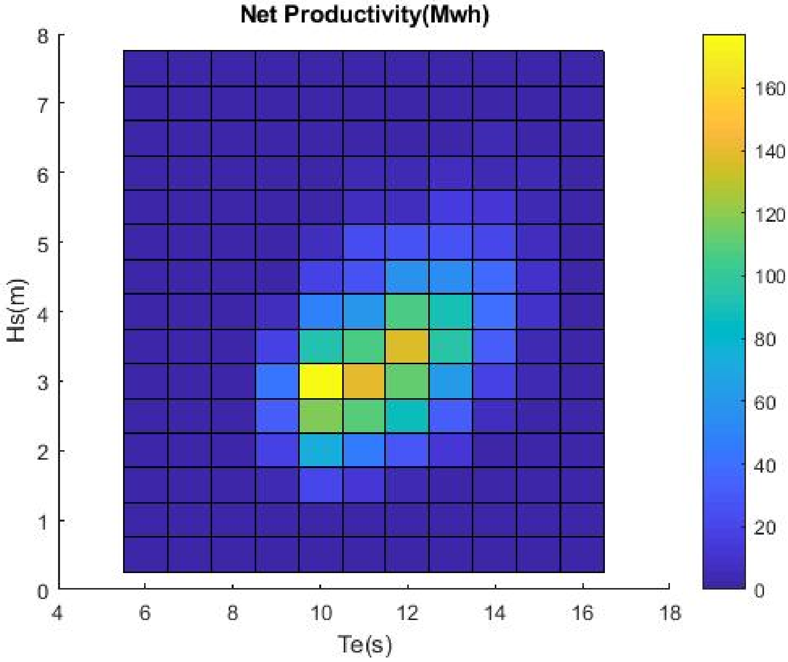

Figure 13: Production scatter of V1 with the optimal use of the U-tank

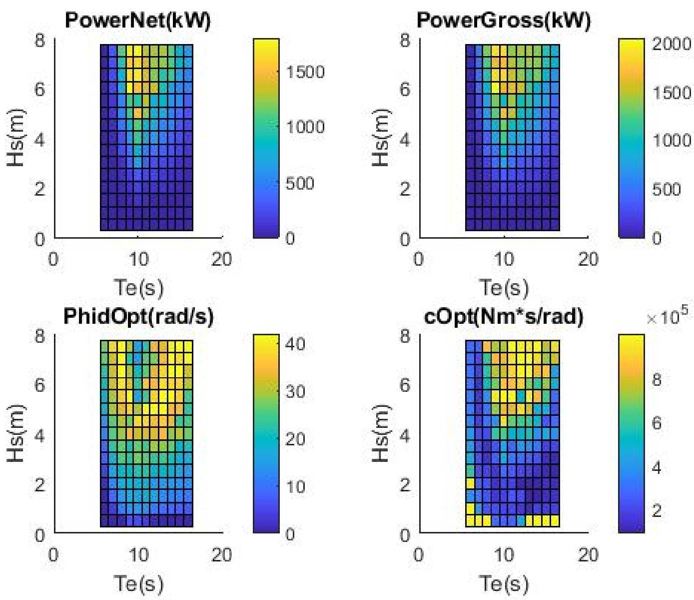

Figure 14: Performance graphs - V1 - group 1

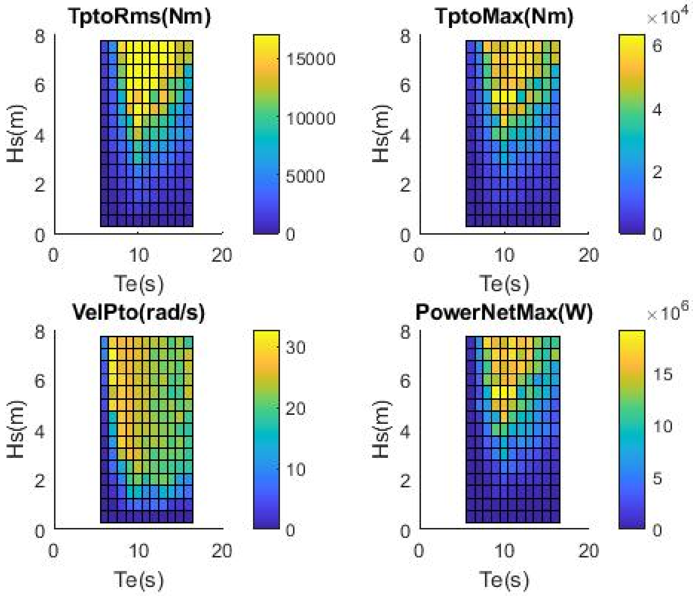

Figure 15: Performance graphs - V1 - group 2

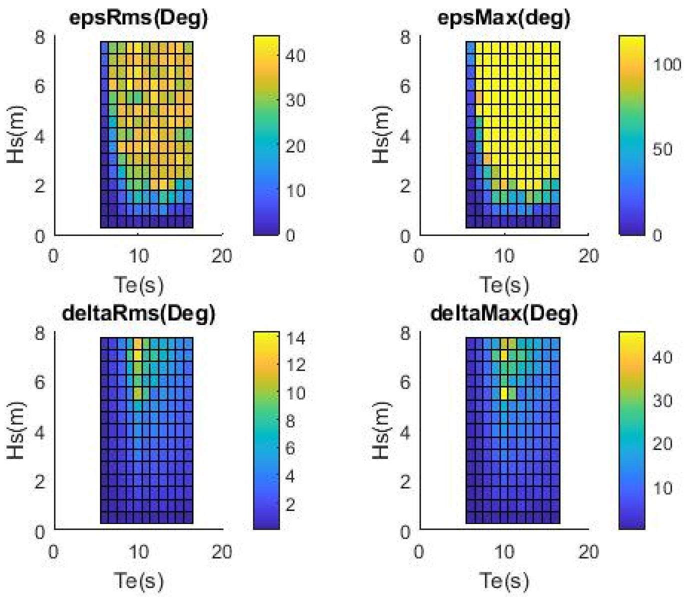

Figure 16: Performance graphs - V1 - group 3

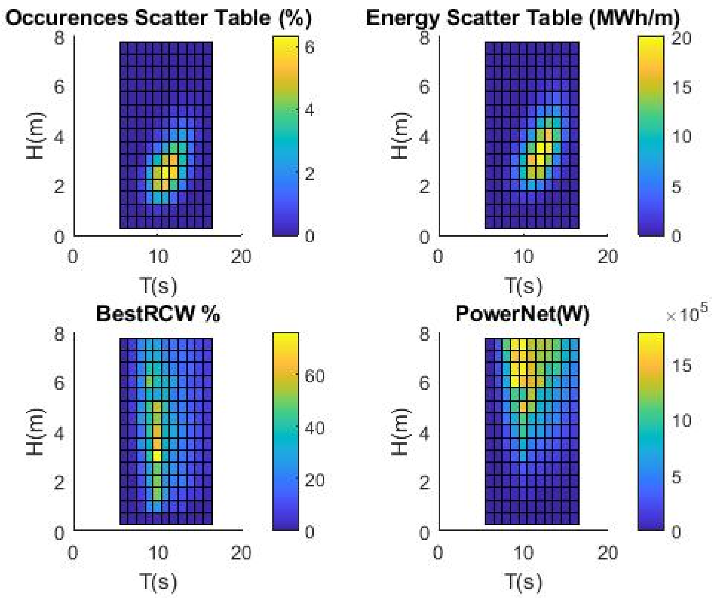

Figure 17: Performance graphs - V1 - group 4

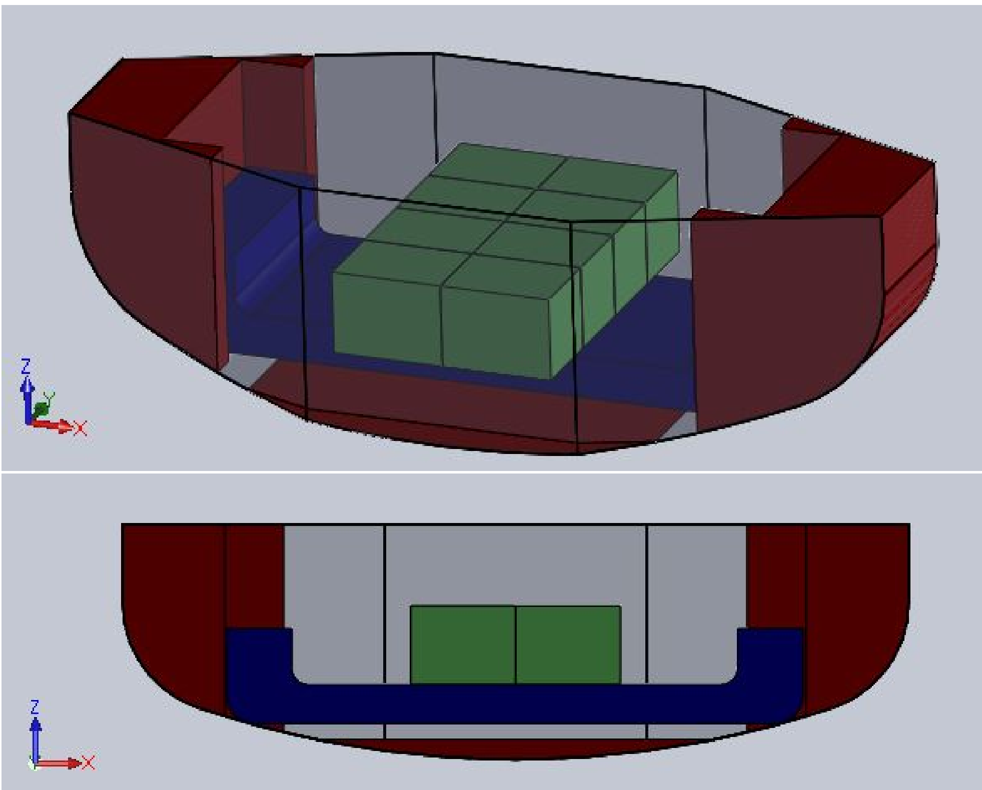

Figure 18: Hull V3 with PRTT

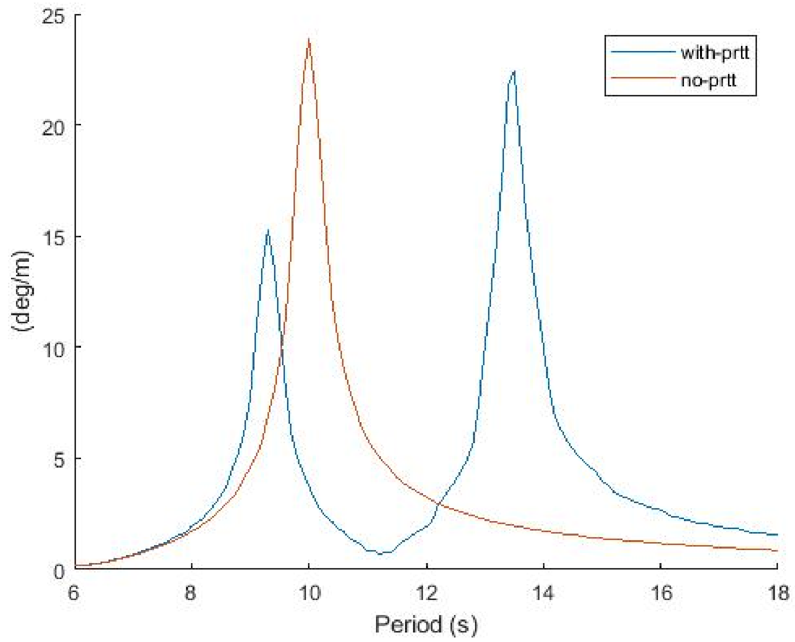

Figure 19: Response of the V3 with PRTT

	V3	V3 - Prtt - optimized	V3 - Prtt - OFF	V3 - Prtt - ON
Phid_Weighted (rpm)	151,03	169,48	168,88	164,43
c_Weighted (Nms/rad)	245760,51	253555,84	237846,64	238153,05
Eps_RmsWeighted (deg)	30,91	29,68	26,94	27,21
Eps_MaxWeighted (deg)	98,86	95,51	91,44	85,83
Delta_RmsWeighted (deg)	2,97	2,65	2,35	2,30
Delta_MaxWeighted (deg)	9,70	8,60	7,93	7,48
T_ptoRmsWeighted (Nm)	3811,25	3809,64	3493,41	3132,54
T_ptoMaxWeighted (Nm)	12617,35	12478,75	11734,03	10216,97
Vel_RmsWeighted (rpm)	58,39	56,00	54,28	49,91
Vel_MaxWeighted (rpm)	187,23	180,62	182,39	162,25
Gross_Productivity (MWh)	2603,45	2524,60	2299,85	1893,05
Net_Productivity (MWh)	2127,38	1984,91	1792,06	1422,65

Table 6: Performance parameters of all V3 versions weighed on the scatter

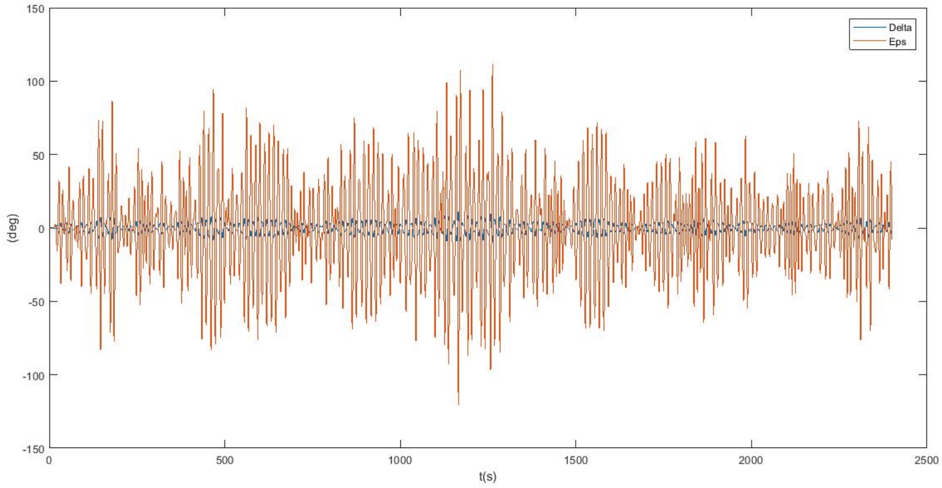

Figure 20: Overlap between δ and ε - V3 - PRTT On

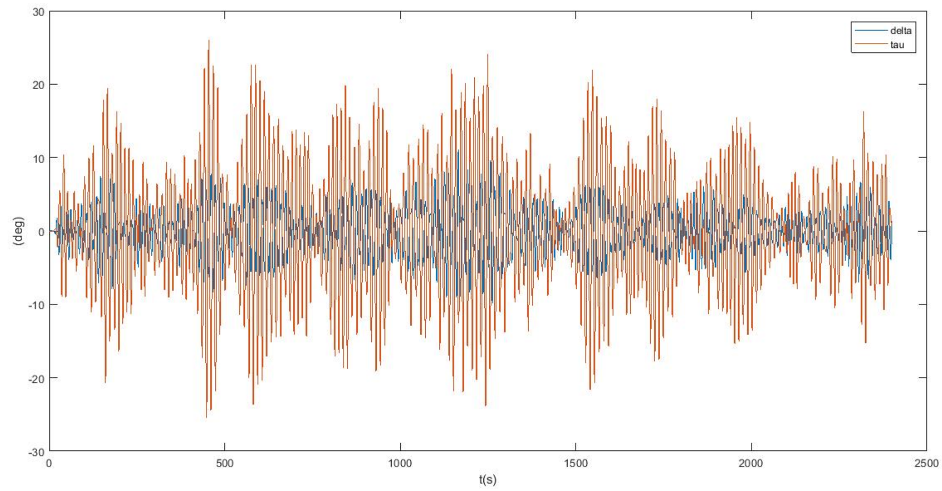

Figure 21: Overlap between δ and τ - V3 - PRTT On

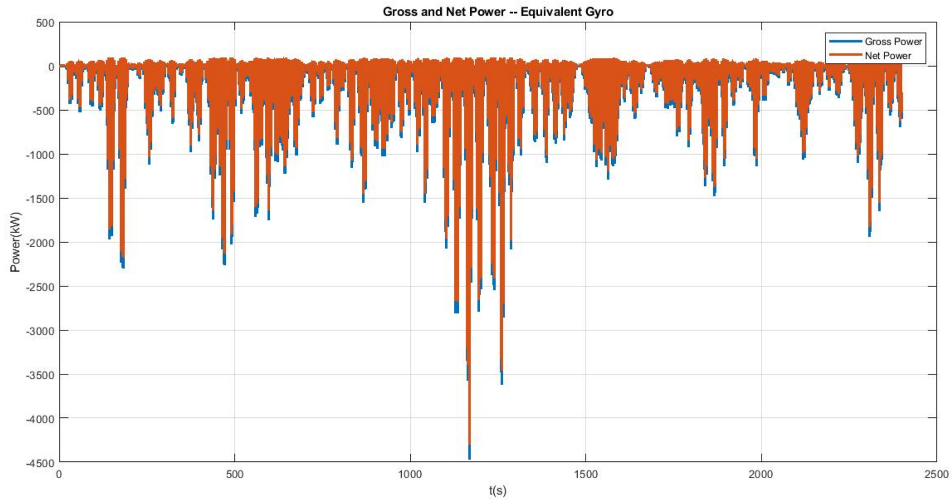

Figure 22: Gross and net productivity - V3 - PRTT On

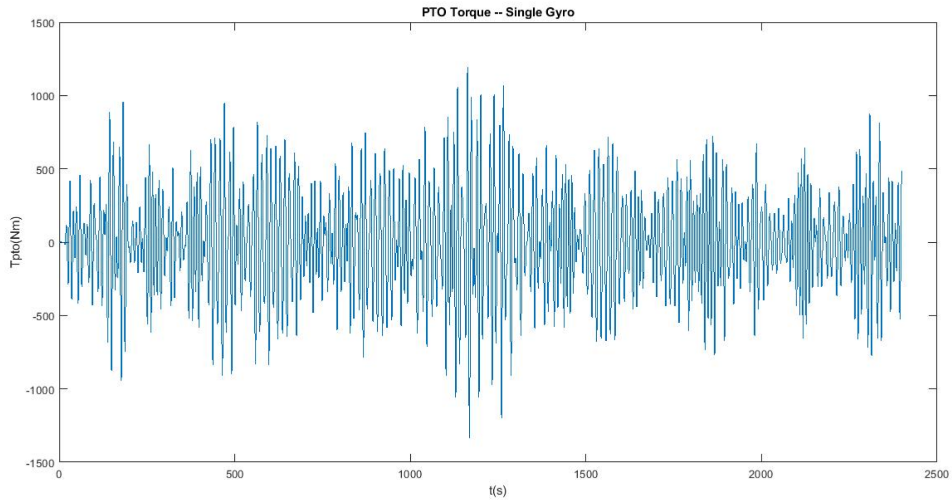

Figure 23: Torque transmitted to the PTO - V3 - PRTT On

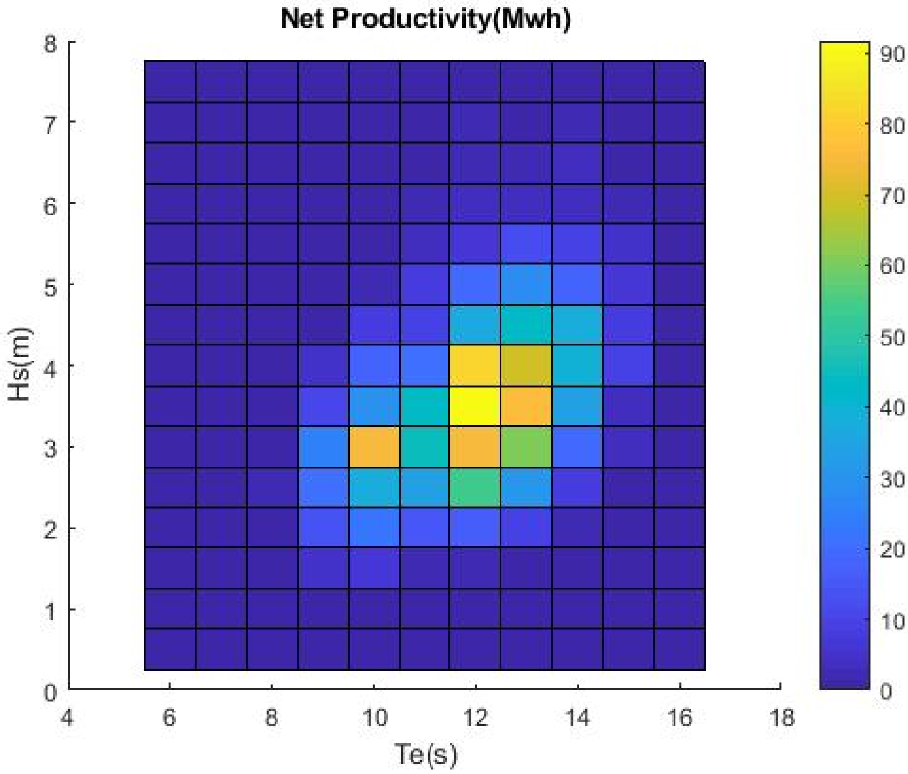

Figure 24: Production scatter - V3 - PRTT enabled

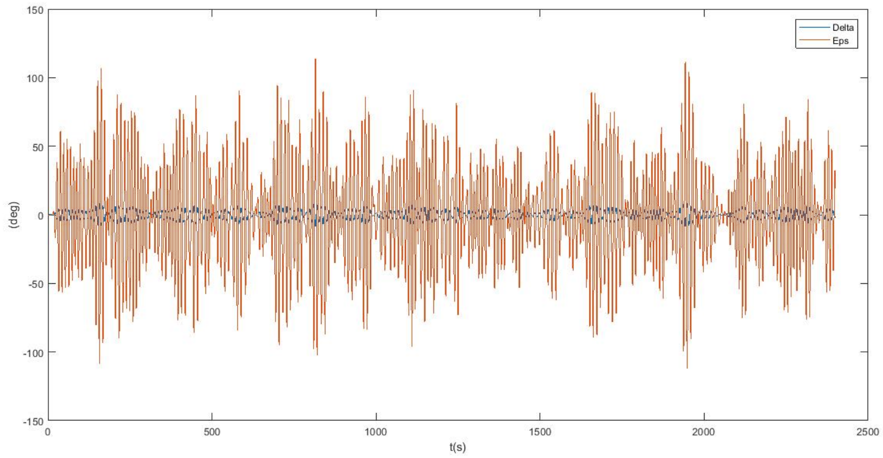

Figure 25: Overlap between δ and ε - V3 - PRTT Off

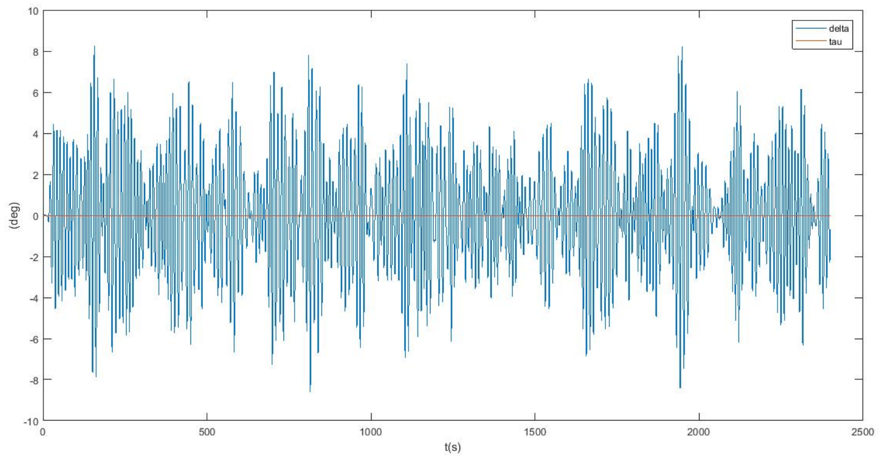

Figure 26: Overlap between δ and τ - V3 - PRTT Off

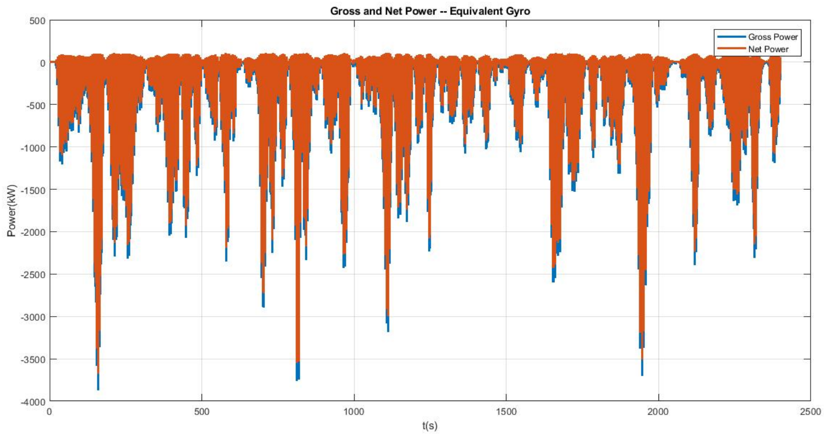

Figure 27: Gross and net productivity - V3 - PRTT Off

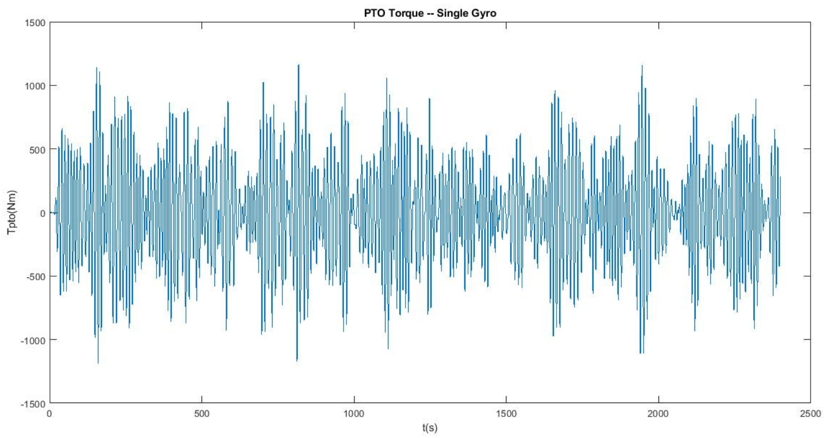

Figure 28: Torque transmitted to the PTO - V3 - PRTT Off

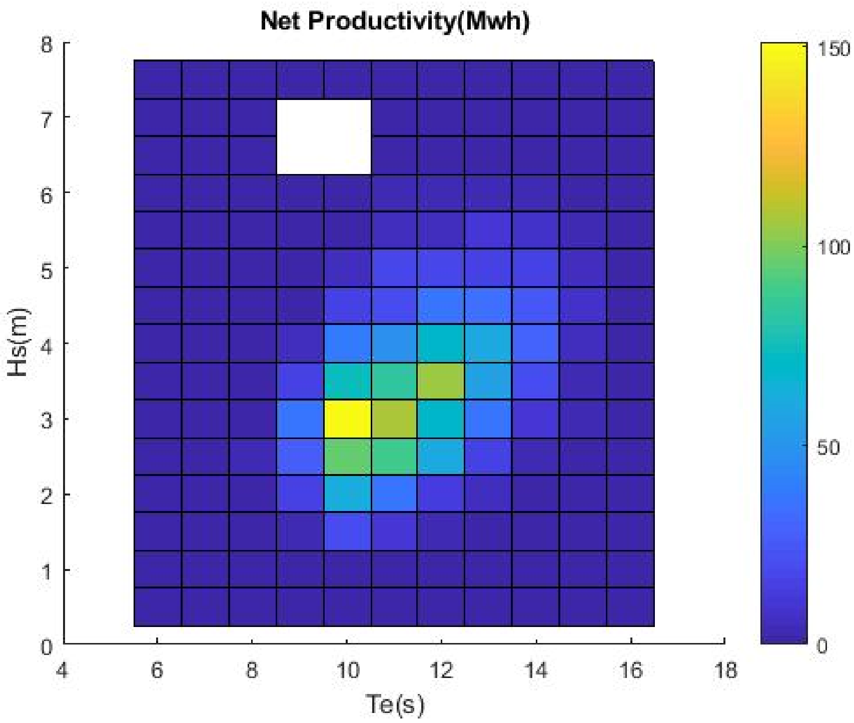

Figure 29: Production scatter - V3 - PRTT disabled

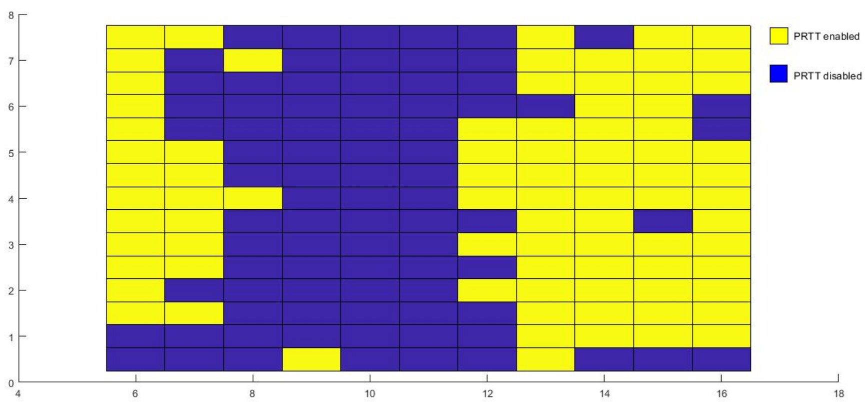

Figure 30: Utilization of the U-tank in dependence of the waves - V3

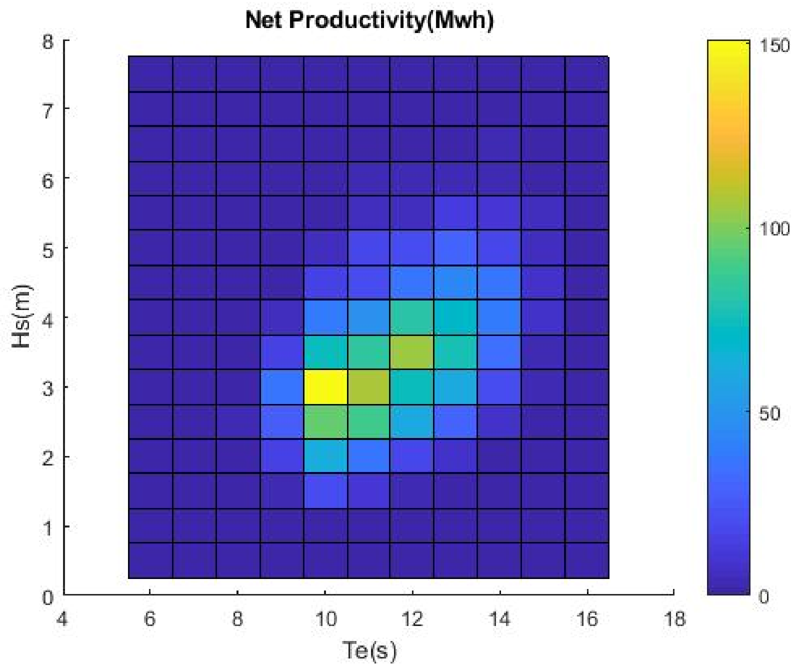

Figure 31: Production scatter of V3 with the optimal use of the U-tank

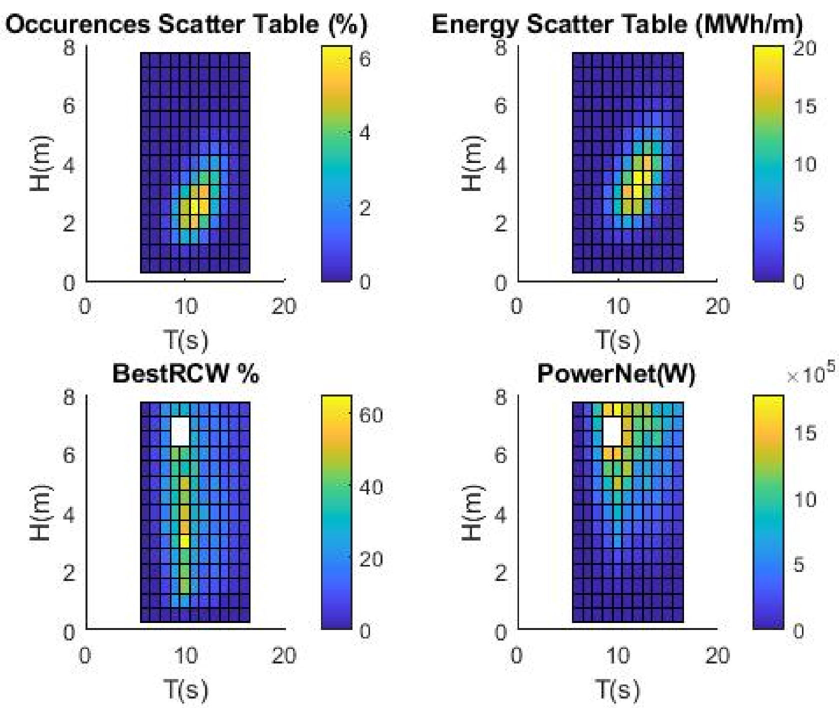

Figure 32: Performance graphs - V3 - group 1

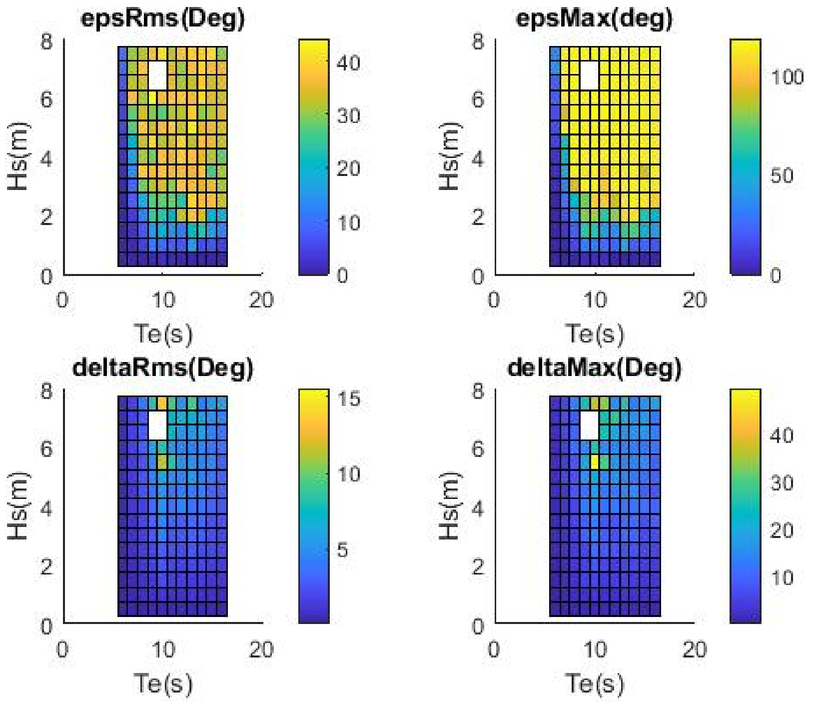

Figure 33: Performance graphs - V3 - group 2

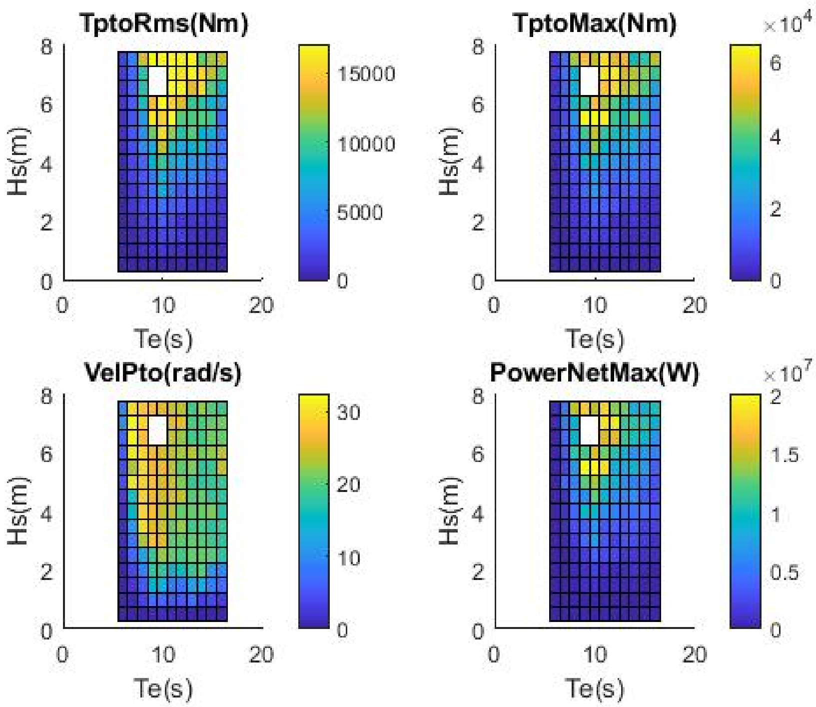

Figure 34: Performance graphs - V3 - group 3

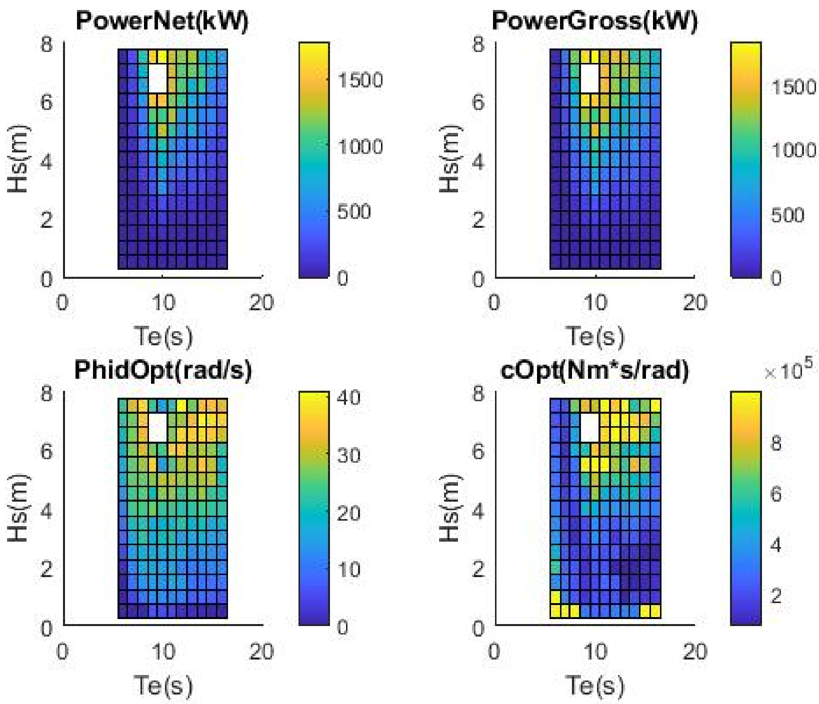

Figure 35: Performance graphs - V2 - group 4

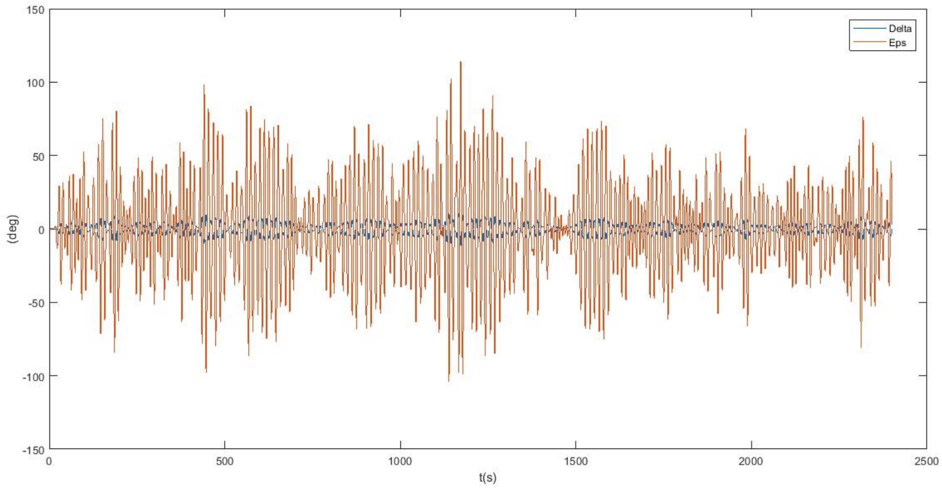

Figure 36: Overlap between δ and ε - V2 RD - PRTT On

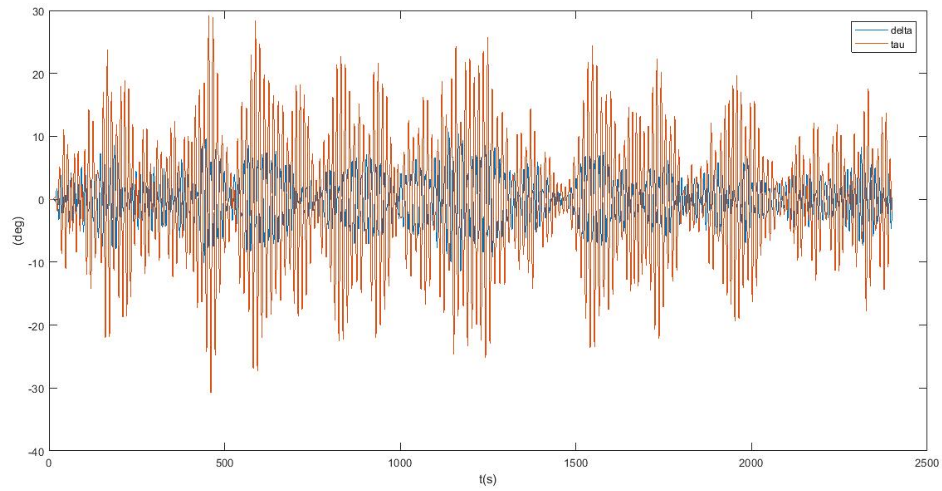

Figure 37: Overlap between δ and τ - V2 RD - PRTT On

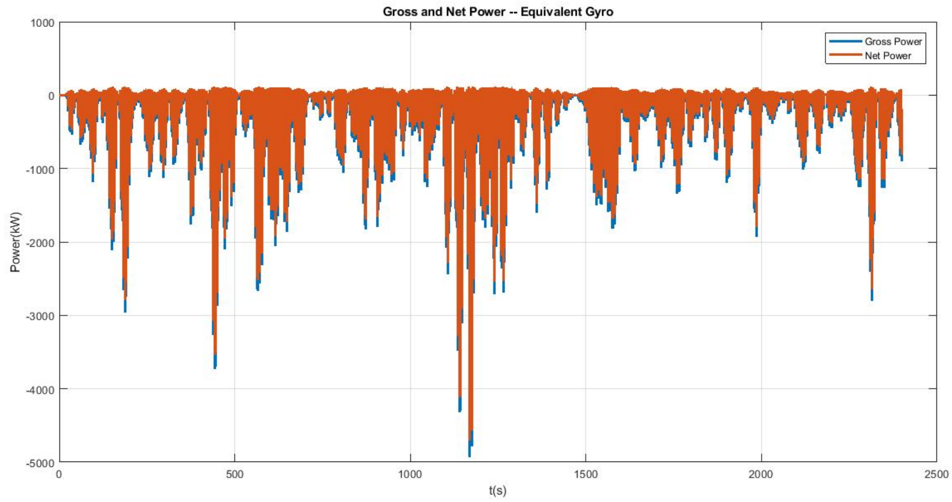

Figure 38: Gross and net productivity - V2 RD - PRTT On

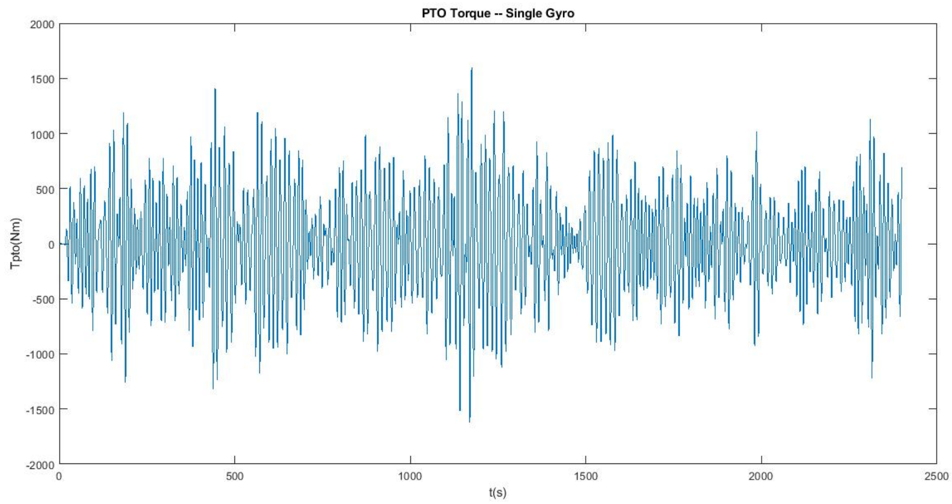

Figure 39: Torque transmitted to the PTO - V2 RD - PRTT On

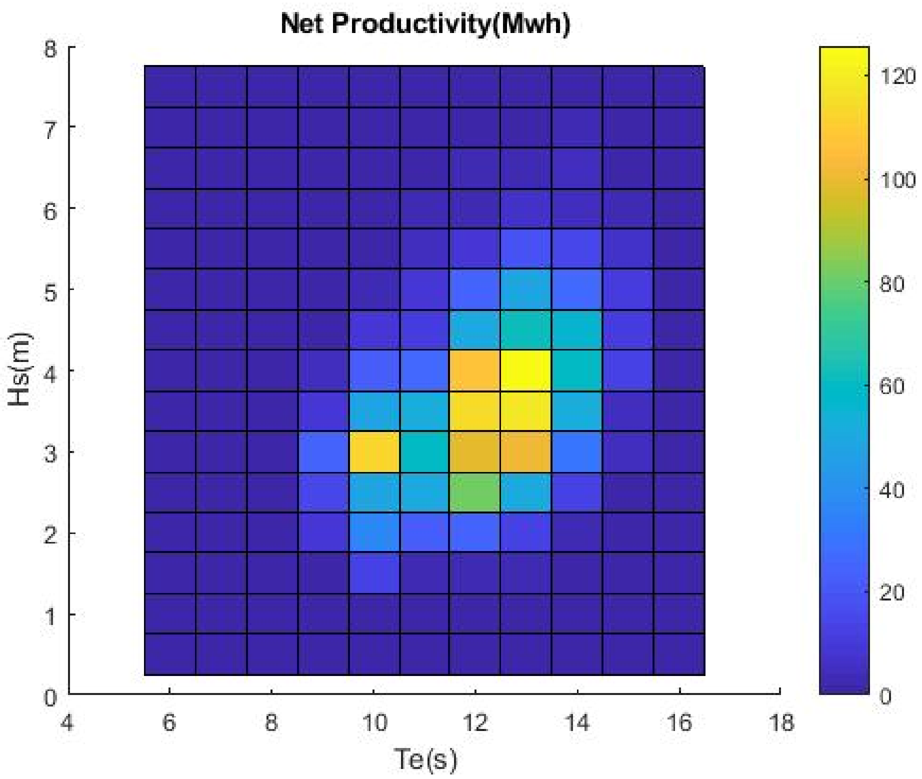

Figure 40: Production scatter - V2 RD - PRTT enabled

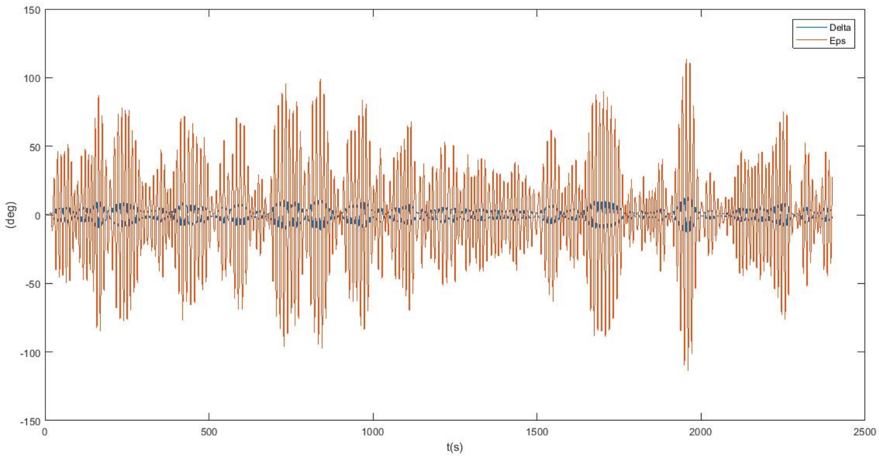

Figure 41: Overlap between δ and ε - V2 RD - PRTT Off

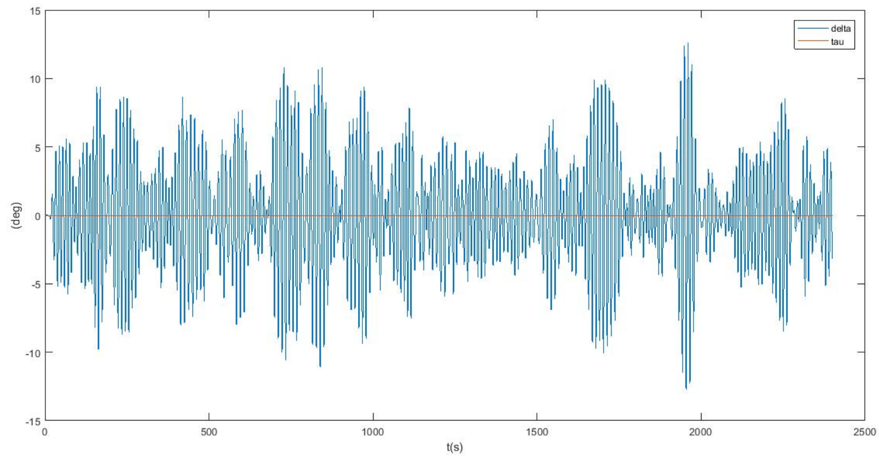

Figure 42: Overlap between δ and τ - V2 RD - PRTT Off

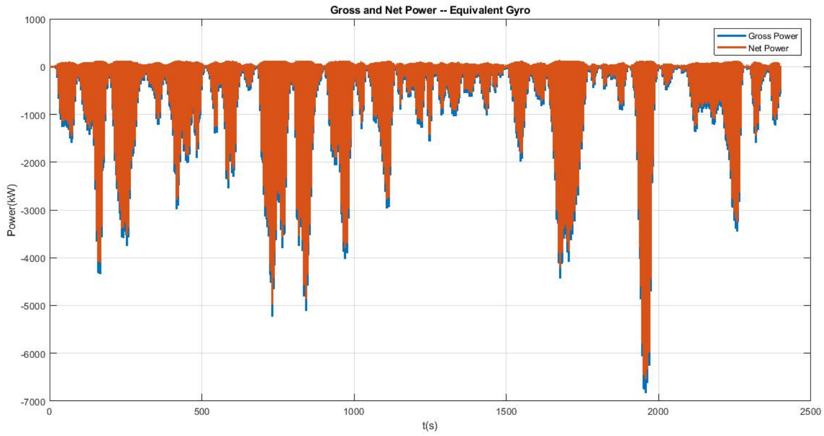

Figure 43: Gross and net productivity - V2 RD - PRTT Off

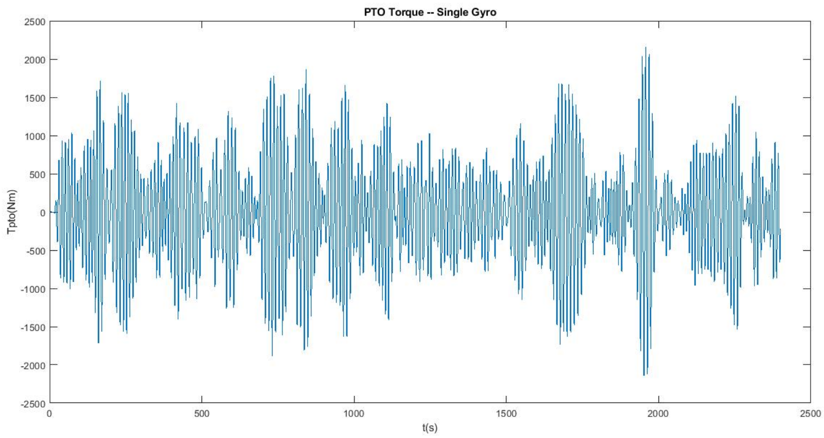

Figure 44: Torque transmitted to the PTO - V2 RD - PRTT Off

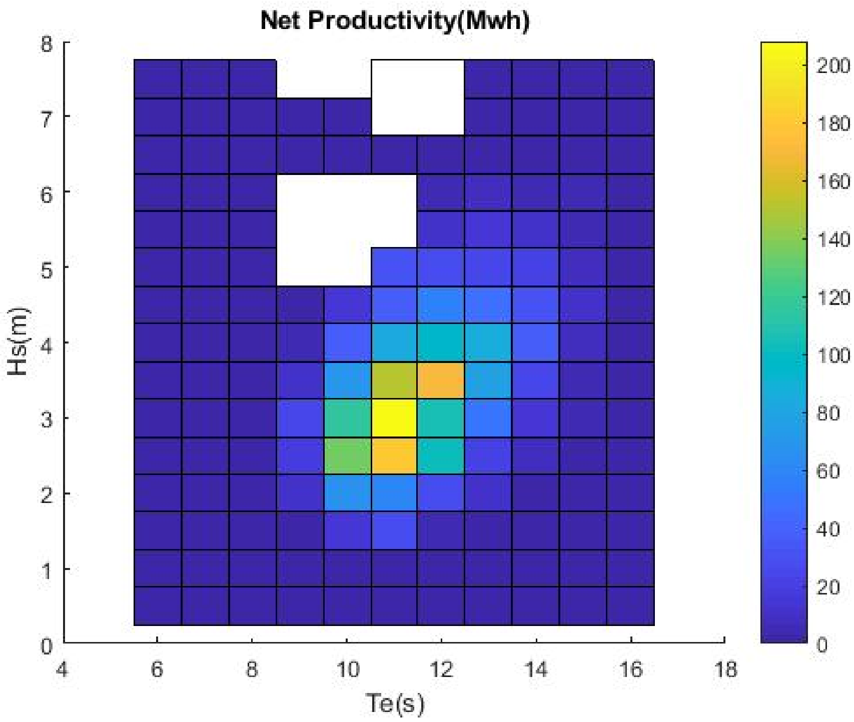

Figure 45: Production scatter - V2 RD - PRTT disabled

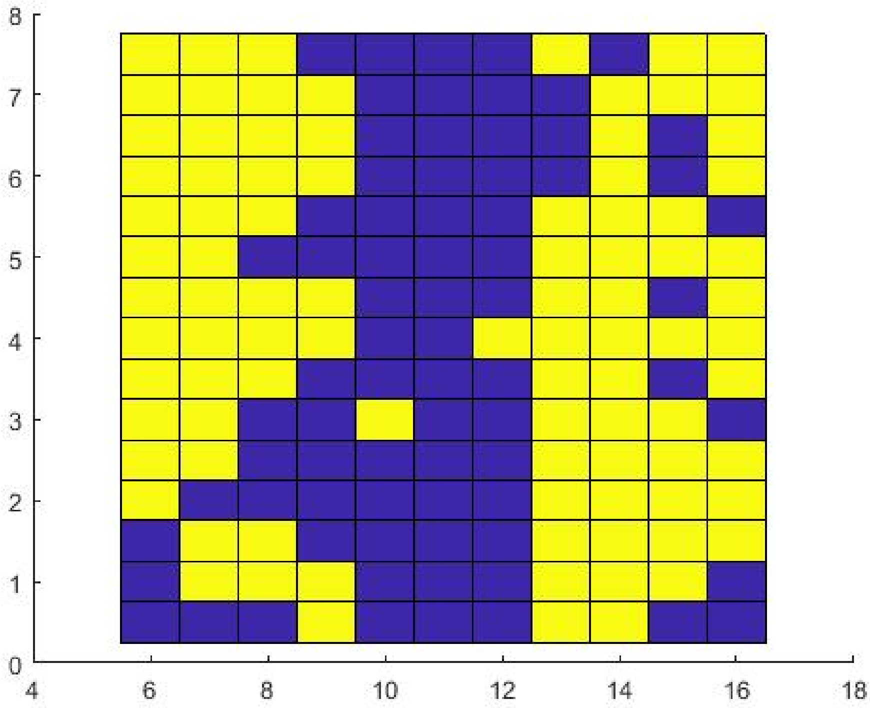

Figure 46: Utilization of the U-tank in dependence of the waves - V2 RD

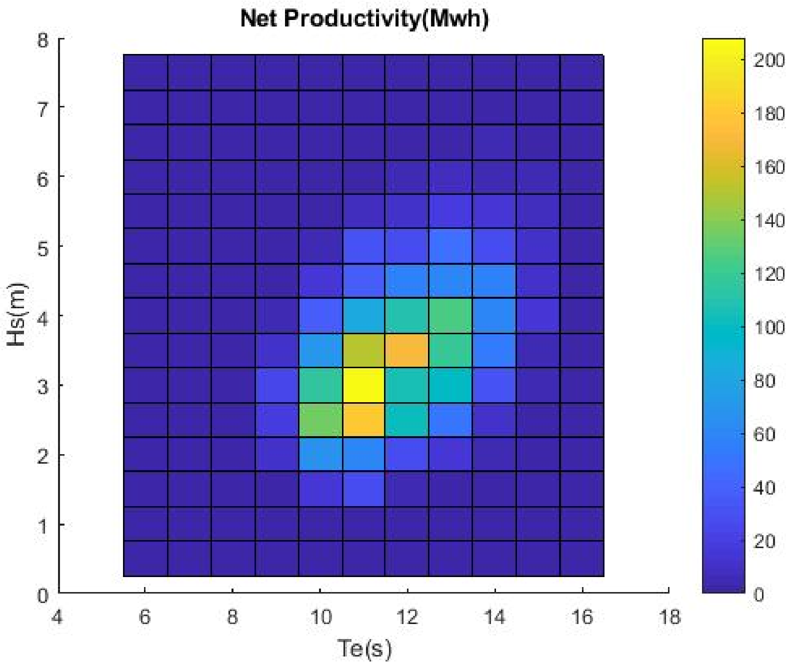

Figure 47: Production scatter of V2 RD with the optimal use of the U-tank

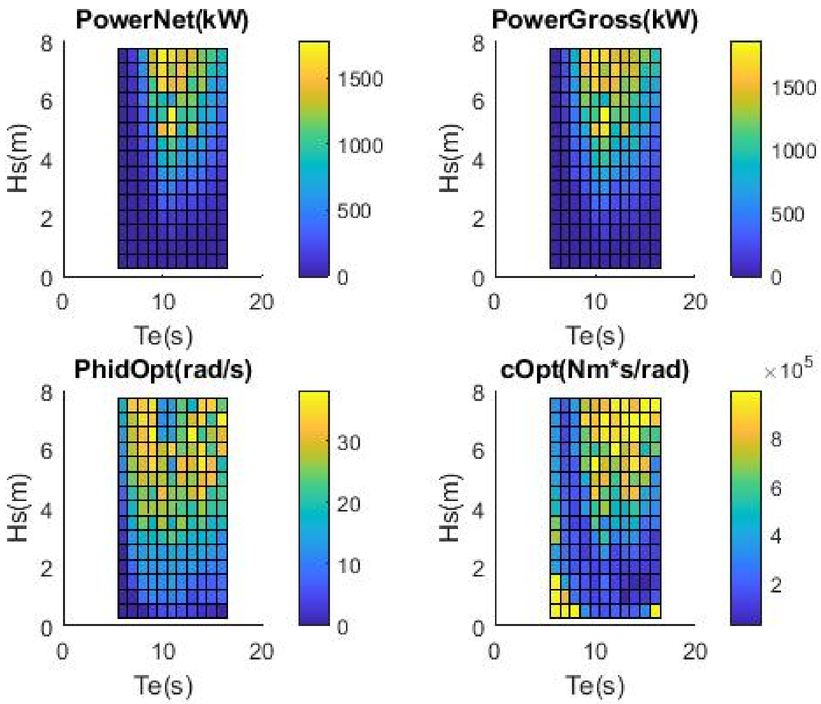

Figure 48: Performance graphs - V2 RD - group 1

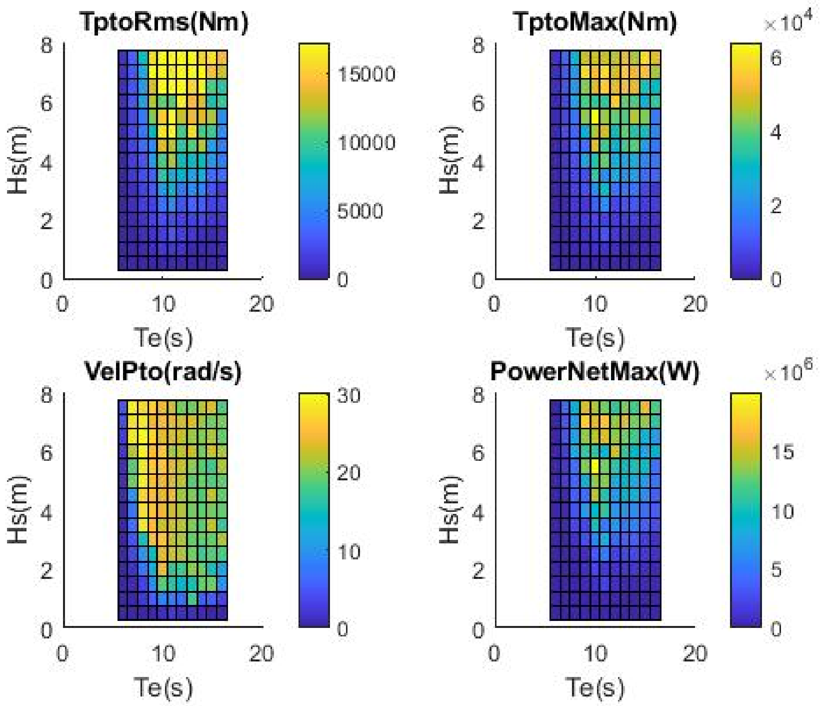

Figure 49: Performance graphs - V2 RD - group 2

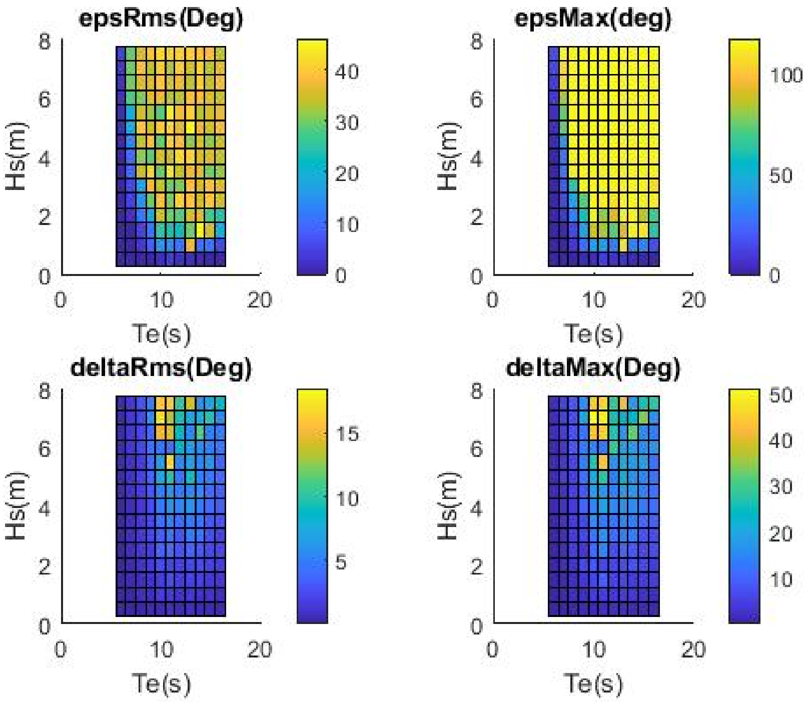

Figure 50: Performance graphs - V2 RD - group 3

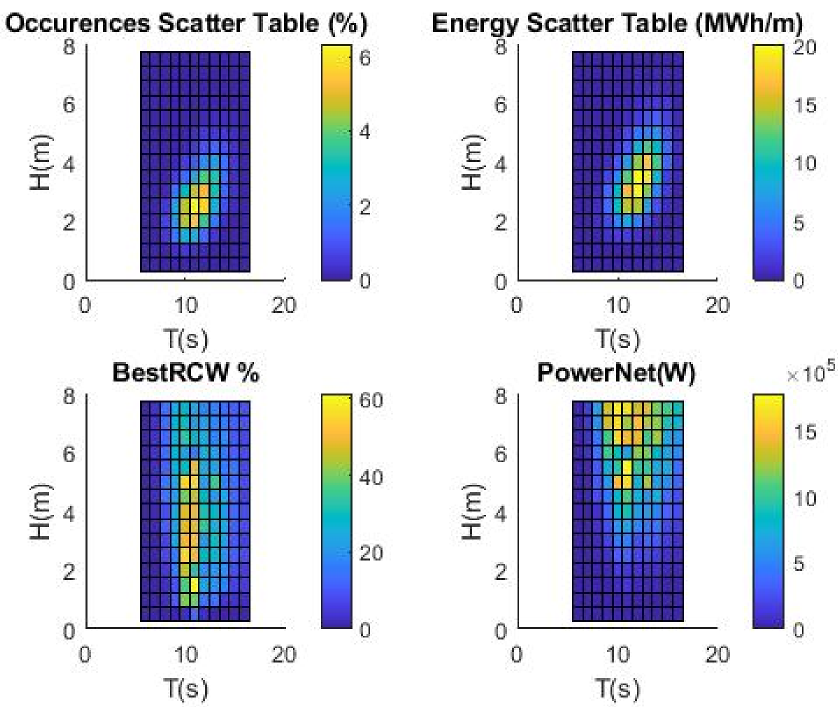

Figure 51: Performance graphs - V2 RD - group 4

Bibliography

[1] John Vidal: *Air pollution rising at an 'alarming rate' in world's cities*, theguardian, 2016.

[2] European Marine Energy Centre: *Wave Devices*, ©2018.

[3] A. Lewis; S. Estefen; J. Huckerby; W. Musial; T. Pontes; J. Torres Martinez: *Ocean Energy, in IPCC Special Report on Renewable Energy Sources and Climate Change Mitigation*, Cambridge University Press, Cambridge, United Kingdom and New York, NY, USA., McGraw-Hill, 2011.

[4] Ocean Energy Europe: *About Ocean Energy*, ©2015.

[5] G. Mattiazzo: *ISWEC: varo del sistema in scala reale nel mare di Pantelleria*, ©Wave for Energy 2014.

[6] G. Bracco; E. Giorcelli; G. Mattiazzo: *Iswec: A gyroscopic mechanism for wave power exploitation*, Elsevier, 2011.

[7] Harald E. Krogstad; Øivind A. Arntsen: *LINEAR WAVE THEORY - PART A*, Norwegian university of science and technology, Trondheim, Norway, 2000.

[8] John N. Newman: *Marine Hydrodynamics*, MIT Press, 1977.

[9] US Army Corps of Engineers: *Shore Protection Manual - Volume 1*, Coastal engineering research center, Washington D.C., 1984.

[10] R. H. Stewart: *Introduction to physical oceanography*, Department of Oceanography, Texas University, 2008.

[11] S.A. Sirigu; B. Passione; G. Vissio; N. Pozzi: *Iowec Predesign Chile*, 2016.

[12] Harald E. Krogstad; Øivind A. Arntsen: *LINEAR WAVE THEORY - PART B*, Norwegian university of science and technology, Trondheim, Norway, 2000.

[13] J.M.J. Journée; W.W. Massie: *OFFSHORE HYDROMECHANICS*, Delft University of Technology, January 2001.

[14] M. Calleri: *Inertial Sea Wave Energy Converter from Mediterranean Sea to Ocean - Design Optimization*, Polytechnic of Turin, 2017.

[15] E. W. Cummins: *The impulse response function and ship motion*, Washington DC, USA, David Taylor model basin, report 1961, Department of the Navy, 1962.

[16] S.A. Sirigu: *ISWEC: a design tool*, Polytechnic of Turin, 2015.

[17] S.A. Sirigu; B. Passione; V. Calamusa; N. Pozzi: *Pitch resonant tuning tank (PRTT) model validation*, Polytechnic of Turin, 2016.

[18] G. Rosati: *Arte navale ed elementi di costruzione navale*, PAS.

[19] L. Di Franco: *Elementi di stabilità, galleggiabilità e assetto delle navi*, Del Bianco, 2005.

[20] R. Nabergoj: *Fondamenti di tenuta al mare*, Trieste, 2007.